TOMAS BATA UNIVERSITY IN ZLIN
Faculty of Technology
Department of Polymer Engineering

The Influence of Thermal Effects on the Thermoplastic Materials Extrusion Process

(Závislost teplotních efektů na vytlačování termoplastických materiálů)

Bc. Patrik Rohrer

2016 Master Thesis

Univerzita Tomáše Bati ve Zlíně
Fakulta technologická
Ústav inženýrství polymerů
akademický rok: 2015/2016

ZADÁNÍ DIPLOMOVÉ PRÁCE

(PROJEKTU, UMĚLECKÉHO DÍLA, UMĚLECKÉHO VÝKONU)

Jméno a příjmení:	**Bc. Patrik Rohrer**
Osobní číslo:	**T14476**
Studijní program:	**N2808 Chemie a technologie materiálů**
Studijní obor:	**Inženýrství polymerů**
Forma studia:	**prezenční**
Téma práce:	**Vliv tepelných efektů na proces extruze termoplastických materiálů**

Zásady pro vypracování:

Vypracování rešerše v oblasti vytlačovacích hlav a dějů vyskytujících se v nich:
-úvod do procesu extruze
-přehled typů vytlačovacích hlav
-termodynamické procesy a teplotní vlastnosti polymerních a kovových materiálů
-simulace extruzního procesu a její význam pro extruzní procesy
Dále pak preliminární experimentální část zaměřená na korelaci simulovaných dějů uvnitř vytlačovací hlavy za pomocí programu Virtual Extrusion Laboratory 6.9 s reálným měřením ve vytlačovací hlavě.

Rozsah diplomové práce:

Rozsah příloh:

Forma zpracování diplomové práce: **tištěná/elektronická**

Seznam odborné literatury:

J. R. Wagner, E. M. Mount, H. F. Giles: Extrusion: the definitive processing guide and handbook
Ch. Abeykoon: Polymer extrusion: a study on thermal monitoring techniques and melting issues
W. Michaeli: Extrusion dies for plastics and rubber: design and engineering computations
T. Osswald, N. Rudolph: Polymer rheology: fundamentals and apllications
T. G. Mezger: Applied rheology

Vedoucí diplomové práce: **doc. Ing. Tomáš Sedláček, Ph.D.**
Centrum polymerních materiálů

Datum zadání diplomové práce: **15. ledna 2016**

Termín odevzdání diplomové práce: **16. května 2016**

Ve Zlíně dne 1. března 2016

doc. Ing. František Buňka, Ph.D.
děkan

UNIVERZITA TOMÁŠE BATI VE ZLÍNĚ
Fakulta technologická
L.S.

Ing. Lubomír Beníček, Ph.D.
ředitel ústavu

Příjmení a jméno: Patrik Rohrer

Obor: Polymerní materiály,
Specializace: Farmaceutické a medicínské mat.

PROHLÁŠENÍ

Prohlašuji, že

- beru na vědomí, že odevzdáním diplomové/bakalářské práce souhlasím se zveřejněním své práce podle zákona č. 111/1998 Sb. o vysokých školách a o změně a doplnění dalších zákonů (zákon o vysokých školách), ve znění pozdějších právních předpisů, bez ohledu na výsledek obhajoby [1];
- beru na vědomí, že diplomová/bakalářská práce bude uložena v elektronické podobě v univerzitním informačním systému dostupná k nahlédnutí, že jeden výtisk diplomové/bakalářské práce bude uložen na příslušném ústavu Fakulty technologické UTB ve Zlíně a jeden výtisk bude uložen u vedoucího práce;
- byl/a jsem seznámen/a s tím, že na moji diplomovou/bakalářskou práci se plně vztahuje zákon č. 121/2000 Sb. o právu autorském, o právech souvisejících s právem autorským a o změně některých zákonů (autorský zákon) ve znění pozdějších právních předpisů, zejm. § 35 odst. 3 [2];
- beru na vědomí, že podle § 60 [3] odst. 1 autorského zákona má UTB ve Zlíně právo na uzavření licenční smlouvy o užití školního díla v rozsahu § 12 odst. 4 autorského zákona;
- beru na vědomí, že podle § 60 [3] odst. 2 a 3 mohu užít své dílo – diplomovou/bakalářskou práci nebo poskytnout licenci k jejímu využití jen s předchozím písemným souhlasem Univerzity Tomáše Bati ve Zlíně, která je oprávněna v takovém případě ode mne požadovat přiměřený příspěvek na úhradu nákladů, které byly Univerzitou Tomáše Bati ve Zlíně na vytvoření díla vynaloženy (až do jejich skutečné výše);
- beru na vědomí, že pokud bylo k vypracování diplomové/bakalářské práce využito softwaru poskytnutého Univerzitou Tomáše Bati ve Zlíně nebo jinými subjekty pouze ke studijním a výzkumným účelům (tedy pouze k nekomerčnímu využití), nelze výsledky diplomové/bakalářské práce využít ke komerčním účelům;
- beru na vědomí, že pokud je výstupem diplomové/bakalářské práce jakýkoliv softwarový produkt, považují se za součást práce rovněž i zdrojové kódy, popř. soubory, ze kterých se projekt skládá. Neodevzdání této součásti může být důvodem k neobhájení práce.

Ve Zlíně 16.5.2016

.....

[1] zákon č. 111/1998 Sb. o vysokých školách a o změně a doplnění dalších zákonů (zákon o vysokých školách), ve znění pozdějších právních předpisů, § 47 Zveřejňování závěrečných prací:
(1) Vysoká škola nevýdělečně zveřejňuje disertační, diplomové, bakalářské a rigorózní práce, u kterých proběhla obhajoba, včetně posudků oponentů a výsledku obhajoby prostřednictvím databáze kvalifikačních prací, kterou spravuje. Způsob zveřejnění stanoví vnitřní předpis vysoké školy.
(2) Disertační, diplomové, bakalářské a rigorózní práce odevzdané uchazečem k obhajobě musí být též nejméně pět pracovních dnů před konáním obhajoby zveřejněny k nahlížení veřejnosti v místě určeném vnitřním předpisem vysoké školy nebo není-li tak určeno, v místě pracoviště vysoké školy, kde se má konat obhajoba práce. Každý si může ze zveřejněné práce pořizovat na své náklady výpisy, opisy nebo rozmnoženiny.
(3) Platí, že odevzdáním práce autor souhlasí se zveřejněním své práce podle tohoto zákona, bez ohledu na výsledek obhajoby.
[2] zákon č. 121/2000 Sb. o právu autorském, o právech souvisejících s právem autorským a o změně některých zákonů (autorský zákon) ve znění pozdějších právních předpisů, § 35 odst. 3:
(3) Do práva autorského také nezasahuje škola nebo školské či vzdělávací zařízení, užije-li nikoli za účelem přímého nebo nepřímého hospodářského nebo obchodního prospěchu k výuce nebo k vlastní potřebě dílo vytvořené žákem nebo studentem ke splnění školních nebo studijních povinností vyplývajících z jeho právního vztahu ke škole nebo školskému či vzdělávacího zařízení (školní dílo).
[3] zákon č. 121/2000 Sb. o právu autorském, o právech souvisejících s právem autorským a o změně některých zákonů (autorský zákon) ve znění pozdějších právních předpisů, § 60 Školní dílo:
(1) Škola nebo školské či vzdělávací zařízení mají za obvyklých podmínek právo na uzavření licenční smlouvy o užití školního díla (§ 35 odst. 3). Odpírá-li autor takového díla udělit svolení bez vážného důvodu, mohou se tyto osoby domáhat nahrazení chybějícího projevu jeho vůle u soudu. Ustanovení § 35 odst. 3 zůstává nedotčeno.
(2) Není-li sjednáno jinak, může autor školního díla své dílo užít či poskytnout jinému licenci, není-li to v rozporu s oprávněnými zájmy školy nebo školského či vzdělávacího zařízení.
(3) Škola nebo školské či vzdělávací zařízení jsou oprávněny požadovat, aby jim autor školního díla z výdělku jím dosaženého v souvislosti s užitím díla či poskytnutím licence podle odstavce 2 přiměřeně přispěl na úhradu nákladů, které na vytvoření díla vynaložily, a to podle okolností až do jejich skutečné výše; přitom se přihlédne k výši výdělku dosaženého školou nebo školským či vzdělávacím zařízením z užití školního díla podle odstavce 1.

Abstrakt

Stabilita toku taveniny je důležitou podmínkou pro dlouhodobou a bezproblémovou produkci během procesu vytlačování. Zmíněná stabilita toku je závislá jak na materiálových vlastnostech (teplota, tlak) ovlivněných procesními podmínkami, tak i na použitých technologických parametrech, jako je design extruzních nástrojů (šnek, hlava). V místech zúžení geometrie či hlavách obsahujících trn je výrazně spotřebováván tlak. Přítomná mechanická energie je pak pomocí disipace přeměněna na tepelnou, což může způsobit nestabilní tok taveniny. Pro pochopení těchto jevů uvnitř vytlačovacích hlav jsou často používány simulace extruzních procesů.

Úvod diplomové práce je věnován teoretickému popisu extruzního procesu a designu zpracovatelských nástrojů. Za účelem pochopení chování zpracovatelských materiálů v průběhu extruzního procesu nestačí pouze znalost procesu a extruzních nástrojů, ale i osvojení reologického a tepelného chování polymerních tavenin. Závěr teoretické rešerše je věnován matematickému popisu zmíněných jevů pomocí metody konečných sítí.

Experimentální výzkum v předkládané práci je zaměřen na pochopení tepelných jevů vytlačovacích hlav. Za tímto účelem byl tok taveniny danou geometrií simulován 2D a 3D modulem programu Virtual Extrusion Laboratory™ 6. 9. Simulace je následně ověřena reálným měřením teplotního spádu zvolené vytlačovací hlavy pomocí infračervených detektorů a termočlánku. Měření teploty taveniny uvnitř vytlačovací hlavy pomocí infračervených senzorů je inovativním a rozvíjejícím se nástrojem v online-monitoringu vytlačovacích procesů.

Výsledkem práce je návrh nové okrajové podmínky usnadňující a zpřesňující výpočet simulací vytlačovacích hlav s trnem.

Klíčová slova:

Extruze, vytlačovací hlava, trn, disipace, simulace, metoda konečných sítí

Abstract

For smooth, long term production is necessary to have steady polymer melt flow. Stability of the polymer melt flow is depended on few parameters, such as material properties (temperature, pressure) controlled by process conditions, and technology parameters as a design of the extrusion tools (screw, extrusion die). Pressure is consumed in places where dimensions of the geometry are decreased. Mechanical energy is present and due to the dissipation mechanical energy is transferred into the thermal energy. It may have influence on the quality of the final product or flow instabilities. Simulation of the extrusion process are often used for better understanding.

Introduction of diploma thesis belongs to the theoretical background of the extrusion process and design of the extrusion tools. Knowledge of extrusion processes and tools is not enough for material behavior understanding. Rheological and thermal behavior of the polymer melt is also important to know. Mathematical description of mentioned influences with help of finite difference method is shown at the end of theoretical background.

Experimental research is aimed on understanding of thermal effects in the extrusion dies. Polymer melt flow was simulated with help of 2D and 3D module in program Virtual Extrusion Laboratory™ 6. 9. For verification of simulation results real measuring of the temperature drop was made by infrared probe devices and thermocouple. Measuring of the temperature gradient by infrared probe devices is innovative and modern way in the online-monitoring of the extrusion process.

The main contribution of submitted thesis is developing of the new boundary condition. This condition makes current module calculations in Virtual Extrusion Laboratory™ 6. 9. faster and simpler. Mainly because during calculation mandrel will not be present.

Keywords:

Extrusion, extrusion die, mandrel, dissipation, simulation, finite difference method

Acknowledgements

I would like to express my heartfelt gratitude to all people which they have supported me and have made my study much easier.

My gratitude belongs to my whole family, mainly to my parents, grandparents and to my sister for their support and endless love.

I would like to thank to my supervisor Assoc. Prof. Tomas Sedlacek, PhD., who was personal guide during my study and he has always showed me the way.

Especially I am thankful to the company Compuplast International® a. s. Mainly to my second supervisor Jiri Svabik, PhD. for his infinite supporting, kindness, suggestions, his patience during teaching me, and mainly for his valuable time. This thesis was made mainly because of him.

The last but not least gratitude is for all my friends which I met at TBU and with whom I enjoyed a lot of parties (Blok 12). Without them it would not be such a funny and memorable journey.

In the end I would like to thank to all lifeless things and passions which they were surrounded me, my work and my life is because of them awesome. Namely it is a music, fashion and my old trustworthy laptop Lenovo Y570 which it was with me all 5 years of my study without any obstacles.

I hereby declare that the print version of my Master thesis and the electronic version of my thesis deposited in the IS/STAG system are identical.

"Everything is theoretically impossible, until it is done."

Robert A. Heinlein

Content-Theoretical Background

INTRODUCTION **12**
1. EXTRUSION PROCESS **14**
1.1 INTRODUCTION **14**
1.2 PRETREATMENT AND CONDITIONING OF POLYMER RESIN **15**
1.3 EXTRUSION **17**
1.4 FINAL TREATMENT **21**
2. EXTRUSION DIES **22**
2.1 INTRODUCTION **22**
2.2 TYPES OF EXTRUSION DIES **23**
2.2.1 SHEETING DIES 23
2.2.2 TUBULAR DIES 25
2.2.3 PROFILE DIES 26
2.3 DESIGN OF EXTRUSION DIE **27**
3. PROPERTIES OF THE POLYMER MATERIALS **29**
3.1 INTRODUCTION **29**
3.2 RHEOLOGY OF THE POLYMER MATERIALS **29**
3.2.1 SHEAR FLOW 33
3.2.2 ELONGATION FLOW 39
3.3 THERMAL PROPERTIES OF THE POLYMER MATERIALS **41**
3.3.1 FIRST LAW OF THERMODYNAMIC 41
3.3.2 THE ENERGY BALANCE EQUATION 43
4. SIMULATION OF THE EXTRUSION PROCESS **47**
4.1 INITIAL AND BOUNDARY CONDITIONS **47**
4.1.1 THE BOUNDARY CONDITION OF THE FIRST KIND (DIRICHLET CONDITION) 48
4.1.2 THE BOUNDARY CONDITION OF THE SECOND KIND (NEUMANN CONDITION) 48
4.1.3 THE BOUNDARY CONDITION OF THE THIRD KIND (FOURIER CONDITION) 49
4.1.4 THE BOUNDARY CONDITION OF THE FOURTH KIND 49
4.2 FINITE DIFFERENCE METHOD **50**
4.2.1 TAYLOR SERIES EXPANSION 51

Content-Experimental Research

5. MOTIVATION AND AIMS OF THE THESIS 56
5.1 MOTIVATION 56
5.2 AIM OF THE MASTER THESIS 57
6. MATERIALS AND GEOMETRY 58
6.1 MATERIAL 58
6.1.1 RHEOLOGY CHARACTERIZATIONS 59
6.1.2 MELT DENSITY 62
6.1.3 MELT THERMAL CONDUCTIVITY 63
6.1.4 HEAT CAPACITY 64
6.2 GEOMETRY 64
7. EXTRUSION PROCESS SIMULATION 67
7.1 INTRODUCTION 67
7.2 3D FLOW DOMAIN 74
7.3 2D FLOW DOMAIN 79
7.3.1 THE ISOTHERMAL CASE OF THE 2D SIMULATION 79
7.3.2 THE ADIABATIC CASE OF THE 2D SIMULATION 82
7.3.3 THE DEVELOPED NEW BOUNDARY CONDITION FOR THE 2D SIMULATION 86
8. REAL EXTRUSION PROCESS 91
8.1 EXTRUDER 91
8.2 EXTRUSION DIE 92
8.3 MEASURING TOOLS 92
8.3.1 INFRARED PROBE DEVICES 93
8.3.2 THERMOCOUPLE WIRE 94
8.3.3 PRESSURE TRANSDUCERS 94
8.4 EXTRUSION PROCESS PARAMETERS 95
8.5 TEMPERATURE AND PRESSURE MEASURING 95
9. RESULTS COMPARISON 98
CONCLUSION 101
REFERENCES 103
LIST OF ABBREVIATIONS 107
LIST OF FIGURES 112
LIST OF TABLES 115

Introduction

Theoretical simulations of extrusion process, predecessor of the computer simulations, were started in 1953 by Carley, Gore, Strub, Jepson, Mallouk and McKelvey in Industrial & Engineering Chemistry magazine. (Carley et al., 1953, Carley and McKelvey, 1953, Carley and Strub, 1953b, Carley and Strub, 1953a, Gore, 1953, Jepson, 1953, Mallouk and McKelvey, 1953, McKelvey, 1953) Few years later the first melting theory was published by Tadmor in 1966 which is one of the most significant theory in polymer science. (Tadmor and Gogos, 2006) *Computer-aided-design* (CAD) is considered as a beginning of the computer simulations and it was developed by Western Electric Engineering Research Centre team in late 1960s and further development of computer simulations still continue. (Patterson, 1968)

Traditional trial-and-error methods are domain of many engineers in field of polymer processing. Computer simulations should be used for extrusion process to avoid errors during extrusion process. Simulation is basically combination of a mathematical model and a numerical method. Creating of the good simulation model is not simple, it requires complex knowledge of material properties and behavior, transport and thermodynamic properties, etc. Nevertheless, simulation is only theoretical and verification of the results with the real process is desirable. For verification it is possible to use different kind of measuring tools, e. g. infrared probe devices and thermocouples when temperature gradient is required.

The submitted thesis is focused on better understanding of thermal effects of the mandrel inside the extrusion die. In cases when mandrel is not big enough for transferring of heat out by convection and conduction transport, overheating is present. This overheating can have crucial effect on the polymer melt flow behaving (such as viscosity). For this purpose, measuring tools as infrared probe devices, thermocouple and pressure sensors are used for a comparison between the developed new boundary condition in software Virtual Extrusion Laboratory^{TM} 6. 9. and real extrusion process measurement.

Theoretical Background

1

Extrusion Process

1.1 Introduction

The basic explanation of extrusion process could be that extrusion is a technology operation where polymer resin is fed into the feed throat, then this polymer resin is melted inside the extruder and after melting the polymer melt is transported or continuously extruded through the extrusion die into a free space. It is possible to imagine this process as squeezing of toothpaste out of tube, mechanical energy is given and toothpaste is extruded.

The shape of plastic products is given by the shape of the extrusion die. Already shaped polymer extrudate is then cooled by water, air or cold surface.

The last part of extrusion is a puller machine which regulates and controls the dimensions of plastic products and also collects the final product. All these steps are part of extrusion process. Different extrusion lines are occurred according to the difficulty of extrusion process. (Rauwendaal, 2014)

Extrusion process is classified by more steps as it is shown in figure 1. Each of these steps is mutually important for the final products. Influence of each steps will be discussed

below. For better clarity, this chapter will be divided to more subheads, namely Pretreatment and Conditioning of Polymer Resin, Extrusion and Final Treatment.

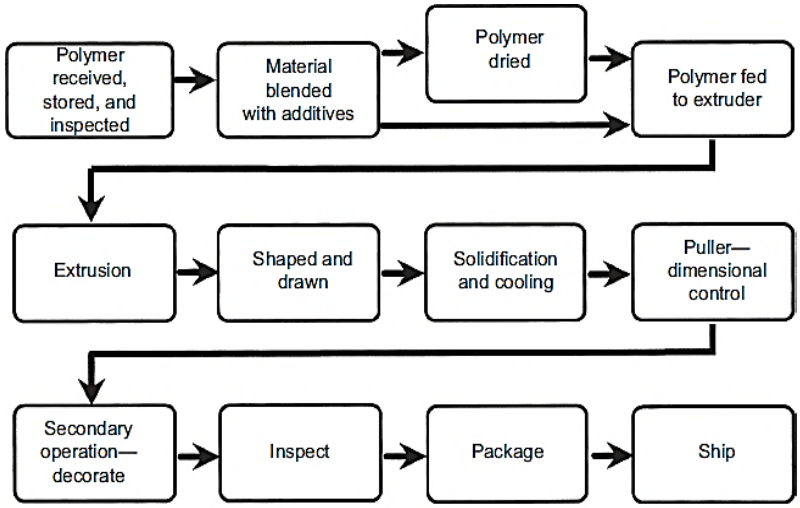

Figure 1: Schematic of a basic extrusion process (Giles et al., 2005)

1.2 Pretreatment and Conditioning of Polymer Resin

Extrusion process, respectively pretreatment and conditioning, starts already when raw materials are received by processing company. Incoming polymer resin can be imported in many forms such as bags, fiber packs, containers, bulk packs, hopper trucks or rail wagons. Received polymer resin is then stored in warehouses without environmental controls (lack of heat or cooling). Polymer resin should be brought to the room temperature before processing. If polymer resin is not brought to the room temperature, instabilities can be achieved. Many properties of polymer resin such as the polymer melting point or the polymer softening point are varying with temperature of pellets.

Another step is blending and mixing of raw material with additives. The problem is that the most of materials are in different states of forms (powder, liquid, pellets, flakes, fibers, etc.). Liquids can be, for example, fed to the feed throat through the feed pump. For materials in a solid state there are two possible ways how to prepare final blend before the extrusion process. The first variant is to use gravimetric feeders. In this way of feeding more feed throats for different materials and additives are necessary to be used. Using of multiple feeders is probably the best method to ensure a repeatable, homogenous distribution of polymer resin and additives together. Gravimetric feeders have few disadvantages. Such as taking up a lot of space and also not every form and state of additives are possible to be fed by gravimetric feeders. Another alternative is to mix and blend all the material components in

mixers. Mixers can possess low or high intensity. In case of high intensity mixers there is serious disadvantage. This disadvantage is obtained during the mixing where a significant amount of heat is generated. So care must be given not to initial melting by the mixers. (Giles et al., 2005)

The third step which has to be done for some specific kinds of polymers before extrusion process is drying. There are two major kinds of polymers, the first is hydroscopic type of polymers with strong affinity for water, for moisture respectively. The second is non-hydroscopic type of polymers (polyethylene, polypropylene, polystyrene, polyvinyl chloride). Non-hydroscopic type of polymers does not need to be dried. Here only surface moisture is accumulated and for most of the operations it is not problem. In the case of hydroscopic polymers (nylon, polyester, polycarbonate, polyethylene terephthalate, polybutylene terephthalate, etc.) the moisture, respectively water molecules, is bonded by strong secondary bonds with functional groups of polymer. It means that water is not just on the surface of polymers but even in the structure of the polymer chains. The danger consists from depolymerization which is destroying polymer chains to shorter and mainly lower molecular weight polymer chains and it cause the final product defects (streaks, bubbles, burning, brittleness, holes). (Grellmann and Seidler, 2013) Here is a lot of types of driers which processor can use, final decision will always depend on properties of material and on the final product. There are for example hot air dryers, desiccant dryers (gold standard), compressed-air dryers, compressed-air micro dryers, infrared dryers or vacuum dryers. Neverless, every processor should set right time and temperature of drying (prevention of overdrying). (Freire et al., 2014)

Next step in the line of the process is feeding of polymer resin to the extruder. There are several types how an extruder can be fed (flood feed, starve feed, crammer and melt feed). Flood feeding is based on principles of gravity. It is the most common supplying device of polymer resin in polymer industry. The speed of feeding, respectively the throughput rate is proportional to the screw speed. (Chung, 2011) Totally different way of feeding is a starve feeding, most common in twin screw extrusion. Feed throats in case of starve feeding have own screw and every material or additive have own feed throat with specific screw speed. The speed of the screws in feed throats specifies the throughput rate. (Rauwendaal, 1991) Crammer feeding and melt feeding are less common ways of polymer resin supplying. Crammer feeding is used for materials with low bulk density, such as recycled flakes. Ma-

terial is pushed due to pressure into the extruder screw, Pressure is generated by the additional screw located in feed throat. Melt feeding is based on supplying of the polymer melt by another extruder directly to the main extruder screw. (Giles et al., 2005) Feeders described above are shown in figure 2.

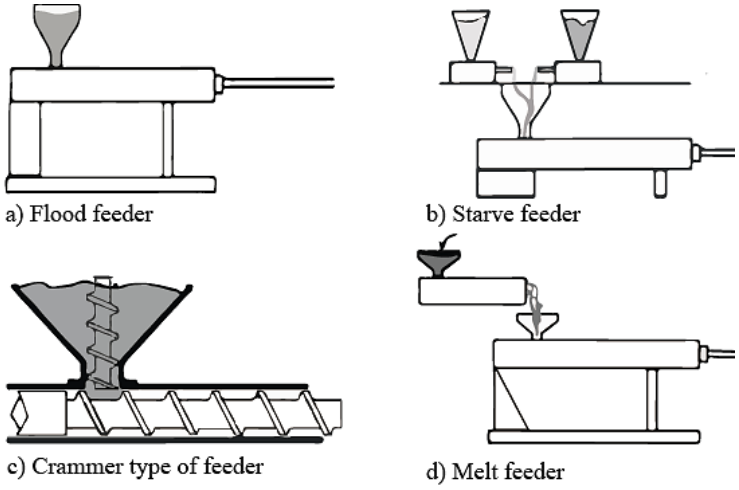

Figure 2: Classification of feeders for polymer materials

1.3 Extrusion

As it was written in the beginning of the chapter 1, extrusion process consists from melting and transporting/pushing of the polymer melt through extrusion die. Every single polymer resin has to go through this process in form of pellets, powder or flakes. For extrusion it is necessary to have extruder machine. There are basically two most commonly used types of extruder, single screw (single-flighted, multi-flighted) and multiscrew extruders. This thesis deals only with single screw extruders but the principles of melting are practically based on the same mechanism. Both of mentioned extruders, single and twin screws, are composed from three zones: Feed, compression and metering section as figure 3 shows. (Drury, 2009) In the next part of the thesis the sections will be discussed in details.

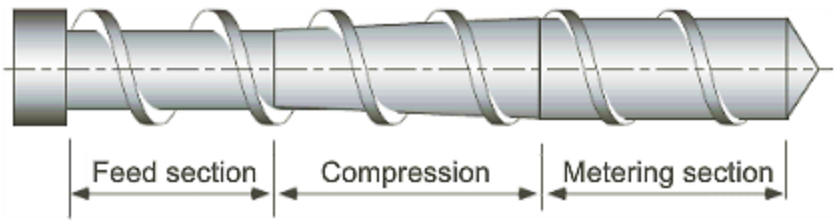

Figure 3: Basic screw zones of extruders (Rauwendaal, 2014)

The main purpose of feed section is mixing, preheating, compression of polymer pellets and mainly getting rid of the air capsules → creating of the solid bed. The barrel is stationary and the screw rotates. Due to this movement the polymer resin is transported to oncoming section. It is important to feed the extruder by required amount of polymer resin without fluctuations. This means that the amount of polymer resin has to be constantly same in every single moment of extrusion. As it is displayed on figure 3, feed section has the deepest channel cross section (depth). Air capsules are consisted between each pellet and volume is then much bigger. Already compressed solid bed is achieved. For successful transport it is important to achieve forward movement of material. To obtain good friction between barrel and polymer resin (reasonable increasing of pressure) and good compression, the barrel have to be cool down under the hopper. An opposite situation is between screw and polymer resin, here it is important to have as small friction as possible (polishing of screw). (Bralla, 2007)

Here it is assumption, the compacted bed of solid pellets flow down the screw channel as a plug. The balance of forces and torque determines the pressure build-up exerted and it is usually expressed in the form:

$$P = P_0 \times \exp(const. f_b - const. f_s) \times Z_b \quad (1)$$

where P_0 is the pressure under the feed throat (normally very small), f_b and f_s are the friction coefficients of the solid bed on the barrel and on the screw and Z_b is the down channel distance at barrel surface. For forward motion, as explained, f_b must be larger than f_s. (Compuplast, 2003)

The source of the heat is generated in the feeding section by friction and heat conduction from the barrel walls (temperature is rising downstream). When the polymer temperature is reached the melting point of crystalline polymer or the glass transition temperature of an amorphous polymer, a melt film forms at the barrel surface. (Manas and Vlcek, 2001) For homogenous melting during extrusion it is necessary to generate a shear force as well as downforce. In case of polymer extrusion these shear force and downforce are provided by decreasing depth of the channel depth. Due to decreasing of channel depth shearing of the polymer melt is generated which means generating of viscous heat (dissipation). These requirements for melting are possible to be imagine as the candle on the hot stove. If downforce is generated, the candle will start to melt. When shear force is generated as well as downforce, faster melting of the candle is occurred. Solid bed is melted mainly with help of viscous heat (dissipation) and particularly with help of heat conduction and friction heat.

Tadmor melting model (shown in figure 4) will be here used for describing of melting process in compression section. (Campbell and Spalding, 2013)

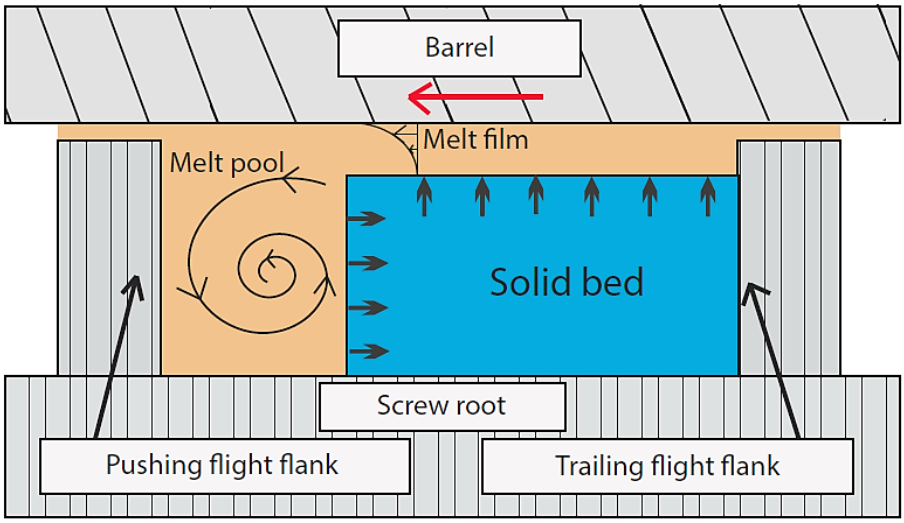

Figure 4: Tadmor melting model

Tadmor melting model from late of 1960s is displayed in figure 4. Assumption in Tadmor model is that the model takes the screw as a cylinder, there are no flanks. Velocity speed is then the highest at the upper wall. Nevertheless, the mechanism of Tadmor model is possible to express as: The solid bed is pushed against the leading flight of the screw as freshly melted polymer is wiped from the melt film into the melt pool by the relative motion between the solid bed and the barrel surface. The solid bed is decreasing its volume and volume of melt pool is increasing. Shear force and downforce are present. This reduction of solid bed has to be gradual otherwise it could create insulted film on the edges of solid bed and melting will not be successful. In extreme cases solid bed is destroyed and little parts of non-melted solid bed are present in melt pool. For effective extrusion, polymer has to be completely melted before the end of the extruder. This is mainly the task of the screw design and processing conditions. (Osswald and Menges, 2012, Stevens and Covas, 1995)

The last section is called a metering section or a melt pumping section. The melting should be already complete at this stage. The main task of this section is mixing and conveying of polymer melt toward to the end of the extruder. In relation to the purpose of the extruder screw the metering section can generate or consume pressure. According to pressure profiles we recognize conveying or mixing types of extruder screw. During extrusion both of flows are present, pressure flow and drag flow as well. Sum of drag flow and pressure flow are significant. This sum gives final flow profile. Pressure flow is characterized by the

forward movement. Drag flow is characterized that the polymer melt is pushed to the backward in the channel, it cause mixing effect. Both flows are shown in figure 5. (Cantor, 2006)

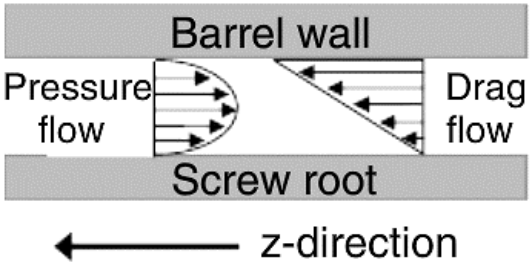

Figure 5: Drag downstream and pressure upstream side by side (Cantor, 2006)

Drag velocity profile at the end of the extrusion screw can be modified also by changing of the channel depth. At first for finding the balance between pressure and drag velocity profiles it is important to assume that friction coefficient is constant and Newtonian fluid is present. That is also reason why curves in figure 6 are linear lines. During real extrusion these curves are not so smoothed. Characteristic curves of the channel depth dependency of pressure are displayed in figure 6. This figure also shows that a restrictive extrusion die would clearly work most productive with a shallow channel screw. On the other hand, less restrictive die would offer the highest productivity with a deep channel screw. (Osswald and Menges, 2012)

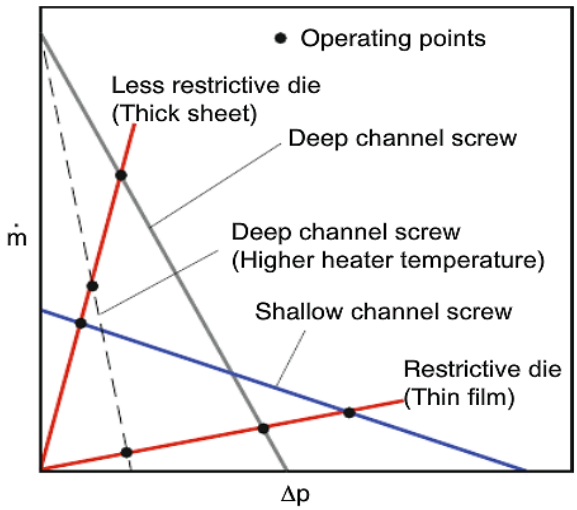

Figure 6: Screw characteristic curves (Newtonian fluid) (Osswald and Menges, 2012)

In the last section it is important to have dominant dissipation in the middle of the barrel. This means to have the highest velocity speed in the middle. In order to ensure the highest efficiency a compromise between all parameters in design of the screw has to be present. (Zatloukal, 2015)

1.4 Final Treatment

The last steps in extrusion process include shaping and drawing, solidification and cooling, pulling, secondary operations and finally inspection, packaging and shipping. When polymer melt is extruded through the extrusion die into the free space, it is called the extrudate. After the polymer (extrudate) leaves the extrusion die, its molecules, which were oriented in the die land area (direction of the melt flow), relax and re-entangle causing die swell. Die swell can be also occurred because of the stored energy of the polymer melt. For orientation of these polymer molecules and stabilization of the extrudate velocity profile it is essential to use a force. Force is provided by puller and then we talk about pulling force which orients molecules in the direction of the extrusion line. (Kutz, 2011) Extrudate is drawn down due to the puller machine and also shaped to the final product form. The speed of the puller machine is equal to the intensity of drawing down, it is called draw down ratio. Draw down ratio also says how polymer molecules are oriented. That is related with mechanical properties of the final product (better tensile and flexural properties in extrusion line direction rather than in transverse direction). (Pethrick et al., 2011) Mechanism of die swell and drawing down is shown in figure 7.

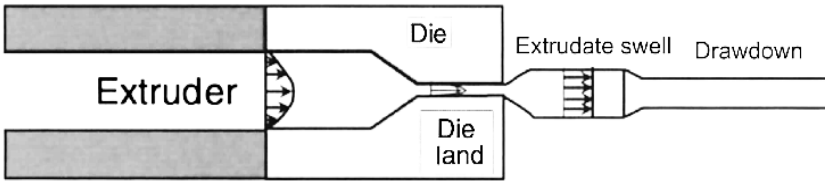

Figure 7: Die swell on exiting the extrusion die (Pethrick et al., 2011)

Cooling of the extrudate is located between the extrusion die and the puller. There are several types of cooling media, the most common are water, air or contact with cold surface. Cooling of materials depends on their thermal properties. However, it has to be always possible to cool down materials to the temperature bellow melting point (semicrystalline polymers) or glass transition temperature (amorphous polymers). Temperature of cooling is depended also on the production rate of an extrusion line and on degree of crystallinity which the processor wants. Shrinkage and warpage of the final product are possible to reduce by uniform cooling on all sides of the product. (Erhard, 2006, Giles et al., 2005, McCrum et al., 1997)

At the end there is an inspection, packaging, shipping and secondary operations such as cutting, drilling, punching holes, corona, flame treatment, decorating. (Giles et al., 2005)

2

Extrusion Dies

2.1 Introduction

This chapter will be focused only on extrusion dies for thermoplastic materials. The two major components of the extrusion dies are the extrusion die itself and the breaker plate. The breaker plate is formed by a plate and sieves with many holes. These sieves are a cleaner between the screw and the extrusion die. The main purpose of the breaker plate is to provide homogenous melt flow without any impurities from the extrusion screw to the extrusion die.

Also rheological and thermodynamic processes in the extrusion die must be taken into account. For example, these thermodynamic and rheological processes can have significant influence on the actual distribution of the polymer melt, mainly flow properties of material, the flow rate through the extrusion die and temperature profile.

Pulsation-free, thermally and mechanically homogenous melt stream with sufficient distribution is required to flow through the extrusion die. When all these required properties are respected, the extrusion die can ensure uniform velocity of the melt flow. When uniform velocity is present then with help of the calibration unit it is possible to produce stabilize dimensions of the semi-finished products.

Due to extrusion die design failures, the flow instabilities can be presented and these instabilities can make the product to become unacceptable. Some of these instabilities could be the channeling, shark skin, die drool, the extrudate swell, die fracture or for blown film extrusion draw resonance. (Kostic and G., 2006, Michaeli, 2004, Osswald and Menges, 2012, Rauwendaal, 2014)

2.2 Types of Extrusion Dies

The extrusion dies are possible can be categorized according to several rules but the most common classification is according to the shape of the extrusion die (figure 8). More information about each type of the extrusion die will be described below.

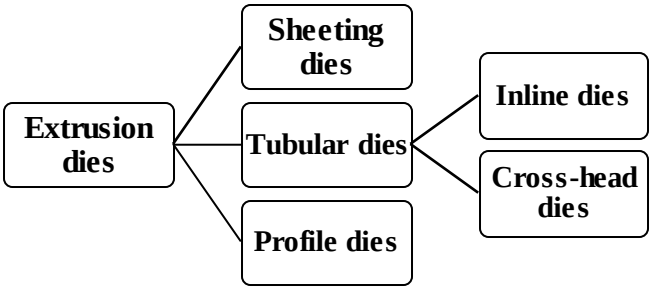

Figure 8: Distribution of extrusion dies

2.2.1 Sheeting Dies

Due to the sheeting dies we can produce films (<0.5 mm) or flat sheets (>0.5 mm), which can be just several microns thick and up to several meters wide. Product requirements are mainly constant thickness and free of surface defects. Uniform flow distribution across the width of the die is desirable to keep. There are two commonly used techniques for minimization of thickness variations. The first technique is to use the flex lip adjustment with a lot of the bolts along the whole width (e. g. led by piezoelectric sensors react on the pressure, hydraulically controlled). An alternative solution with the same mechanism is using of the choker bar. These techniques are based on the regulation of channel depth. Another solution could be also using of local heaters or coolers which affect temperature, respectively viscosity of polymer flow. The flex lip, the choker bar and pressure distribution in die channel are shown in figure 9. (Rauwendaal, 2014)

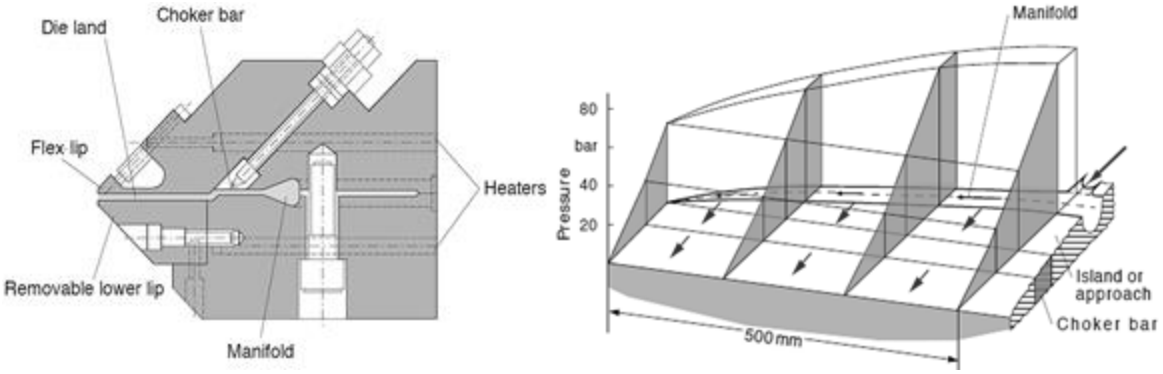

Figure 9: Cross section and pressure distribution of the coat-hanger die (Osswald and Menges, 2012)

There are three most common types of sheeting dies: the T-shape die, the fishtail die and the coat-hanger die (shown in figure 10). The first most common type of sheeting die is the T-shape die. It is mainly used for extrusion coating. The geometry of a T-shape flat die is easy to be machined. The polymer flow rate is not constant in the channel and that is the reason why T-shape extrusiom die is not appropriate for thermal unstable, high viscosity materials.

The fishtail sheeting die has already better polymer flow rate uniformity but still it is not an optimum. The best polymer flow rate distribution with streamlined flow and gradual leakage can be probably reached by the coat-hanger type of die, commonly used for sheet extrusions. The geometry of the flow channel is more difficult to machine in comparison with the previous two types. (Michaeli, 2004)

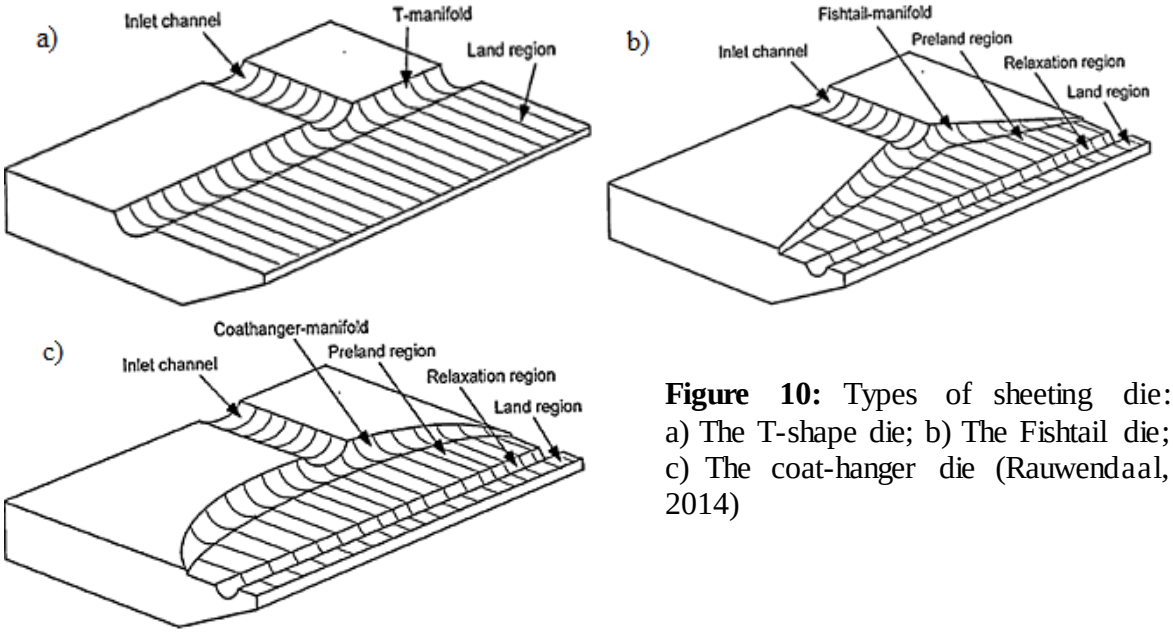

Figure 10: Types of sheeting die: a) The T-shape die; b) The Fishtail die; c) The coat-hanger die (Rauwendaal, 2014)

2.2.2 Tubular Dies

Tubular dies are used for manufacturing of tubes (< 10 mm), pipes (>10 mm) and tubular films (blown process). The melt leaves the tubular die through an annulus, this annular product can be then extruded on inline or cross-head dies. Examples of these dies are shown in figure 11. Another way how tubular dies can be categorized is according to the applications. We recognize the spider dies, the slide fed dies, the spiral mandrel dies and the flat spiral dies.

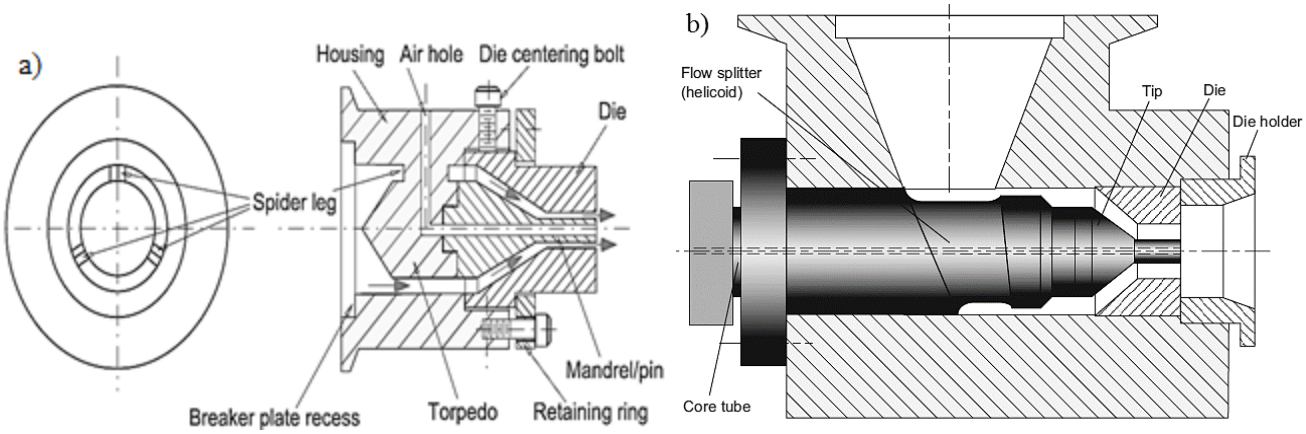

Figure 11: Examples of a) in-line die; b) cross-head die (Rauwendaal, 2014)

The easiest tubular die is a spider die. The spider die consists from the axisymmetric mandrel which is fixed to the other body through legs (3 or more). The polymer melt has to flow around these legs and the weld lines are then made. The weld lines, representing the weakest area of the product, are created when entangled polymer statistical coils have to break own bonds and then recreate those entangled bonds between the statistical coils. The time necessary for entangling is called a healing time. Healing time can be modified, on one hand increased by the temperature, on the other hand decreased by the molecular weight of the material. Another modification can be occurred by the pressure or the time.

The weld lines are practically unavoidable for this type of the die. But in case of the weld lines should be trend to minimize them in every product. Examples how to try to minimize the weld lines are shown in figure 12. The polymer melt has to have healing time to make new entanglements after melt flows along those legs.

Problems with weld lines are particularly solved by the spiral dies often used for extrusion of films in blown process. (Kostic and G., 2006, Michaeli, 2004, Osswald and Menges, 2012, Rauwendaal, 2014)

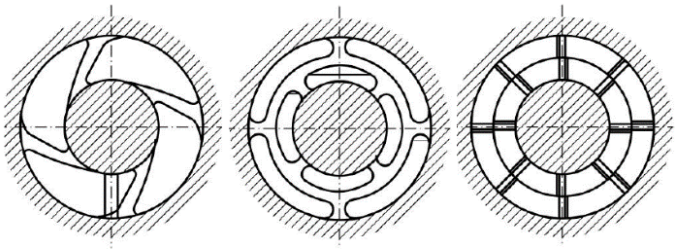

Figure 12: Examples how to avoid weld lines (Michaeli, 2004)

2.2.3 Profile Dies

Besides films, sheets, pipes or tubes there are many other difficult product shapes. For this complex types of products, the profile dies are used. The extrusion of profile products became one of the most difficult type of extrusion. Mainly because it is difficult to predict the required geometry for the flow channel and which dimensions will product achieve. Simulation software has to be used. (Figure 13)

According to the wall thickness we have profiles with relatively thin walls (easy for modeling using simplified techniques) and profiles with relatively thick walls (difficult, 3D modeling with 3D flow effects included). In case of profiles with different wall thickness one big problem arise. The most volume of the material wants to flow preferably through more thick walls (high speed of the melt) and until then through thin walls (lower speed of the melt). Thus pressure resistance is not linear and material flows through the path of the least resistance. It can be described by equation 2:

$$\dot{Q} = S \times v \tag{2}$$

Where $\dot{Q}$ is polymer flow rate, S represents channel area and v is speed of the melt. Variables as the polymer flow rate, stress rate, viscosity, etc. can be affected by varying in thickness. In equation 2 the variation in thickness is represented as an area. Instabilities, as an undulation of the extrudate profile, can be caused then by the different polymer flow rates. Troubleshooting is based on the linear resistance at the end of the extrusion die. (Kostic and G., 2006, Osswald and Menges, 2012, Rauwendaal, 2014, Zatloukal, 2015)

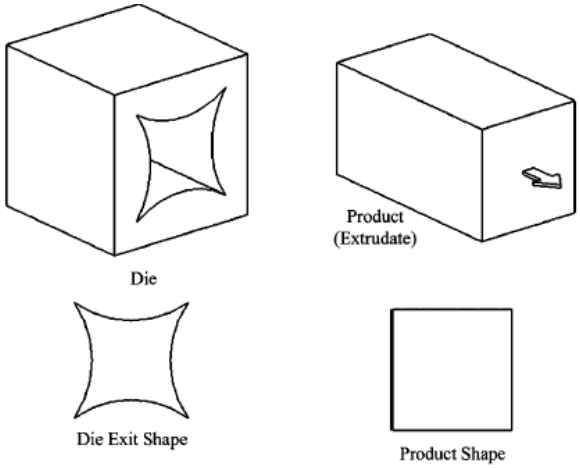

Figure 13: Difficulty of profile die designs (Kostic and G., 2006)

2.3 Design of Extrusion Die

According to the Michaeli´s diagram (Appendix 1), there is seven section of designing of the extrusion dies. They are based on few input information such as: the geometry of the product to be extruded (e.g. pipes, flats, films, profiles), type of extrusion die which processor should use (angles, longitudinal, transverse, single/multi extrusion die), materials and combination of materials, rheological and thermodynamic behavior of materials, throughput and temperature inside the die.

After solving input information of the Michaeli´s diagram requirements it continues to the second section. The second section is aimed on selection, calculation and design of the flow channel (pressure drop and geometry of the flow channel). As well rough idea of the tempering system of the extrusion die is mentioned in section two.

In section three the basic dimensions of extrusion die are established, such as types and placing of the bolts or types of materials according to strengthens of the die body. Last four steps of the Michaeli´s diagram are about feasibility, manufacturing aspects, calculations of tempering system, precise design and dimensions of the die until the die acceptance. (Michaeli, 2004)

In summary for designing of extrusion dies here are some specific general rules:

- Reasonable pressure drop for single screw extrusion is 5 MPa < p < 20 MPa. The lowest value 5 MPa is due to the sensible polymer melt flow speed, suppression of degradation. On the other hand, value 20 MPa is limited mainly because of energy saving during extrusion process. Relevant pressure is expressed:

$$\Delta T = \frac{\Delta p}{\rho \times C_p} \tag{3}$$

Where ΔT is temperature difference between temperature at the wall and in the middle caused by dissipation, Δp is pressure loss, ρ and C_p are density and specific heat capacity, respectively.

- The temperature of the melt increases beyond the set values on the die wall due to viscous dissipation. Designer must examine these places for potential hot spots, which should always be avoided → steady velocity profile across the entire die exit is required
- No dead spots in the flow channel, minimization of residence times which they cause degradation of materials
- Easy assembly and disassembly of extrusion die and cleaning
- Shear stress at the walls in area of 30 kPa – 140 kPa
- The count of the weld lines must be the lowest as possible with optimal orientation
- Functionality for more materials (Kostic and G., 2006, Michaeli, 2004, Zatloukal, 2015)

3

Properties of the Polymer Materials

3.1 Introduction

For understanding of the extrusion process it is not important to know just the extrusion tools, but also the properties of the polymer melt. This chapter is focused on the main rheological and thermal properties. Rheological properties show the behavior of the materials when stress is applied. On the other hand, thermal properties show the thermal dependence of polymer melt. These properties are discussed below.

3.2 Rheology of the Polymer Materials

Rheology as a field of the science is focused on flow and deformation of matter after applied force with time. From the perspective of very long time even glass can flow. Martin Reiner expressed this with help of bible "Mountains flowed before the Lord". The variable which determines how much the matter flows is so called Deborah number:

$$De = \frac{\lambda}{\theta} \tag{4}$$

Here λ is relaxation time and θ is observation time. Each material has different Deborah number. The water, for example, has $\lambda = 10^{-12}$ s and the De is then approaching zero value. The glass has λ = 100 years and then De is getting large (practically to infinity). Polymer materials have λ between liquids and solids and then we can observe them behaving as it would be both states of matter, it is called viscoelastic behaving. Such a behavior can be approximated by simple Maxwell fluid model, which combines the simplest fluid model (Newtonian model) and the simplest solid model (Hookean model):

$$\dot{\gamma} = \dot{\gamma}_{fluid} + \dot{\gamma}_{solid} \tag{5}$$

$$\dot{\gamma} = \frac{\tau}{\mu} + \frac{\dot{\tau}}{G} \tag{6}$$

$$\tau + \frac{\mu}{G} \times \dot{\tau} = \mu \times \dot{\gamma} \tag{7}$$

Then $\frac{\mu}{G}$ is replaced by relaxation time λ and we got Maxwell fluid model:

$$\tau + \lambda \times \dot{\tau} = \mu \times \dot{\gamma} \tag{8}$$

Where τ is stress tensor, $\dot{\tau}$ can be determined as $\frac{d\tau}{dt}$, μ is material coefficient and $\dot{\gamma}$ is shear rate possible determined as $\dot{\gamma} = \frac{dv_x}{dy}$.

In many flow situations we can recognize two simple types of flow, the shear flow and the elongation flow. In both cases the deformation rate may be dependent or independent of time. For example, when steady flow is present, the flow is time independent, the deformation rate is constant in time. In case of transient flow, the deformation rate is time dependent. When we assume for a while that the polymer in molten state is a system of elements (molecules, chains), then we can imagine these two flows as being composed from two different systems with different responses and different relative motion of their elements. The shear flow represents the forward motion of elements having the same or different velocity, while the elongation flow is a motion of elements toward each other or away from each other.

It is useful here to describe the particular stress and deformation components in Cartesian coordinates (Figure 14).

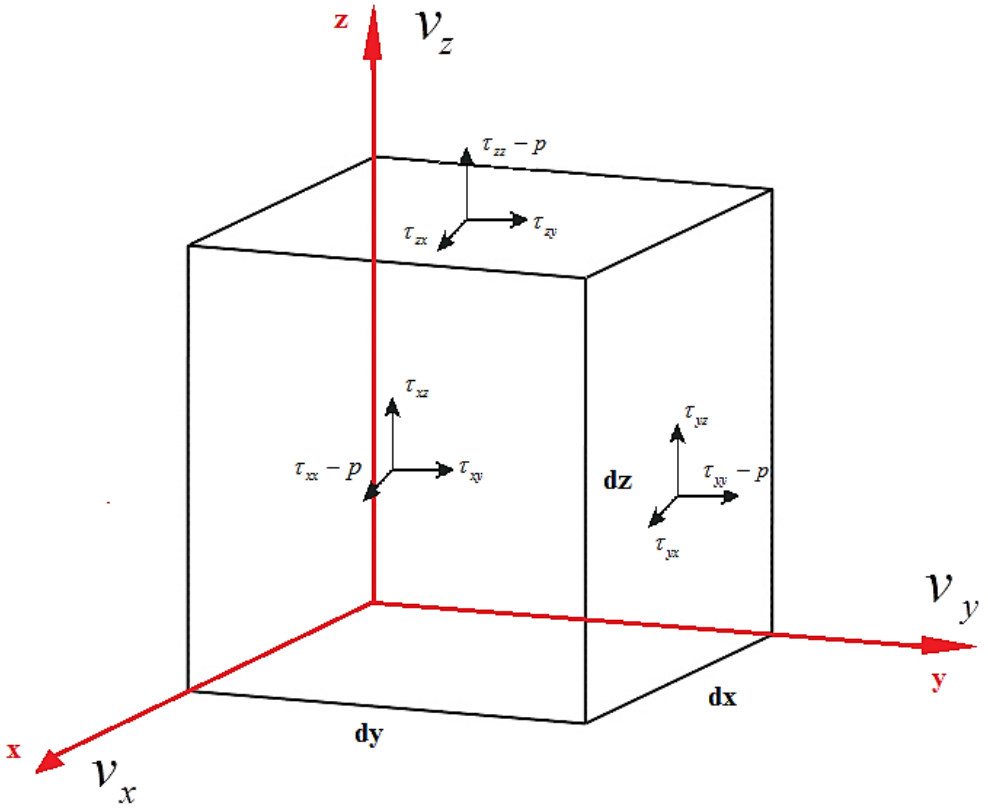

Figure 14: Divided flow system into Cartesian coordinates

The force causing the stress on a reference, infinitesimal cube can be acting in any direction but we can express its influence in the Cartesian three direction. As such the force acts on particular Cartesian planes – in the particular Cartesian directions. In total of nine stresses, three of which are the normal stresses and six are the shear stresses.

Using these parameters, we can analyze flow behavior inside the matter. This behavior is monitored with the help of the total rate of the deformation tensor D_{ij} (general form):

$$2 \times D_{ij} = \begin{bmatrix} 2\frac{\partial v_x}{\partial x} & \frac{\partial v_y}{\partial x} + \frac{\partial v_x}{\partial y} & \frac{\partial v_z}{\partial x} + \frac{\partial v_x}{\partial z} \\ \frac{\partial v_x}{\partial y} + \frac{\partial v_y}{\partial x} & 2\frac{\partial v_y}{\partial y} & \frac{\partial v_z}{\partial y} + \frac{\partial v_y}{\partial z} \\ \frac{\partial v_x}{\partial z} + \frac{\partial v_z}{\partial x} & \frac{\partial v_y}{\partial z} + \frac{\partial v_z}{\partial y} & 2\frac{\partial v_z}{\partial z} \end{bmatrix} \tag{9}$$

The total rate of the deformation comes from velocity gradient tensor L:

$$L_{ij}(t) = \frac{\partial v_i(x,t)}{\partial x_j} \tag{10}$$

Velocity gradient tensor can be decomposed into symmetric (d) and asymmetric parts (ω), where symmetric part is responsible for shearing and asymmetric part for rotation:

$$L = d + \omega \tag{11}$$

Symmetric part is then expressed as:

$$d_{ij} = \frac{1}{2} \times (\frac{\partial v_i}{\partial x_j} + \frac{\partial v_j}{\partial x_i}) \tag{12}$$

And asymmetric part as:

$$\omega_{ij} = \frac{1}{2} \times (\frac{\partial v_i}{\partial x_j} - \frac{\partial v_j}{\partial x_i}) \tag{13}$$

With knowledge of these equations the total rate of the deformation can be written as:

$$D_{ij} = \begin{bmatrix} \frac{\partial v_x}{\partial x} & 0 & 0 \\ 0 & \frac{\partial v_y}{\partial y} & 0 \\ 0 & 0 & \frac{\partial v_z}{\partial z} \end{bmatrix} + \begin{bmatrix} 0 & \frac{1}{2} \times (\frac{\partial v_x}{\partial y} + \frac{\partial v_y}{\partial x}) & \frac{1}{2} \times (\frac{\partial v_x}{\partial z} + \frac{\partial v_z}{\partial x}) \\ \frac{1}{2} \times (\frac{\partial v_x}{\partial y} + \frac{\partial v_y}{\partial x}) & 0 & \frac{1}{2} \times (\frac{\partial v_y}{\partial z} + \frac{\partial v_z}{\partial y}) \\ \frac{1}{2} \times (\frac{\partial v_x}{\partial z} + \frac{\partial v_z}{\partial x}) & \frac{1}{2} \times (\frac{\partial v_y}{\partial z} + \frac{\partial v_z}{\partial y}) & 0 \end{bmatrix} + \tag{14}$$

$$+ \begin{bmatrix} 0 & \frac{1}{2} \times (\frac{\partial v_x}{\partial y} - \frac{\partial v_y}{\partial x}) & \frac{1}{2} \times (\frac{\partial v_x}{\partial z} - \frac{\partial v_z}{\partial x}) \\ -\frac{1}{2} \times (\frac{\partial v_x}{\partial y} - \frac{\partial v_y}{\partial x}) & 0 & \frac{1}{2} \times (\frac{\partial v_y}{\partial z} - \frac{\partial v_z}{\partial y}) \\ -\frac{1}{2} \times (\frac{\partial v_x}{\partial z} + \frac{\partial v_z}{\partial x}) & -\frac{1}{2} \times (\frac{\partial v_y}{\partial z} + \frac{\partial v_z}{\partial y}) & 0 \end{bmatrix}$$

Where each matrix represents specific motion. The first matrix represents stretching, the second matrix shearing and the last matrix represents rotation. As the rotational part does not cause any flow deformation, it is usually omitted.

Another useful variable monitoring the flow behaving inside the matter is the stress tensor τ_{ij} which is in general form expressed as:

$$\tau_{ij} = \begin{bmatrix} \tau_{xx} - p & \tau_{xy} & \tau_{xz} \\ \tau_{yx} & \tau_{yy} - p & \tau_{yz} \\ \tau_{zx} & \tau_{zy} & \tau_{zz} - p \end{bmatrix} \tag{15}$$

Here indexes *i* and *j* represent orientation of the force and the corresponding surface, respectively, p is the pressure. Diagonal elements of this matrix $\tau_{xx} - p$, $\tau_{yy} - p$ and $\tau_{zz} - p$ represent normal stresses and the rest of elements represent shear stresses.

3.2.1 Shear Flow

In this chapter we will assume that the polymer material melt is incompressible and isotropic. Shear flow can be then divided into two types of flow, the drag flow and the pressure driven flow. In the first case, the speed is invoked by moving one of the channel walls and velocity profile has a shape of right angle triangle (highest speed on the moving wall). In the case of pressure driven flow the velocity is invoked by pressure difference and the velocity profile has a shape of semi parabola (highest speed in the middle).

The first case, drag flow, is possible to be imagined as moving polymer layers, each having constant velocity in the direction of the polymer flow, the dragged plate moves. The movement of the next plates, due to internal friction between the plates, will lead to the motion. It can be understood by studying a single infinitesimal element being dragged on the top surface with the bottom surface fixed. As it is shown in figure 15 the layers in-between move each with their own speed.

The second case, pressure driven flow, is based on the pressure gradient. The polymer melt flows from a section with higher pressure to the section with lower pressure. It is known as *Poiseuille flow*. (Bird et al., 1987, Musil, 2008, Tadmor and Gogos, 2006, White and Potente, 2003)

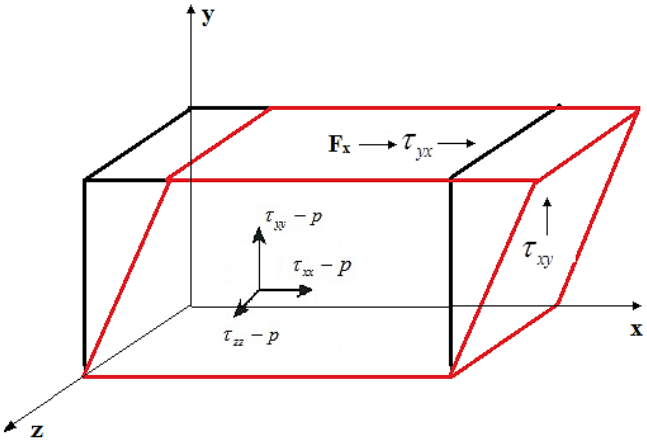

Figure 15: Shear flow deformation

Difference of speed between imaginary plates is:

$$\dot{\gamma} = \frac{dv_x}{dy} \Rightarrow v_x = \dot{\gamma} \times y \tag{16}$$

And velocity profile in shear flow is given as:

$$v_x = \dot{\gamma} \times y\,; \qquad v_y = 0\,; \qquad v_z = 0 \tag{17}$$

Because of zero velocity in y and z direction, the deformation rate tensor becomes:

$$D_{ij} = \frac{1}{2} \times \begin{bmatrix} 0 & \dot{\gamma} & 0 \\ \dot{\gamma} & 0 & 0 \\ 0 & 0 & 0 \end{bmatrix} \tag{18}$$

And stress tensor has then a form:

$$\tau_{ij} = \begin{bmatrix} \tau_{xx} - p & \tau_{xy} & 0 \\ \tau_{yx} & \tau_{yy} - p & 0 \\ 0 & 0 & \tau_{zz} - p \end{bmatrix} \tag{19}$$

But during the shear flow of polymer melts we can observe also normal stresses (N_1 and N_2).

$$N_1 = \tau_{xx} - \tau_{yy} \tag{20}$$

$$N_2 = \tau_{yy} - \tau_{zz} \tag{21}$$

Since normal stresses are not equal to zero in case of the polymer melts, it leads to unusual behavior of the polymer melts. The normal stress differences N_1 cause effects known as Weissenberg effect.

We can define viscosity as a dependency of shear stress on shear rate (similarly as it has been defined for Newtonian fluids):

$$\eta = \frac{\tau_{xy}}{\dot{\gamma}} \tag{22}$$

For normal stresses the coefficient of the first and the second normal stress difference can be defined:

$$\psi_{1/2} = \frac{N_{1/2}}{\dot{\gamma}^2} \tag{23}$$

Thus coefficient of the first and the second normal stress difference can be expressed in terms of shear rate as:

$$\tau_{xx} - \tau_{yy} = \psi_1 \times \dot{\gamma}^2 \tag{24}$$

And

$$\tau_{yy} - \tau_{zz} = \psi_2 \times \dot{\gamma}^2 \tag{25}$$

For shear flow the most critical material factor is the shear viscosity. Viscosity is influenced by many parameters. The main variables influencing viscosity is the temperature in close relation to dissipation, shear rate, polydispersity and pressure.

Viscosity dependency on temperature may be described for example by an exponential equation:

$$\eta \approx e^{\frac{-A}{T}} \tag{26}$$

Or expressed in a form of Arrhenius equation:

$$\eta = \eta_{ref} \times e^{(\frac{Ea}{R} \times (\frac{1}{\Delta T}))} \tag{27}$$

Another form of Arrhenius equation could be:

$$\eta = \eta_{ref} \times e^{(\beta \times \Delta T)} \tag{28}$$

Here Ea is an activation energy (for polymers 25 to 85 kJ/mol), R is gas constant and β is thermal sensitivity constant for polymer. Basically each of these equations (Eq. 27 and 28) are saying the same, with increasing temperature the viscosity decreases (Figure 16, polymer with three different temperatures). Here, the type of polymer and its internal structure maters. In some cases, the polymers at processing conditions do not depend on temperature too much, while for some other polymers the sensitivity of the viscosity to temperature is strong. The polymer melt at flow also dissipates energy:

$$D = \eta \times \dot{\gamma}^2 \tag{29}$$

Dissipation is transforming of the mechanical energy into thermal energy. With the fact that the shear rate at the walls reaches its maximum value we can assume that the highest dissipation occurs at the walls, too. That means we may reach high temperatures and low viscosity, there.

Shear rate dependency of viscosity is significant. It is shown on figure 16. In this figure we can divide each of these three curves made by nodes on three regions. The first region is called Newtonian plateau where the viscosity is relatively constant. The second region of these curves is the processing region (shear rates during extrusion). This represents the typical processing extrusion conditions. It starts to decrease the viscosity with the shear until it reaches some limit value. The third region is called the second Newtonian plateau and it is characteristic with nearly constant viscosity again.

Curve shape in figure 16 is also possible to be described according to disentangling and entangling speed of statistic coils of polymer chains in dependency of viscosity on shear rate. With higher speed of shear rate it is harder for statistical coils to get entangled cause of energy which is necessary for entangling. In the first region the speed of entangling is equal to speed of disentangling, viscosity is then stable and it creates a plateau, shear rate is here too low. In the second region the speed of disentangling is higher than that of entangling due to transcending of critical shear rate. The viscosity in the second region is dramatically decreasing. The third region is a Newtonian plateau again, because there is such a high shear rate that entangling of statistical coils is not possible for polymer chains.

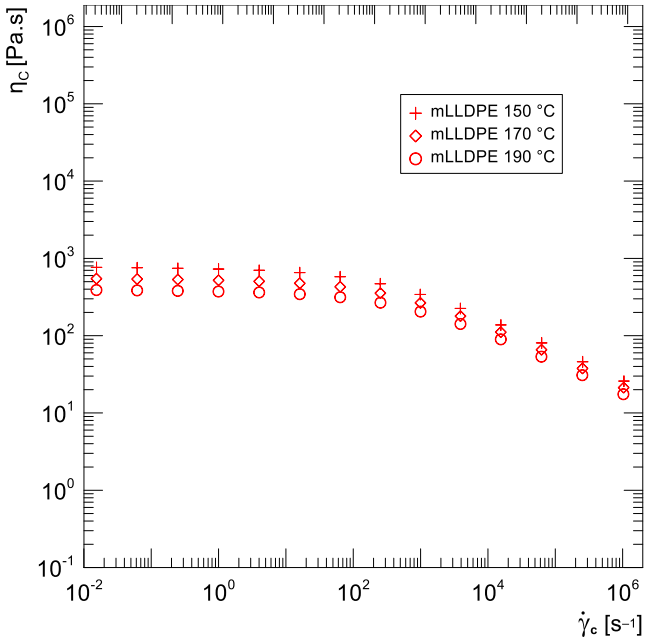

Figure 16: Influence of temperature and shear rate on viscosity

Preparation of raw materials (polymerization) has significant influence on polydispersity (molecular weight). During standard polymerizations without any sophisticated control, the chains lengths varies a lot, having broad distribution. On the other hand, when controlled polymerization is presented, length of the polymer chains is also controlled (narrow molecular weight distribution). We recognize two types of polydispersity, first type is with narrow molecular distribution → small polydispersity, characteristic with similar chains which then exhibit much longer Newtonian plateau and less sensitivity to shear. The second type is the one with broad molecular distribution, characteristic with a lot of non-similar large and small polymer chains. Such a melt exhibits strong sensitivity to shear. It is because of energy which is necessary for disentangling of polymer statistical coils. In case of similar chains, it is needed to get more energy for disentangling then in case of non-similar large chains which they need much smaller energy for disentangling. (Masoco, 1993, Chhabra and Richardson, 2008, Han, 2007, Malkin and Isayev, 2012, Osswald and Rudolph, 2015)

Equations describing the dependency of viscosity on molecular distribution is:

$$\eta = K \times M_V^{\alpha} \tag{30}$$

Here K, α are material constants and M_v is an average molecular weight.

Polydispersity can be calculated as:

$$Polydispersity\_index = \frac{M_W}{M_N} \tag{31}$$

Where M_W is weight average molecular weight and M_N is number average molecular weight.

For proper characterization of viscosity behavior and subsequent use in modelling, it is useful to fit measured data with appropriate viscosity models, which represent the behavior of polymer materials at flow. Most common viscosity models are the Power-Law Model, White-Metzner Model and Carreau-Yasuda Model.

Equation for Power-Law Model is:

$$\eta(T,\dot{\gamma}) = m \times \alpha \times \dot{\gamma}^{n-1} \tag{32}$$

Here m is index of consistency, α is temperature sensibility from Arrhenius equation and n is index of Newtonian behavior. This equation fits very well the segment of the viscosity curve which has, in the logarithmic scale, a straight shape. This is the most important shear thinning, processing region.

Carreau-Yasuda Model is more capable to describe the whole viscosity curve as:

$$\eta(T,\dot{\gamma}) = \frac{\eta_0 \times \alpha}{\left[1+\left(\lambda_0 \times \alpha \times \dot{\gamma}\right)^a\right]^{(\frac{1-n}{a})}} \tag{33}$$

Where a is coefficient of transition from Newtonian region to the pseudoplastic one.

Equation for White-Metzner Model is:

$$\tau + \lambda(II_D,T) \times \dot{\tau} = 2 \times \eta(II_D,T) \times D \tag{34}$$

Here II_D is second invariant of velocity-deformation tensor. For calculation of White-Metzner Model one needs the relaxation time (35) and viscosity from (22) as well.

$$\lambda(II_D,T) = \frac{K_1 \times \alpha}{1+K_2 \times \sqrt{II_D}} \tag{35}$$

Here K_1 and K_2 are constants. (Compuplast, 2003, Morrison, 2001, Osswald and Rudolph, 2015)

3.2.2 Elongation Flow

In previous case of shear flow the velocity was changing in the perpendicular direction (moving plates). Elongation flow is characteristic that the velocity of elements (rate of streamline) is being changed in the direction of the polymer melt flow, in the longitudinal direction. Most often the particles increase or decrease their speed because they are forced to flow through the narrowing or the diverging part of the channel geometry. Elongation then can take place in one or in two directions. According to the melt flow it can be uniaxial elongation flow, a planar elongation flow or biaxial elongation flow. Elongation viscosity can be expressed as:

$$\eta_E = \frac{\tau_{xx} - \tau_{yy}}{\dot{\varepsilon}} \tag{36}$$

Where $\dot{\varepsilon}$ is elongation rate.

In contrast to shear flow, the velocity of elongation flow in the other main directions is not zero. Velocity field here is:

$$v_x = \frac{1}{2} \times \dot{\varepsilon} \times (1 + b) \times x; \quad v_y = \frac{1}{2} \times \dot{\varepsilon} \times (1 - b) \times y; \quad v_z = -\dot{\varepsilon} \times z \tag{37}$$

Here b represents elongation parameter. According to type of flow the parameters $\dot{\varepsilon}$ and b can reach different values:

- Uniaxial elong. flow: b= 0; $\dot{\varepsilon}$ >0
- Planar elong. flow: b= 1
- Biaxial elong. flow: b=0; $\dot{\varepsilon}$ <0

As well as in shear flow the normal stress differences are present ($\tau_{xx} - \tau_{yy}; \tau_{yy} - \tau_{zz}$). However, in case of uniaxial and biaxial flows (elongation parameter b equal to zero) only one normal stress difference is important, namely $\tau_{yy} - \tau_{zz}$.

In the uniaxial elongation flow the material is stretched just in one direction and in the other directions it is compressed. (Figure 17) This type of flow occurs for example in fiber spinning and injection molding.

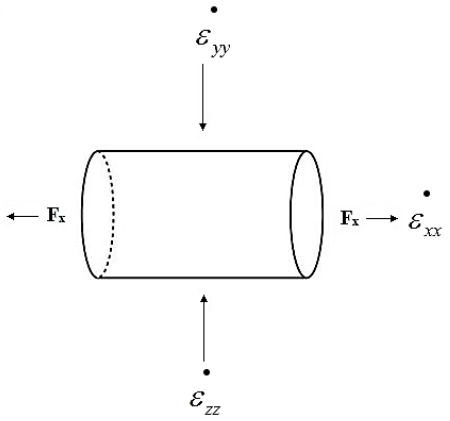

Figure 17: Uniaxial elongation flow

For such a situation the deformation rate tensor simplifies to:

$$D_{ij} = \begin{bmatrix} \dot{\varepsilon} & 0 & 0 \\ 0 & -0.5\dot{\varepsilon} & 0 \\ 0 & 0 & -0.5\dot{\varepsilon} \end{bmatrix} \tag{38}$$

Since the elongation rates in direction y and z are the same, we can write both of them as -0.5 $\dot{\varepsilon}$. Negative value of $\dot{\varepsilon}$ is because in these directions the material is compressed.

The stress tensor then can be expressed as:

$$\tau_{ij} = \begin{bmatrix} \tau_{xx} - p & 0 & 0 \\ 0 & \tau_{yy} - p & 0 \\ 0 & 0 & \tau_{zz} - p \end{bmatrix} \tag{39}$$

Planar elongation flow is another case of elongation flow when a reference volume is stretched in one direction, in another direction it is without any response ($\dot{\varepsilon}_{yy} = 0$) and in third direction it is compressed. For this case the equation for stress tensor is the same as in previous case and the deformation tensor is:

$$D_{ij} = \begin{bmatrix} \dot{\varepsilon} & 0 & 0 \\ 0 & 0 & 0 \\ 0 & 0 & -\dot{\varepsilon} \end{bmatrix} \tag{40}$$

Biaxial elongation flow is characteristic by stretching of the reference volume in two directions, in the third direction the cube is compressed. Stretching in two directions can be the same but can also be different.

Stress tensor here has same form as in previous cases, the equation for the deformation rate tensor is (Halley and George, 2009, Malkin, 1984, Zatloukal, 2015):

$$D_{ij} = \begin{bmatrix} \dot{\varepsilon} & 0 & 0 \\ 0 & \dot{\varepsilon} & 0 \\ 0 & 0 & -2\dot{\varepsilon} \end{bmatrix} \tag{41}$$

3.3 Thermal Properties of the Polymer Materials

In the extrusion process the polymer is heated up, melted, processed at elevated temperature and then cooled again. For that reason, the thermal properties are very important. For polymer engineers it is probably one of the most crucial parameter of polymer materials. Structure of the used polymer (molecular structure) is crucial for final thermal properties. In thermal properties are orientation and length of macromolecular chains, molecular weight, number, size and distribution of side chains, crystalline ratio, mobility of polymer chains and energy of the present bonds the most significant parameters (Torres et al., 2011, Ibrahim and Kadum, 2010)

This law is closely connected with thermal energy balance equation which is crucial for our thesis.

3.3.1 First Law of Thermodynamic

Thermodynamic is a field of science which is focused on macroscopic objects and relations between them, mainly energy transformation relations. Classical thermodynamic perceive those macroscopic objects as a continuum and not as individual particles. Another simplification is that those macroscopic objects will be closed to the thermodynamic system with bonds and walls with specific properties. Sometimes a wall is no more than an imaginary 2D closed surface through which the connection to the surrounding is direct. We recognize impermeable, permeable, semipermeable, diathermal and adiabatic walls. These walls say which system is defined, close system, open system or isolated system. Isolated system is characterised by no transport of matter or energy with surroundings. An open system is a system that freely exchanges energy and matter with its surroundings. A close

system is such a system where it is possible to transport only energy and not the matter. In all the systems we can recognize two groups of variables. The external variables, these are, for example, volume of the system or external forces. The internal variables are for example pressure, temperature, density or internal energy. External and internal variables together are called state variables and they describe actual conditions of the system. (Rathakrishnan, 2005, Kolat, 2001)

When state variables change their values, then system is going from initial conditions to the final steady conditions. Thermodynamic process is then present.

The first law of thermodynamic is a statement of the principle of conservation of energy. Conservation of energy means that the energy cannot be created or destroyed; energy can be only transferred or converted to another form of energy. In a system, the internal energy has to be equal to the sum of energy entering and exiting the system. It means it must be equal to the heat added to the system and the work done by the system:

$$\Delta E = W - Q \tag{42}$$

Here ΔE is the change of internal energy, W is the work done by the system and Q is the heat absorbed by the system from its surroundings. Unlike ΔE, the variables Q and W are not depended on the transformation from the initial condition to final condition.

The total internal energy is possible to be split into three components:

$$\Delta E = \Delta U + \Delta E_k + \Delta E_p \tag{43}$$

In equation 43 ΔU is internal change of energy, ΔE_k is kinetic energy change and ΔE_p is potential energy change. However, ΔU represents all energies in microscopic scale which are the kinetic and potential energies of molecules, atoms and subatomic particles. Equation is also possible to be expressed as:

$$\Delta U + \Delta E_k + \Delta E_p = Q - W \tag{44}$$

When sum of $\Delta E_k + \Delta E_p$ does not change, then equation 45 can be expressed as:

$$\Delta U = Q - W \tag{45}$$

And in differential form as:

$$dU = \delta Q - \delta W \tag{46}$$

Variable U is in differential form dU because it is a variable dependent on the state of the system. Integration would then give the difference between the initial and final states. Values Q and W have the form of differential equation δQ and δW because these values are not properties of the system but they are dependent on the process, integration of δQ and δW is giving then just values Q and W.

For better explanation of the energy equation balance it is necessary to implement another variables, enthalpy and heat capacity. Equation for enthalpy is:

$$H = \Delta U + p \times V \tag{47}$$

Where H is enthalpy, p is pressure and V is volume.

Heat capacity can be expressed with constant volume or pressure. The equations for these heat capacities are (Lyons et al., 2016, Rauwendaal, 2014, Roos and Drusch, 2016, Tannous, 2015):

$$C_V = \left(\frac{\partial U}{\partial T}\right)_V ; \quad C_P = \left(\frac{\partial H}{\partial T}\right)_P \tag{48}$$

3.3.2 The Energy Balance Equation

The Energy balance equation is based on the first law of thermodynamic. This law is also called the law of energy conservation.

The sum of right side terms of equation 49 has to be equal to those of the left side. Right side is represented by the sum of rate of the energy accumulation with rate of the energy convection due to motion. Left side is represented by the sum of the conduction energy with rate of the energy dissipation and the sum with energy source term:

$$\dot{E}_{acc} + \dot{E}_{conv} = \dot{E}_{cond} + \dot{E}_{diss} + \dot{S} \tag{49}$$

The particular components of this equation are expressed in equations 50 – 54.

Energy of accumulation:

$$\dot{E}_{acc} = \rho \times C_P \times \frac{\partial T}{\partial t} \tag{50}$$

Convection energy:

$$\dot{E}_{conv} = \rho \times C_P \times \left(v_x \times \frac{\partial T}{\partial x} + v_y \times \frac{\partial T}{\partial y} + v_z \times \frac{\partial T}{\partial z} \right) \tag{51}$$

Conduction energy:

$$\dot{E}_{cond} = k \times \nabla^2 T = \frac{\partial}{\partial x} \times (k \times \frac{\partial T}{\partial x}) + \frac{\partial}{\partial y} \times (k \times \frac{\partial T}{\partial y}) + \frac{\partial}{\partial z} \times (k \times \frac{\partial T}{\partial z}) \tag{52}$$

Dissipation energy:

$$\begin{aligned} \dot{E}_{diss} = \tau : \nabla == 2 \times \mu \times \left[\left(\frac{\partial v_x}{\partial x} \right)^2 + \left(\frac{\partial v_y}{\partial y} \right)^2 + \left(\frac{\partial v_z}{\partial z} \right)^2 \right] + \\ + \mu \times \left[\left(\frac{\partial v_x}{\partial y} + \frac{\partial v_y}{\partial x} \right)^2 + \left(\frac{\partial v_y}{\partial z} + \frac{\partial v_z}{\partial y} \right)^2 + \left(\frac{\partial v_z}{\partial x} + \frac{\partial v_x}{\partial z} \right)^2 \right] \end{aligned} \tag{53}$$

Energy source term:

$$\dot{S} = H_r \frac{\partial c}{\partial t} \tag{54}$$

Energy source term represents the rate of energy entering the system in a form of dielectric heating, chemical reactions, etc. Unit c in equation 54 represents the degree of cure and unit H_r represents amount of heat per unit volume. (Chung, 2011, Compuplast, 2003, Gordon, 1987, Rauwendaal, 2014, Wilkinson and Ryan, 1998, Tucker, 1989)

From equations 50 – 54 we can construct the energy balance equation, which can be expressed as:

$$\begin{aligned} (\rho \times C_P \times \frac{\partial T}{\partial t}) + (\rho \times C_P \times \left(v_x \times \frac{\partial T}{\partial x} + v_y \times \frac{\partial T}{\partial y} + v_z \times \frac{\partial T}{\partial z} \right)) = (\frac{\partial}{\partial x} \times (k \times \frac{\partial T}{\partial x}) + \frac{\partial}{\partial y} \times (k \times \frac{\partial T}{\partial y}) + \frac{\partial}{\partial z} \times (k \times \frac{\partial T}{\partial z})) + \\ + 2 \times \mu \times \left[\left(\frac{\partial v_x}{\partial x} \right)^2 + \left(\frac{\partial v_y}{\partial y} \right)^2 + \left(\frac{\partial v_z}{\partial z} \right)^2 \right] + \mu \times \left[\left(\frac{\partial v_x}{\partial y} + \frac{\partial v_y}{\partial x} \right)^2 + \left(\frac{\partial v_y}{\partial z} + \frac{\partial v_z}{\partial y} \right)^2 + \left(\frac{\partial v_z}{\partial x} + \frac{\partial v_x}{\partial z} \right)^2 \right] + H_r \frac{\partial c}{\partial t} \end{aligned} \tag{55}$$

According to Charles Tucker (Tucker, 1989) the energy balance equation can be expressed as:

$$\rho \times \frac{DU}{Dt} = -(\nabla \bullet q) - P(\nabla \bullet v) + (\tau : \nabla v) + \dot{S} \tag{56}$$

Here in equation 56, P means the rate of reversible work associated with volume changes, τ represent dissipation energy (irreversible work). From equation 56 internal energy can be eliminated in favor of temperature as (equation 48):

$$\rho \times C_V \times \frac{DT}{Dt} = -(\nabla \bullet q) - T \times \left(\frac{\partial P}{\partial T}\right)_V \times (\nabla \bullet v) + (\tau : \nabla v) + \dot{S} \qquad (57)$$

With an assumption of a constant material density, the term $\left(\frac{\partial P}{\partial T}\right)_V$ is zero and we can neglect right side of equation. Constant density is a practical simplification of the complex pVT relationship. In the modelling of the melt flow the incompressibility assumption is reasonably adequate.

With this assumption equation 57 becomes:

$$\rho \times C_P \times \frac{DT}{Dt} = k \times \nabla^2 T + \frac{1}{2} \times \mu \times (\dot{\gamma} : \dot{\gamma}) + \dot{S} \qquad (58)$$

Now we will discuss each term of the energy balance equation and its meaning for polymer materials.

3.3.2.1 Convection energy

This form of energy is present due to the bulk motion of the melt stream, heat is moving with the flowing melt. So here it is very important to know the material properties such as density and heat capacity and also the speed and temperature gradient of the moving melt at the beginning and at the end of the flow. Then, the difference between initial and final conditions is a result of the final convection heat. (see eq. 51).

3.3.2.2 Conduction energy

From equation 52 is obvious that conduction energy (heat flux) is strongly depended on thermal conductivity and temperature gradient. For polymers is thermal conductivity usually very low. Temperature is a scalar and in a body is given by value. Heat flow is given by numerical value but also by direction, it is a vector. The heat flow, respectively its magnitude and direction are dependent on the temperature distribution. Then heat flow vector is in direction of decreasing temperature. Heat flux is usually marked as q and in equation for conductivity k is the thermal conductivity which is material constant. Equation (52) for conduction was found by J. B. J. Fourier. (Özişik, 2002, Pavlou, 2015)

3.3.2.3 Dissipation energy

During polymer processing it is necessary to transport the polymer melt from the feed throat to the extrusion die. As the deformation is present, all of these processes require source of energy. The energy comes from the extruder machine, it means mechanical energy. This mechanical energy is during extrusion transformed due to friction, dissipation and other form of work to the internal energy, respectively heat energy (equation 53).

The energy necessary for deformation of the viscous material is irreversibly converted into an internal energy. The deformation of elastic and viscoelastic materials is particularly reversible; it can be transformed in form of potential energy and then transformed to mechanical energy. In both cases the equation 53 can be used. The dissipation in case of viscous material is positive, in case of elastic and viscoelastic materials is positive or negative. (Gordon, 1987, Singler and Pollock, 1992)

4

Simulation of the Extrusion Process

4.1 Initial and Boundary Conditions

For solution of the energy balance equation it is necessary to know the initial and boundary conditions. These conditions define temperature distribution inside and on the surface of a body. Inside a body we have to assume that the temperature is a function of directions x, y, z and also a function of time.

Initial conditions, respectively the state of a body on the beginning of the process (start of the heat flow), are necessary to be specified when unsteady problem is presented. Such a condition is usually expressed as a prescribed value. Initial temperature for all points of body is (Ghoshdastidar, 2012):

$$\lim_{t \to 0} T(x, y, z, t) = T(x, y, z) \tag{59}$$

Boundary conditions are used to complete the description of the boundary limits of a body during experiment. If we want to set a simulation project we have to know parameters of a body and surrounding space, the particular flow equations, the size and shape of the system

(body), initial conditions and physical and chemical properties of a body. Boundary conditions which are describing the conditions at the surface or inside a body can be linear or nonlinear. We recognize four kinds of linear boundary conditions: Dirichlet condition, Neumann condition, Fourier condition and boundary condition of the fourth kind. In subheads below we will focus just on linear type of boundary conditions. (Özişik, 2002, Poehls and Smith, 2009)

4.1.1 The Boundary Condition of the first kind (Dirichlet condition)

The Dirichet condition basically says that the temperature of the body surface is prescribed by temperature distribution. It means a value of heat transfer coefficient α at the interface between two surfaces is very high.

In submitted thesis Dirichet boundary condition has meaning as an isothermal boundary condition.

In general case the temperature is function of time and position:

$$T = f_i(r,t) \tag{60}$$

Here r is a position.

Special type of Dirichlet condition is when temperature is constant or zero, then we speak about homogenous boundary condition of the first kind. (Özişik, 2002, Pal and Bhunia, 2015)

4.1.2 The Boundary Condition of the second kind (Neumann condition)

When the normal derivative of temperature along the body surface should be prescribed, we can use Fourier law equation:

$$q = -k \times \nabla T = -k \times \frac{\partial T}{\partial n} \tag{61}$$

Here q is heat flux, k is thermal conductivity and $\frac{\partial T}{\partial n}$ is a temperature gradient along a body surface. Then, the magnitude of heat flux is prescribed by temperature drop of a body surface.

Neumann boundary condition has for submitted thesis meaning as an adiabatic boundary condition.

Special type of Neumann condition is when surfaces of a body are insulted, then temperature gradient is zero:

$$\frac{\partial T}{\partial n} = 0 \tag{62}$$

Another special state of Neumann condition is an effect of the radiation:

$$-k \times \frac{\partial T}{\partial n} = \varepsilon \times \sigma \times \left(T^4 - T_S^4\right) \tag{63}$$

Where T and T_s are absolute temperatures of the heated surface/of the source of radiation, ε is the emissivity and σ is the Boltzmann constant.

4.1.3 The Boundary Condition of the third kind (Fourier condition)

The third kind of boundary condition is based on principle of energy balance, respectively on mechanism of continuous flows. It means that input in form of conductive flow has to be in balance with output in form of convective flow from medium. Then we can use an equation, where conductive heat flow variables are in balance with Newtonian´s law variables (heat transfer is proportional to temperature difference) of cooling:

$$-k \times \frac{\partial T}{\partial n} = \alpha \times (T - T_m) \tag{64}$$

or

$$k \times \frac{\partial T}{\partial n} + \alpha \times T = \alpha \times T_m = f_i(r,t) \tag{65}$$

Where T_m is temperature of medium surrounding the body and α is heat transfer coefficient. In case, when α is high, respectively significant, then third kind of boundary condition is changed to the first kind of boundary condition. Another case could be homogenous boundary condition, when heat energy by convection from the boundary surface into a medium at zero degree Celsius. Then element $\alpha \times T_m = 0$ in equation 65 is equal to zero.

4.1.4 The Boundary Condition of the fourth kind

The last kind of boundary condition is based on mechanism of two material surfaces which they have perfect contact each other. Both of them have own thermal conductivity and different temperature, respectively different temperature gradient. It is possible to expressed that as:

$$k_i \times \frac{T_i}{n_i} = k_j \times \frac{T_j}{n_j} \tag{66}$$

The boundary condition of the fourth kind could transform into the boundary condition of first kind when surroundings has much higher thermal conductivity than a body. Then out body will have temperature gradient same as surrounding medium. (Bird et al., 2007, Özişik, 2002, Placek, 2002, Pepper and Carrington, 2009)

4.2 Finite difference method

The polymer process simulations use various numerical methods. When it is necessary to solve any flow model a series of differential equations is presented. These differential equations are discretized. This process converts those partial differential equations into a series of algebraic equations (techniques of linear algebra). There is several ways how to divide domain to many little subdomains (elements) as it is shown in figure 18. Namely the finite element method, the boundary element method and the finite difference method.

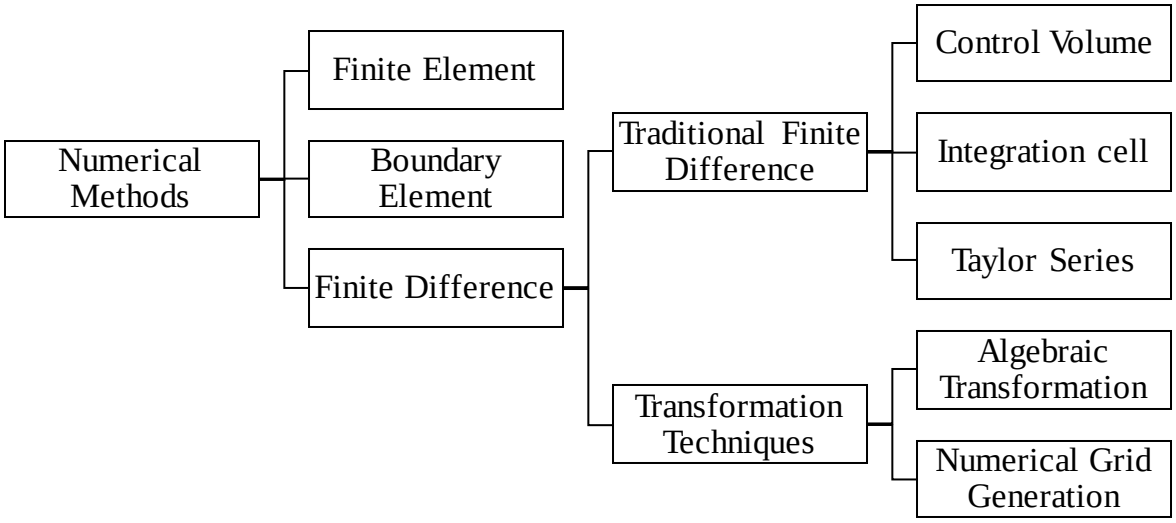

Figure 18: Schema of numerical methods

The simulations used in our thesis will use commercial programs based on Finite element method. For our study of the heat conditions inside the mandrel, we will also use a simple energy balance equation. In this case we will exploit the finite difference method.

Solution with help of finite difference method in general incorporates three subsequent steps. First it is necessary to build a grid over solved domain (figure 19). This grid divides the

domain (geometry of solved body) into many little domains and nodes. Each node has some unknown variables and we need to get corresponding set of algebraic equations through discretizing the partial differential equations. Based on the real shape of solution domain different coordinate systems (non-orthogonal, Cartesian, etc.) can be used.

The second step is to transform the partial differential equations into algebraic equations with help of discretization. Then the last, step is to solve the algebraic system numerically. Here it is important to respect the nature of algebraic equations.

In this work we choose for modeling of energy balance inside a mandrel the Taylor series approach which is usually considered as a traditional finite difference method. This type of approach is restricted to regular/simple geometries.

The grid coordinates of function value, respectively node coordinates of function value, will be written by subscripts separated with a comma, it means node with location (i, j) will be written as $f_{i,j}$. (Nicoud, 2015, Schubert, 2015, Pal and Bhunia, 2015, Tucker, 1989, Civan, 2016, Osswald and Hernández-Ortiz, 2006)

4.2.1 Taylor Series Expansion

This method helps us to analyze the order of the approximation. It can also estimate truncation errors to compare the accuracy of different discretization formulas. In figure 19 the typical discretization grid is shown.

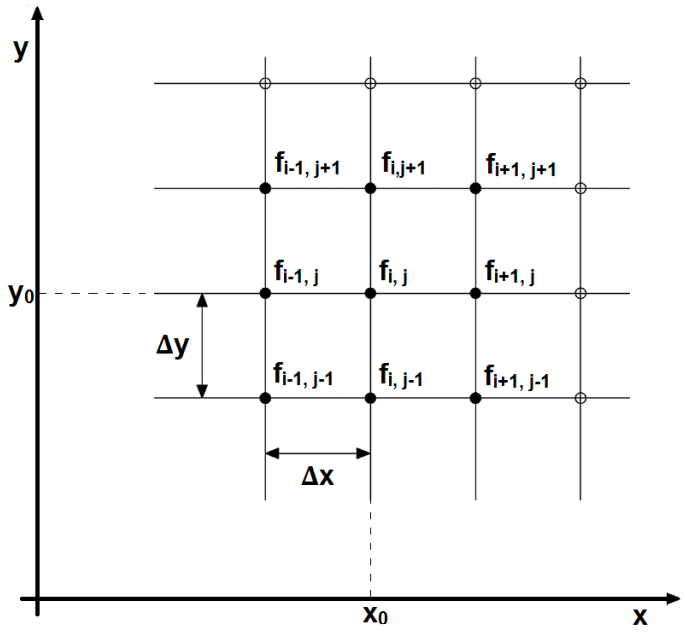

Figure 19: Construction of a grid for finite difference approximations

The grid is divided into many nodes, located by x, y coordinates (nodal location). When a node in the middle, with coordinates x_0, y_0, is marked as a function with the indices i, j ($f_{i,j}$), then the nodes surrounding can be similarly marked as $f_{i+1,j}$; $f_{i-1,j}$; $f_{i,j+1}$; $f_{i,j-1}$. If the function f is continuous over the domain, then the value of $f_{i+1,j}$, which expands the function f in the positive x-direction, can be expressed in terms of $f_{i,j}$ by a Taylor series expansion as:

$$f_{i+1,j} = f_{i,j} + \left.\frac{\partial f}{\partial x}\right|_{i,j} \times (\Delta x) + \left.\frac{\partial^2 f}{\partial x^2}\right|_{i,j} \times \frac{(\Delta x)^2}{2!} + \left.\frac{\partial^3 f}{\partial x^3}\right|_{i,j} \times \frac{(\Delta x)^3}{3!} \ldots \tag{67}$$

Then the first derivative of $f_{i,j}$ at the location x_0, y_0 can be expressed as:

$$\left.\frac{\partial f}{\partial x}\right|_{i,j} = \frac{f_{i+1,j} - f_{i,j}}{\Delta x} - \frac{1}{2} \times \left.\frac{\partial^2 f}{\partial x^2}\right|_{i,j} \times \Delta x + \ldots \tag{68}$$

or as

$$\left.\frac{\partial f}{\partial x}\right|_{i,j} = \frac{f_{i+1,j} - f_{i,j}}{\Delta x} + O(\Delta x) \tag{69}$$

Here O(Δx) means the order of the additional terms in the series. If we neglect the high order terms O(Δx), the equation 69 will be expressed as:

$$\left.\frac{\partial f}{\partial x}\right|_{i,j} = \frac{f_{i+1,j} - f_{i,j}}{\Delta x} \tag{70}$$

Equations 70 is called a forward difference expression for the first derivative. Forward because it expands in positive x-direction. Hiding of O(Δx), respectively elimination of higher order terms, is called truncation error.

In similar way the function f can be expressed also in the negative x-direction, this is called a backward expansion:

$$f_{i-1,j} = f_{i,j} - \left.\frac{\partial f}{\partial x}\right|_{i,j} \times (\Delta x) + \frac{1}{2} \times \left.\frac{\partial^2 f}{\partial x^2}\right|_{i,j} \times (\Delta x)^2 - \frac{1}{6} \times \left.\frac{\partial^3 f}{\partial x^3}\right|_{i,j} \times (\Delta x)^3 \ldots \tag{71}$$

And again, with dropping of O(Δx) the equation 71 is expressed as backward difference expression for the first derivative of the function f at (x_0, y_0):

$$\left.\frac{\partial f}{\partial x}\right|_{i,j} = \frac{f_{i,j} - f_{i-1,j}}{\Delta x} \tag{72}$$

The difference between forward (67) and backward (71) equations give central difference expression for the first derivate:

$$\left.\frac{\partial f}{\partial x}\right|_{i,j} = \frac{f_{i+1,j} - f_{i-1,j}}{2 \times \Delta x} \tag{73}$$

Central difference expression has an exception that the truncation error is not expressed as $O(\Delta x)$ but as $O(\Delta x)^2$. Equations 70 and 72 are then called as first order expressions for the first derivate, unlike of them equation 73 is called second order expression for the first derivate.

Central difference is possible to be expressed also for second derivate at x_0, y_0:

$$\left.\frac{\partial^2 f}{\partial x^2}\right|_{i,j} = \frac{f_{i+1,j} - 2 \times f_{i,j} + f_{i-1,j}}{(\Delta x)^2} + O\left[(\Delta x)^2\right] \tag{74}$$

By dropping of element $O\left[(\Delta x)^2\right]$ in equation 74 we can express the second order, central difference expression for the second derivative of the function f at x_0, y_0.

For better understanding we will discuss here also the derivative expressions for y-direction. First order, forward difference as:

$$\left.\frac{\partial f}{\partial y}\right|_{i,j} = \frac{f_{i,j+1} - f_{i,j}}{\Delta y} \tag{75}$$

First order, backward difference as:

$$\left.\frac{\partial f}{\partial y}\right|_{i,j} = \frac{f_{i,j} - f_{i,j-1}}{\Delta y} \tag{76}$$

Second order, central difference:

$$\left.\frac{\partial f}{\partial y}\right|_{i,j} = \frac{f_{i,j+1} - f_{i,j-1}}{2 \times \Delta y} \tag{77}$$

Last but not least examples of Taylor series will be for the function values at nodes f_{i+2} and f_{i-2} because casual grids consist from more than just two nodes:

$$f_{i+2,j} = f_{i,j} + \left.\frac{\partial f}{\partial x}\right|_{i,j} \times (2 \times \Delta x) + \left.\frac{\partial^2 f}{\partial x^2}\right|_{i,j} \times \frac{(2 \times \Delta x)^2}{2!} + \left.\frac{\partial^3 f}{\partial x^3}\right|_{i,j} \times \frac{(2 \times \Delta x)^3}{3!} + \ldots \tag{78}$$

$$f_{i-2,j} = f_{i,j} - \left.\frac{\partial f}{\partial x}\right|_{i,j} \times (2 \times \Delta x) + \left.\frac{\partial^2 f}{\partial x^2}\right|_{i,j} \times \frac{(2 \times \Delta x)^2}{2!} - \left.\frac{\partial^3 f}{\partial x^3}\right|_{i,j} \times \frac{(2 \times \Delta x)^3}{3!} + \ldots \qquad (79)$$

With some modifications the Taylor series expansion is also possible to be used for unregular shapes with unequally spaced nodes.

In appendix II there is a table of common finite difference expressions for uniformly spaced grids. Derivatives in governing equations can be replaced by those finite difference expressions, see appendix II. (Pal and Bhunia, 2015, Tucker, 1989, Osswald and Hernández-Ortiz, 2006)

Experimental Research

5

Motivation and Aims of the Thesis

5.1 Motivation

Many studies were already focused on thermal behavior understanding of the polymer melt. Nevertheless, many problems connected with thermal behavior were not solved yet. Thermal behavior in the flow channel of the extrusion die is crucial for important variables as for example viscosity.

Submitted thesis is focused on understanding of the thermal behavior of the polymer melt in the extrusion die. Understanding and description of important properties as dissipation, heat conduction, heat convection or energy balance equation are one of the aims.

However, thermal behavior of the polymer melt in the extrusion die is huge topic. Longitudinal part of the extrusion dies, where the highest thermal effects are reached, is the main aim of submitted thesis. Many engineers and scientists assume in longitudinal part constant temperature. This statement is incorrect because of different thermal conductivity. Thermal conductivity of the steel tools is high, that is why dimensions of the steel tools are important. For example, from barrels all heat is removed out. On the other hand, in case of

small size tools inside the extrusion die, such as mandrels, surrender by the polymer melt (isolation because of low thermal conductivity), heat is kept inside the tools.

For better understanding of thermal behavior of the polymer melt and mandrels the computer modeling was used. Nowadays isothermal or adiabatic boundary condition for mandrel walls is considered as a standard in computer modeling. This assumption is incorrect as it was mentioned above. When isothermal condition is chosen, all heat is removed out and mandrel has constant temperature. Whereas adiabatic condition assumes that no heat is removed out from the mandrels.

Mandrel can be successfully described as a part of calculations connected with the flow calculations (3D module). Nevertheless, this solution leads to the difficult mathematical models, it is expensive, complicated and it take a lot of time.

Our motivation is to design fast, simple and exact solution of the boundary condition. This condition should describe and also help us to clearly understand to the thermal behavior of the mandrel and surrender polymer melt as well.

5.2 Aim of the Master Thesis

- Measuring of the thermal conditions of the polymer melt and of the mandrel inside the extrusion die
- Understanding of thermal effects inside the extrusion die due to simulations of limit situations and due to real extrusion process measuring
- Description of heat flow inside the mandrel and calculation of the heat flow in software Maple by finite difference method
- Comparison of real extrusion process measuring with the extrusion simulation which will include the new boundary condition
- With help of the 1D finite difference method develop the new boundary condition and calculations for neglecting of the mandrel during the extrusion simulation in the computer program Virtual Extrusion Laboratory ™ 6.9.

6

Materials and Geometry

6.1 Material

In this chapter basic properties of used polymer materials will be discussed. Material was used for simulation of extrusion process and for real extrusion process as well.

Molecular distribution was crucial for purposes of this thesis, narrow molecular distribution, respectively. These kinds of material are characterized by small polydisperzity, similar small chains and by longer Newtonian plateau than polymer materials with broad molecular distribution.

In this thesis was being chosen, after several measuring of different polymer materials, special type of high density polyethylene (HDPE), Liten ML 71. Other types of polymer materials, as a metallocene linear low density polyethylene (mLLDPE), linear low density polyethylene (LLDPE) or HDPE with low MFR, were not being suitable for our application. Few of them generated huge pressure in area of the slit, few of them had not inclination to make a dissipation energy in area of the slit.

HDPE Liten ML 71 is a homopolymer with narrow molecular distribution and UV stabilization. Typical using of Liten ML 71 is injection molding or applications where high rigidity, good impact resistance and oxidation stability is required. The material properties of Liten ML 71 are given in table 1.

Table 1: Typical material properties of Liten ML 71

Property	Unit	Value	Test Method
Solid Density	kg/m³	961	ISO 1183
Yellowness Index	standard	max. A	ASTM D 1925
Yield Stress	MPa	59	ISO 527-1
Flexural Modulus	MPa	1100	ISO 178
Melt Flow Rate (190 °C /2.16 kg)	g/10 min	7.2-9.2	ISO 1133
Vicat Softening Temperature	°C	126	ISO 306
DSC Melting Point	°C	135	ASTM D3418-03
Coefficient of Friction	[1]	0.29	ASTM D1894
Conductivity	W/m.°C	0.49	ISO 22007-1
Specific Heat	J/Kg.°C	2250	ASTM E1269-05
Emissivity	[1]	0.9	ASTM C835-06

6.1.1 Rheology Characterizations

Rheological or flow curve, shear rate dependency of viscosity, were measured on the capillary rheometer Göttfert RG 50 (50 kN force range). Two capillaries with L/D 20/1 and 0/1 were used. Length of barrel system was 250 mm. Pressure sensors 200 and 500 bar were used with accuracy 0.2 % from total range.

During measuring on capillary rheometer two types of corrections are significant. Only apparent values of variables are obtained and it is reason of those corrections. After correction correct values are obtained:

At first volume flow rate can be calculated as:

$$\dot{Q} = A \times v = \frac{\pi \times d_{cn}^{2}}{4} \times v \tag{80}$$

Where A is area, d_{cn} is diameter of capillary (capillary number) and v is velocity. With knowledge of volume flow rate apparent values of shear rate (81), shear stress (82) and viscosity (83) are expressed as:

$$\dot{\gamma}_a = \frac{4 \times Q}{\pi \times r_{cn}^{\ 3}} \tag{81}$$

$$\tau_{XY,a} = \frac{\Delta P \times r_{cn}}{2 \times L} \tag{82}$$

$$\eta_a = \frac{\tau_{XY,a}}{\dot{\gamma}_a} \tag{83}$$

Where r_{cn} is radius of capillary, L is length of capillary channel and ΔP is total pressure loss. Pressure loss in capillary is reason of first correction, Bagley correction. In equation 82 is calculated only with total pressure loss and not real pressure loss of capillary. Bagley correction is solved this accuracy:

$$\tau_{XY,c} = \frac{\Delta P_{capillary} \times r_2}{2 \times L} = \frac{(\Delta P - \Delta P_{end}) \times r_2}{2 \times L} \tag{84}$$

Where ΔP_{end} is sum of entry and exit pressure loss (equation 86), $\Delta P_{capillary}$ is real pressure loss of capillary given by equation 87:

$$\Delta P = \underbrace{\Delta P_{entry} + \Delta P_{capillary} + \Delta P_{exit}} = \Delta P_{end} + \Delta P_{capillary} \tag{85}$$

$$\Delta P_{end} = \Delta P_{entry} + \Delta P_{exit} \tag{86}$$

$$\Delta P_{capillary} = \Delta P - \Delta P_{end} \tag{87}$$

Due to the directive of curve (y=kx + q) shown in figure 20 total pressure ΔP is given as:

$$\Delta P = \left[\frac{P_{L2} - P_{L1}}{(\frac{L}{d_2})_2 - (\frac{L}{d_2})_1} \right] \times (\frac{L}{d_2})_1 + \Delta P_{end} \tag{88}$$

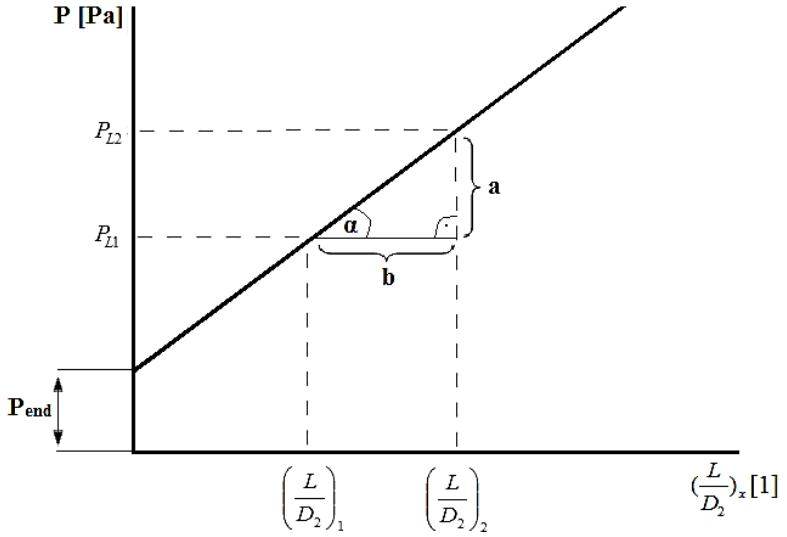

Figure 20: Curve for calculation of ΔP

On the other hand, Rabinowitsch correction is given as:

$$\dot{\gamma}_c = \dot{\gamma}_a \times \left(\frac{3 \times N + 1}{4 \times N}\right) \tag{89}$$

Where N is index of non-Newtonian behavior and term $\left(\frac{3 \times N + 1}{4 \times N}\right)$ is in equation 89 Rabinowitsch correction. Apparent shear rate is given only for Newtonian liquids. This distinction is solved by index of non-Newtonian behavior. This index has to be calculated from directive of polynomial curve of apparent shear rate dependence of correct shear stress.

$$N = 2 \times a \times \log(\dot{\gamma}_a) + b \tag{90}$$

Where parameters a and b are given from directive of polynomial curve.

When both variables, correct shear stress and correct shear stress, are known correct viscosity is given as:

$$\eta_c = \frac{\tau_{XY,c}}{\dot{\gamma}_c} \tag{91}$$

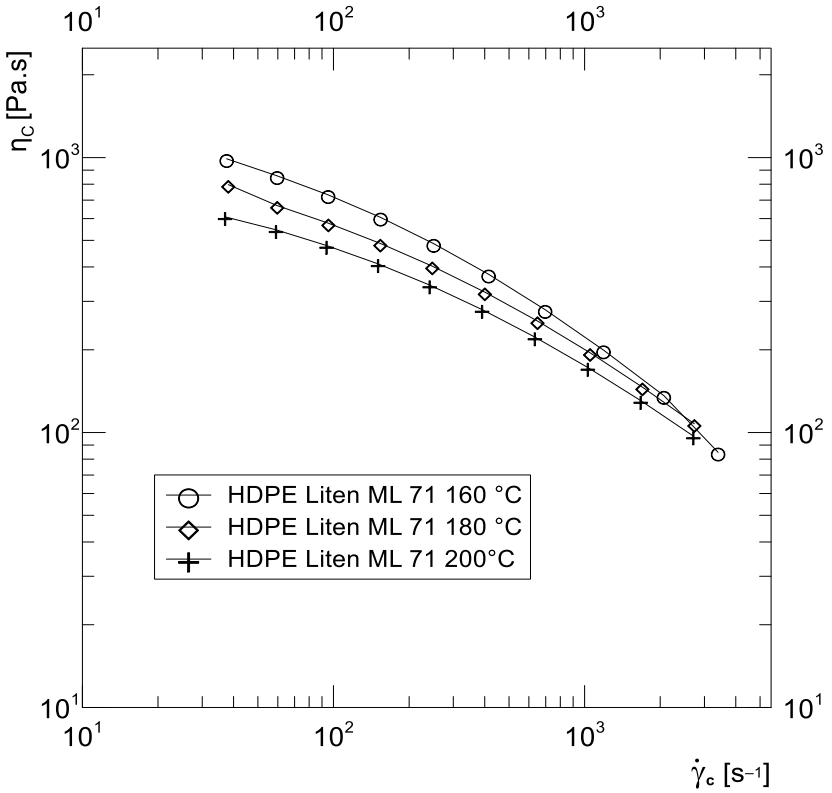

Figure 21: Flow curve of HDPE Liten ML 71

In figure 21 is shown the flow curve of HDPE Liten ML 71. The flow curve has declining trend, with increasing shear rate viscosity is gradually decreasing. Until critical shear rate viscosity has very stable trend. It is probably because of narrow molecular distribution. Extrusion process operates at shear rates often range up to several hundred s^{-1}. Newtonian plateau in area of low shear rate values (0.1 – 50 s^{-1}) is expected. Decreasing of viscosity is most likely because of unstoppable disentangling of the statistical coil.

6.1.2 Melt density

Melt density of HDPE Liten ML 71 was measured at 160 °C. As a machine for measuring was used melt indexer Tinius Olsen MP 600. Measuring was made according to standard ISO 1133. Length of the piston was 14.3 cm and area of barrel channel was 0.711 cm^2. The melt density of polymers is always lesser than density of solids (shown in table 1). The melt density is depended on temperature. With increasing temperature, melt density is decreasing its value. (Campbell and Spalding, 2013) The melt density equation can be expressed as:

$$\rho = \frac{m}{V} = \frac{m}{S \times l} \tag{92}$$

HDPE Liten ML 71 resin was measured 3 times at the same temperature 160 °C. Results are shown in table 2. Average value of melt density from three measuring is 780.28 kg/m^3.

Table 2: Values for weight and density of measured samples:

Sample no.	Weight [kg]	Density [kg/m^3]
Sample 1	0.0081	796.67
Sample 2	0.0079	777.00
Sample 3	0.0078	767.17
Average	0.0079	780.28

6.1.3 Melt Thermal Conductivity

The thermal conductivity of HDPE Liten ML 71 was measured at the temperature 160 °C. Value of thermal conductivity was measured on Göttfert RG 50 (50 kN force range). For measuring was used special piston including electric heater. Polymer melt was pressed on set value of force, in our case 1784 N. After 10 min where tempering was carried out, measuring was started. Piston was heated by electricity for 2 min, during those 2 min thermal conductivity was measured. Value of thermal conductivity was obtained as a linear regression from curve in figure 22. Result of thermal conductivity was calculated as $\lambda = 0.246\,\mathrm{W/m.°C}$ with R^2=0.995.

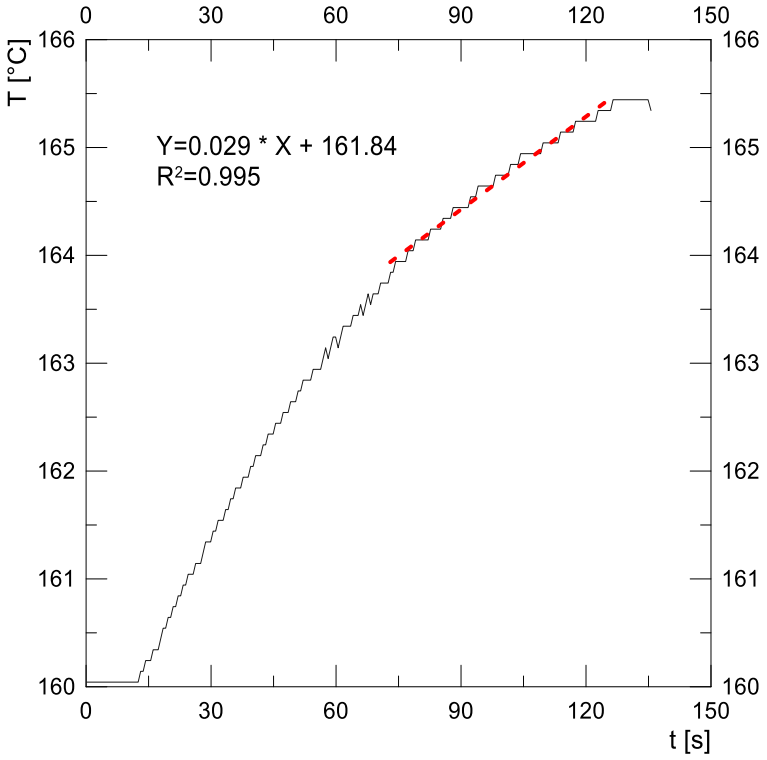

Figure 22: Temperature dependency of time for measuring of thermal conductivity

6.1.4 Heat Capacity

Value of heat capacity for HDPE ML 71 was measured by Mettler Toledo DSC 1. Range of temperatures was chosen from 150 °C to 200 °C in inert atmosphere (nitrogen). Speed of heating was chosen 2 °C per minute. Value of heat capacity at 160 °C is significant for us. Aluminum was used as a crucibles material. In figure 23 is shown curve temperature dependency of heat capacity.

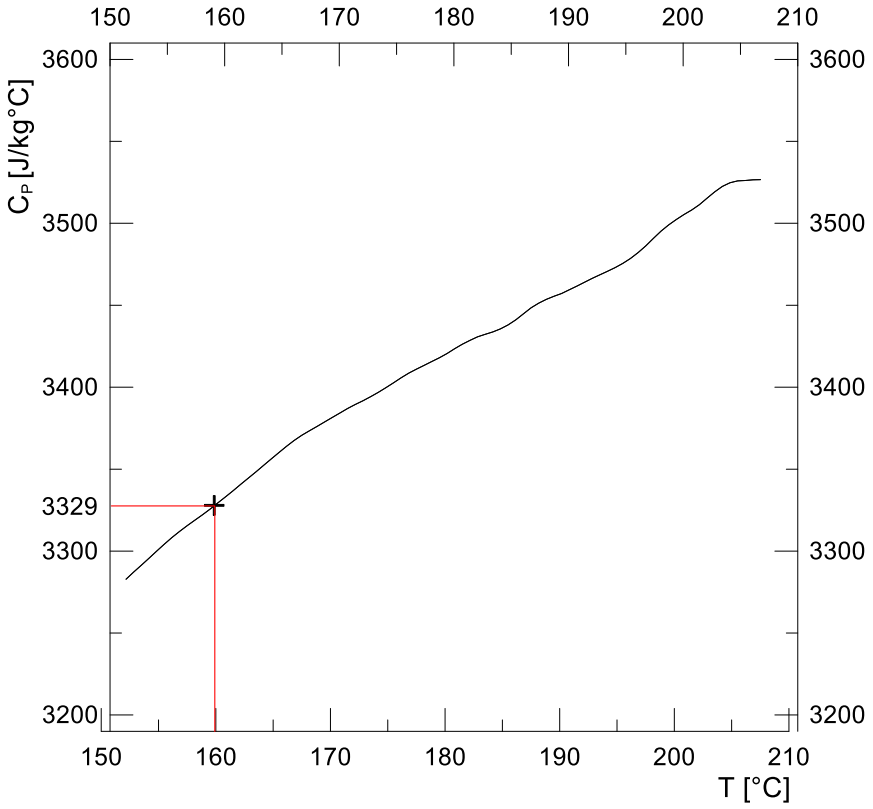

Figure 23: Heat capacity dependency of temperature curve

In figure 23 is shown heat capacity dependency of temperature. This curve has increasing trend. When temperature is increasing then heat capacity as well. Curve in figure 23 has practically linear character. The most important temperature for submitted thesis is at 160 °C, value of heat capacity at 160 °C is 3329 J/Kg.°C.

6.2 Geometry

For purposes of submitted thesis laboratory extrusion die was modified by company Compuplast s. r. o. In figures 24-28 is shown used extrusion die. This extrusion die is composed from input, flow channel where mandrel is placed and output with the tourniquet. Because of pressure modification tourniquet is part of the extrusion die. Heaters are placed

from both sides. Holes in the extrusion die walls showed in figures bellow are for measuring devices, such as infrared probe devices and pressure sensors. Dimensions of the flow channel are: length 159 mm, width 24.8 mm and depth 6 mm. Dimensions of the mandrel are: length 59.33 mm, width 24 mm and depth 5 mm.

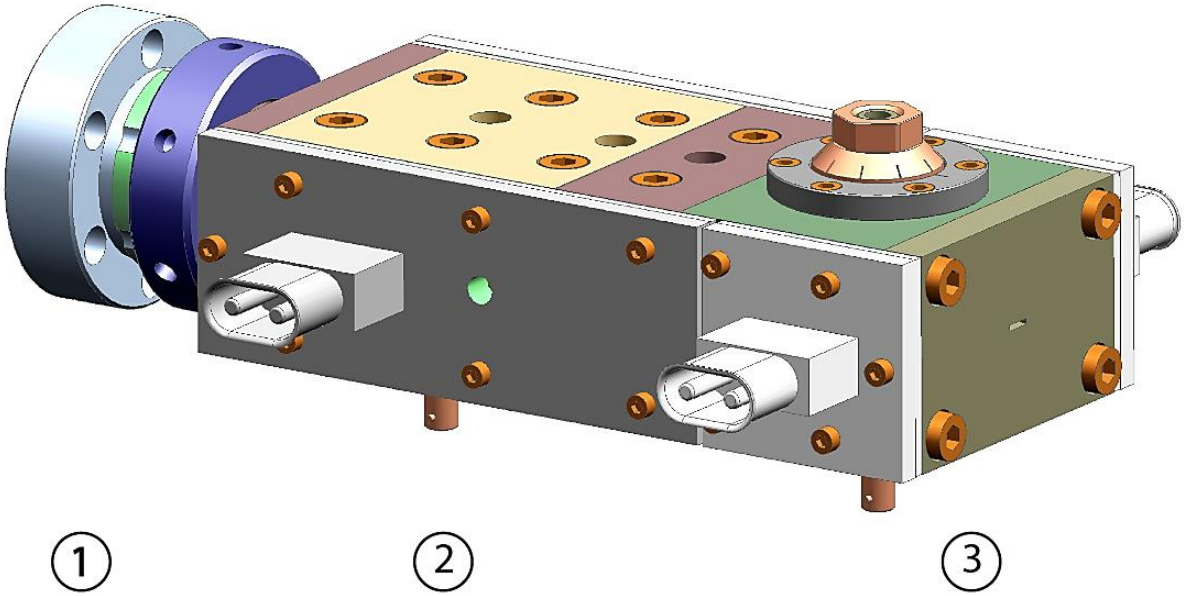

Figure 24: Extrusion die: 1 Input; 2 Flow channel; 3 output with the pressure controller

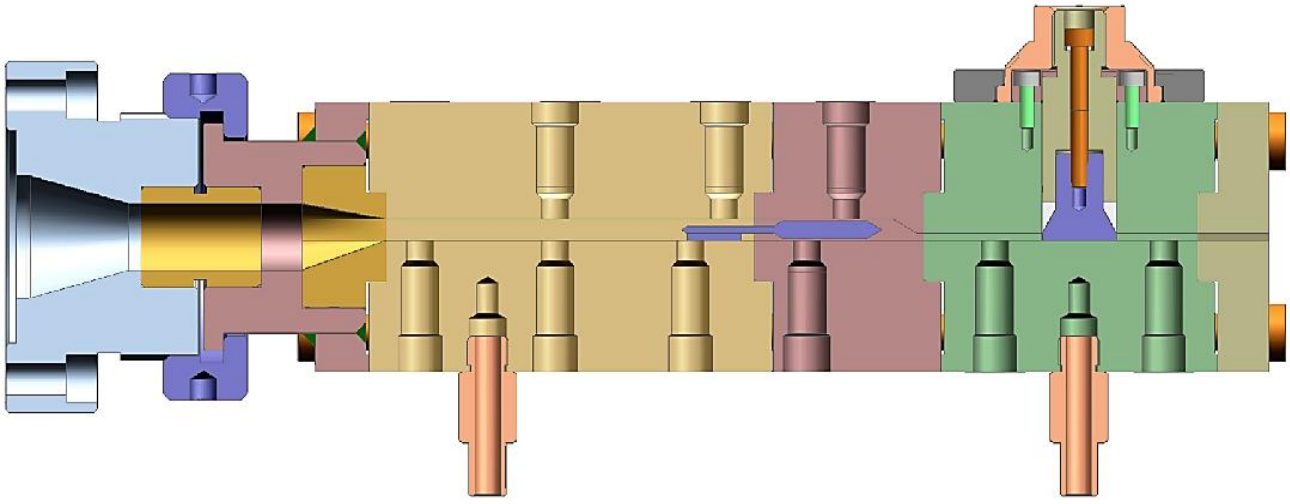

Figure 25: Cross section of the extrusion die

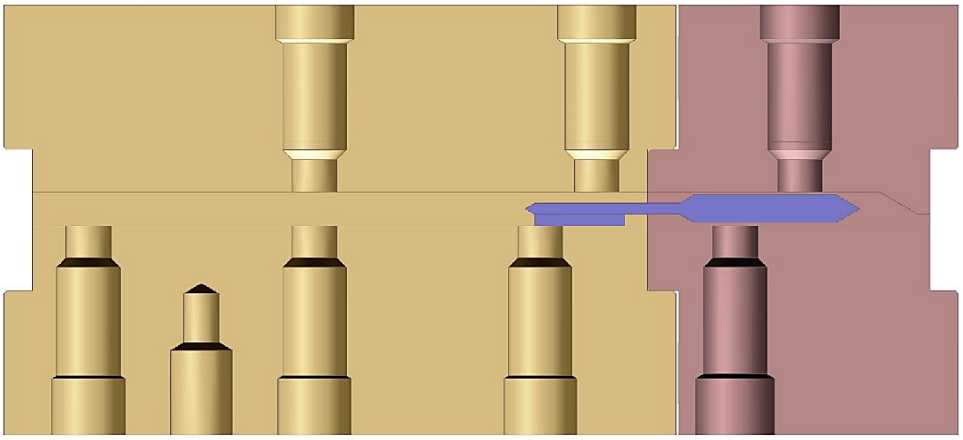

Figure 26: Cross section of the channel flow where dissipation is occurred

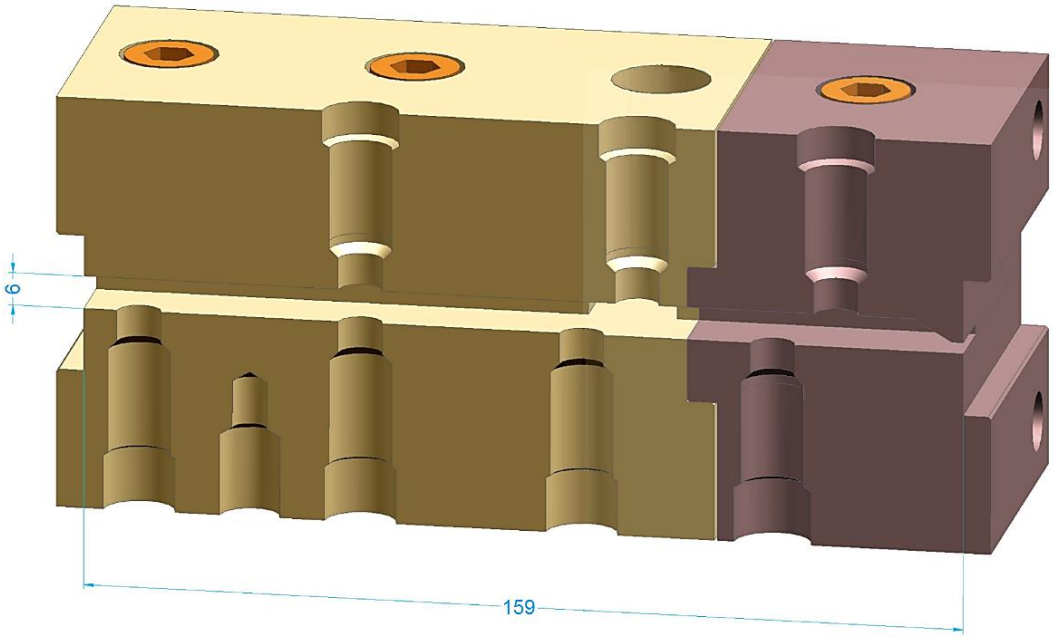

Figure 27: Cross section of the channel flow where mandrel is placed

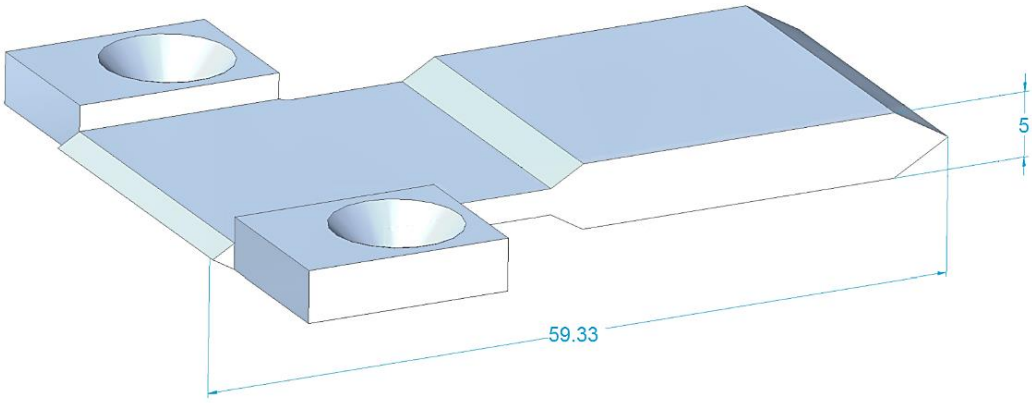

Figure 28: Mandrel of the extrusion die

7

Extrusion Process Simulation

7.1 Introduction

Thermal effects during extrusion, which they are present in the extrusion die and the mandrel, are complex and difficult to understand. The polymer melt interacts with the steel wall and the energy dissipated is partly conducted away from the melt. Thus, the real process simulation includes the steel body in the energy balance as well. In most of the cases, however, the simulation is performed in a simple form, the wall is replaced by boundary condition. Examples of typical simulations using isothermal and adiabatic boundary conditions will be discussed below for better understanding. These two represent some ideal states assuming either infinite or negligible wall heat transfer coefficient. During polymer flow inside a die channel none of these ideal states describes the real conditions well enough. The real solution could be found simply somewhere in-between the isothermal and adiabatic solutions.

The case with isothermal boundary condition is appropriate for some flow situations when the heavy block of the steel (high thermal conductivity) is capable to conduct away all

the heat flux the flow generates. The wall is then kept at prescribed temperature. When the steel is thin or surrounded by other polymer layers, the heat cannot be removed. In such a case the adiabatic boundary condition is appropriate.

When the wall is made from material with low thermal conductivity or simply the heat cannot be conducted away (for example when the wall is very thin or surrounded by the melt), the adiabatic boundary condition is more appropriate. The melt is insulated. Differences between these two ideal cases can be seen on the temperature plots along melt/steel interface and temperature plots across the steel and flow channel below.

The simulations are made for a simple 2D flat flow channel. The flow channel has length 20 mm, width 15 mm and depth 1 mm. Mass flow rate was set to 10 kg/h and the initial temperature, temperature of walls (isothermal case) and temperature of incoming material were set to 160 °C. Simulation was made in software VEL^{TM} 3DFem module.

Figure 29 shows different views on a flow domain with isothermal boundary conditions. Walls of the flow channel have the same temperature across the whole area. All heat flux at the polymer-metal interface generated by the flow viscous heating is absorbed and conducted away.

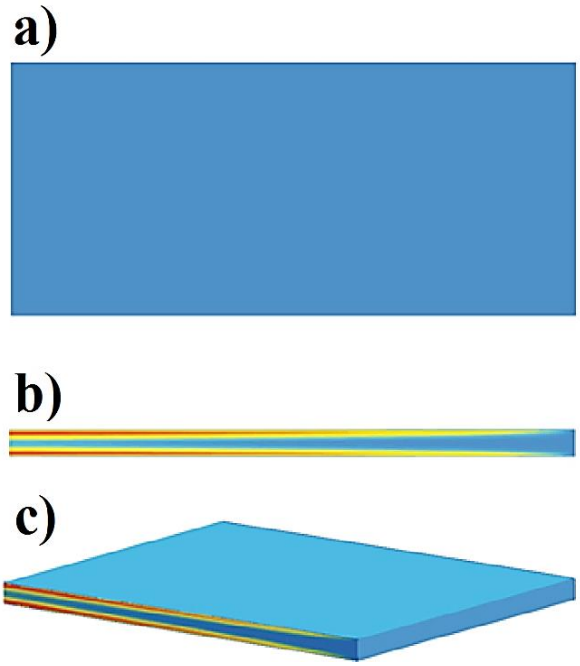

Figure 29: The flow situation with isothermal boundary condition of the surface (Temperature field displayed): a) view on top, b) longitudinal section, c) 3D view of a body

From figure 30 (temperature profile across the die) it is obvious that the polymer melt dissipates energy and is cooled down by walls. The temperature is the lowest at the steel walls and reaches its maximum near the walls. That indicates high temperature gradient. Polymer melt flow is symmetric. Thermal conductivity has main influence on the heat exchange between the melt and steel body. In comparison of thermal conductivities, thermal conductivity of our polymer material is 0.246 W/m°C and thermal conductivity of steel is 40 W/m°C. That is the reason why steel walls are able to conduct all heat the polymer is able to supply. The polymer melt is cooled down by walls.

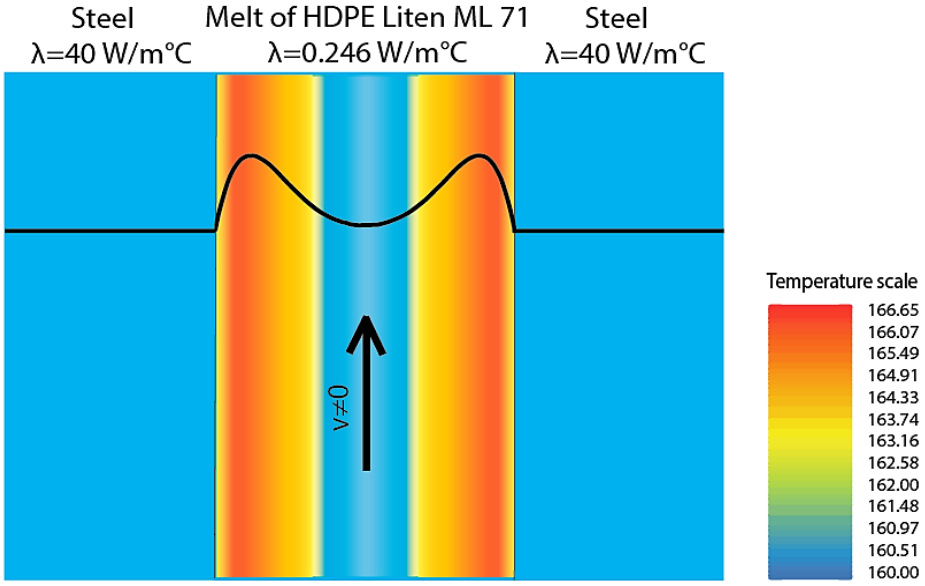

Figure 30: Temperature profiles across the flow channel at the end of the die with different thermal conductivity (isothermal boundary condition)

Figure 31a) shows temperature along the melt/steel interface. At the isothermal wall the temperature has the prescribed value, 160 °C. On the other hand, the maximum value of temperature generated by dissipation is in case of isothermal condition 166.65 °C.

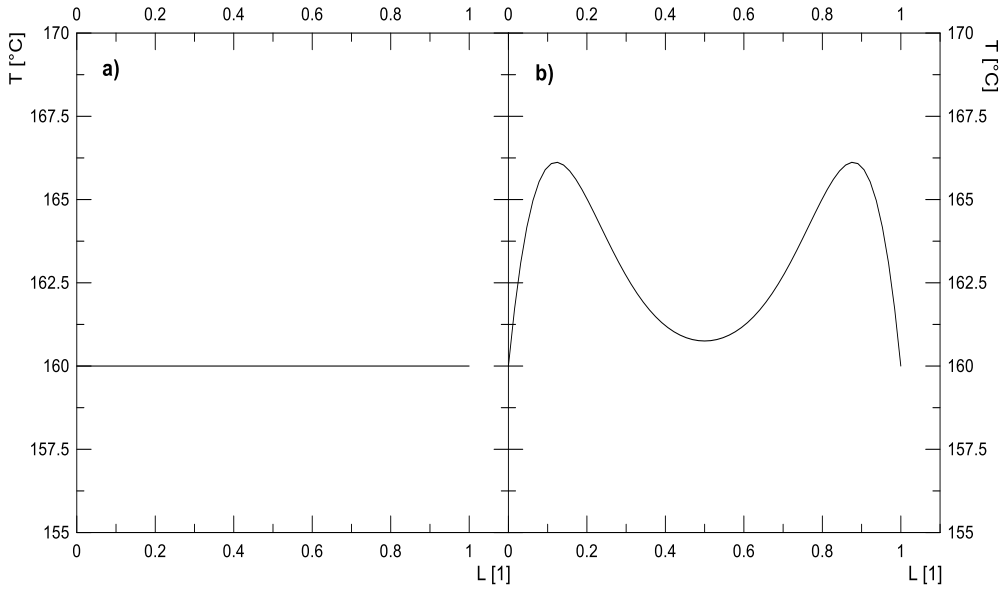

Figure 31: Temperatures in the steel body and flow channel for isothermal boundary condition: a) values at the polymer melt/steel interface - along, b) values across the flow channel

To understand better, the thermal effect we should look at the energy balance equation of the polymer melt. For isothermal boundary condition the energy balance equation will be calculated as difference between the sum of convection, conduction and dissipation. Result of equation 93 should be in ideal instance equal to zero. Energy balance equation of the polymer melt for an isothermal condition can be expressed as:

$$\left[k \times (2 \times (A_{wall} \times \frac{\Delta T}{L}))\right] + \left[\rho \times C_p \times 2 \times A_{input/output} \times \left[(\int v_{output} \times \int T_{output}) - (\int v_{input} \times \int T_{input})\right]\right] = \tau : \nabla \tag{93}$$

After substitution of variables obtained from simulations equation 93 is expressed as:

$$Conduction + Convection = Dissipation$$
$$7.674W + 4.736W = 12.53W$$
$$12.41W = 12.53kW$$

A little difference between the terms on each side could be caused by low density of the finite element mesh.

The second situation is with adiabatic boundary condition.

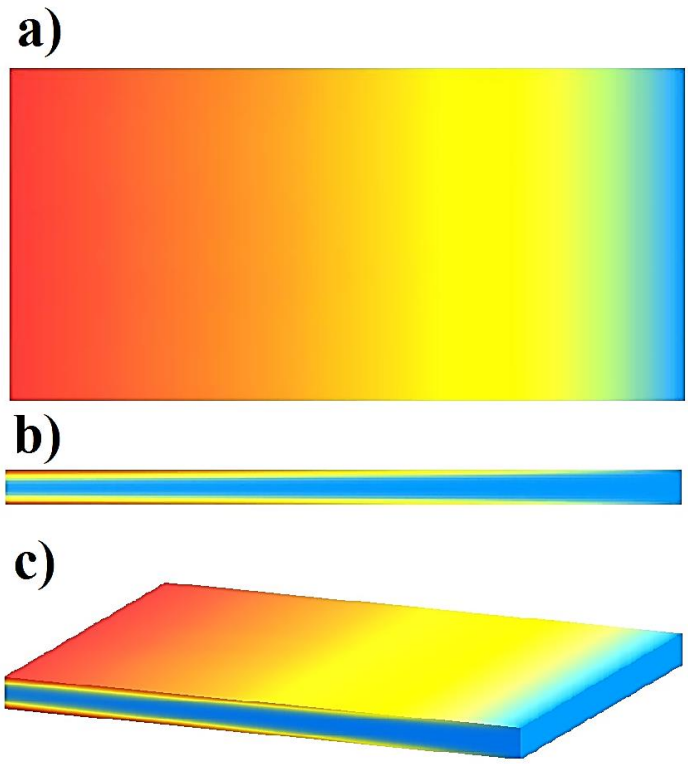

Figure 32: The flow situation with adiabatic boundary condition of the surface (Temperature field displayed): a) view on top, b) longitudinal section, c) 3D view of a body

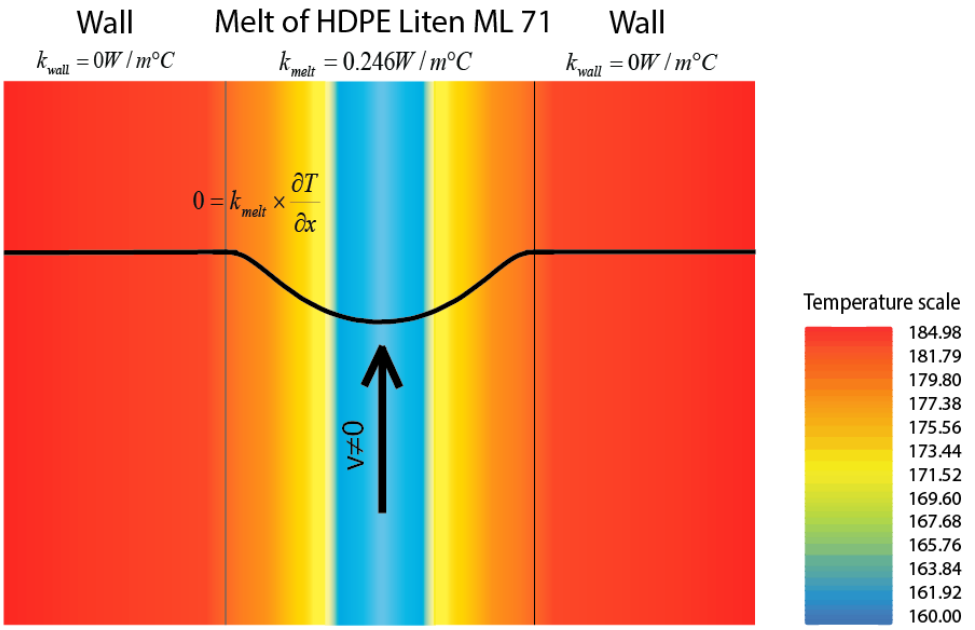

Figure 33: Temperature profiles across the flow channel at the end of the die with different thermal conductivity (adiabatic boundary condition)

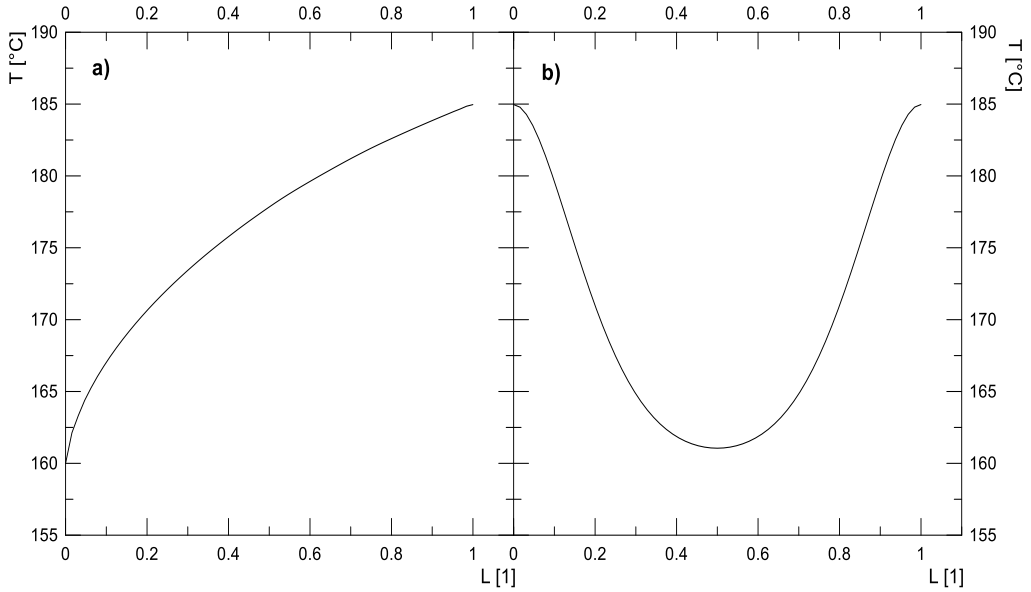

Figure 34: Temperatures in the steel body and flow channel for adiabatic boundary condition: a) values at the polymer melt/steel interface - along, b) values across the flow channel

Different views on a body with adiabatic boundary condition are shown in figure 32. In comparison with isothermal boundary condition it is possible to see increasing temperature in direction of the flow (Fig. 32a)). Also there is shown that walls are not cooled down by the polymer melt. Heat accepted from polymer melt is kept inside the walls.

In figure 33 is shown cross section temperature profile. The highest temperature is at the walls and also in the walls. On the other hand, the lowest temperature profile is in the middle of the channel. Curve of the increasing temperature profile has practically linear character until it reaches the maximum value of temperature at the wall. In comparison of ranges of temperature scale with isothermal condition, adiabatic condition has much higher values of temperature, from 160 °C in the middle to 184.98 °C at the walls. In this case thermal conductivity does not have such a big influence on the final temperature profile.

Figure 34 shows longitudinal section temperature profile across area of a body. As it was said, temperature increases in direction of the flow until it is reached walls. Dissipation energy generated by polymer melt is kept inside the walls.

Energy balance equation for adiabatic boundary condition can be written as:

$$\left[\rho \times C_p \times A_{wall} \times \left[\left(\int v_{output} \times \int T_{output}\right) - \left(\int v_{input} \times \int T_{input}\right)\right]\right] = \tau : \nabla \qquad (94)$$

$$Convection = Dissipation$$
$$11.76W = 11.83W$$

As in previous case, a little difference is caused by low solution mesh density.

As it was written on the beginning of this chapter, thermal behavior of the mandrel is somewhere between isothermal and adiabatic boundary condition.

The figure 35 shows the temperature as a function of mandrel length. Geometry composed from a body, flow domain and the mandrel is shown below in figure 35 under the curve. Geometry of the mandrel is followed by the curve. The first half of the mandrel is cooled down by polymer melt. However, in the second half mandrel is heated up by the dissipation energy. Pressure, mechanical energy is transform onto dissipation energy, respectively. These two thermal effects give final curve (fig. 35). Model situation is shown in figure 35. Mandrel and barrel have dimensions of mandrel used in submitted thesis. Temperature in the middle of the mandrel is 164.8 °C. In the first half the mandrel is cooled down to 160.4 °C. In the second half the mandrel is heated up to 168.8 °C. Mentioned cooling down and heating up can have crucial influence on the polymer melt flow. This knowledge has significant role for our new boundary condition.

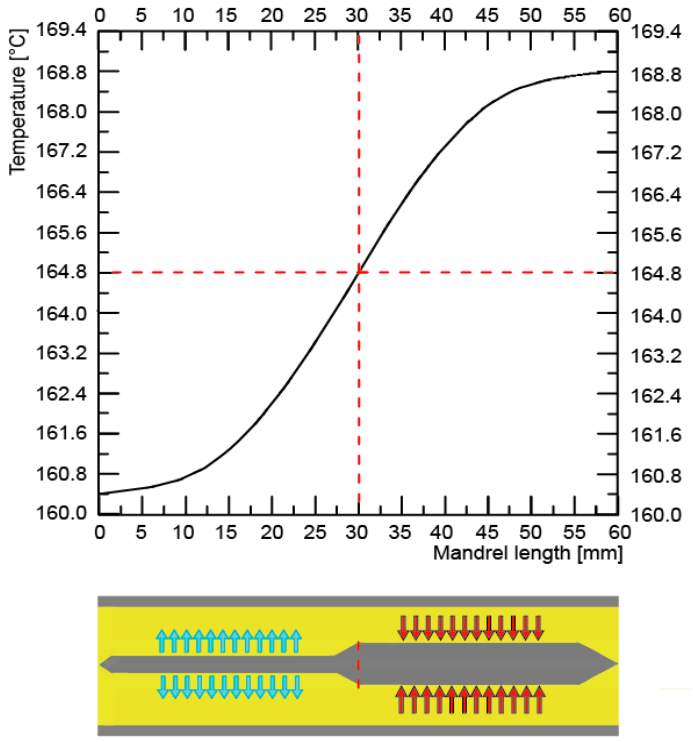

Figure 35: Longitudinal section temperature profile of the mandrel

7.2 3D Flow Domain

S To understand better, the thermal effects including viscous heating, conduction and convection we use an experimental die which includes narrow gaps, small isolated steel parts as well as heavy block of steel. This is the geometry presented in this chapter. The flow domain starts as a rectangular channel, then a mandrel is introduced creating narrow gap. This flow situation represents a typical flow condition observed in many extrusion dies.

In the previous chapter it has been explained, that the steel and melt stream interact thermally to minimize the overall resistance.

Simulation software VEL^{TM} 3DFem module provides a unique solution where steel can be a part of the thermal calculation, it is coupled with the flow domain! This approach has, however, also some drawbacks. For example, meshes of the flow domain and the mandrel have to be dense enough. In real life cases this can lead to millions of elements. Moreover, the connecting surfaces of these two meshes have to be exactly topologically conform - connected together. As a consequence, it leads to expensive solution, relatively long calculation times (often more than 24 hours). On the other hand, the 3DFem module solution provides exact solution of the problem and it is possible to construct even the most difficult flow domains and geometries.

For us the 3DFem solutions used as a verification of our modelling results. Here the boundary condition for outside melt/body surface was chosen to be the isothermal condition (as the body is usually big block of steel with sufficient thermal conductivity). Due to double symmetry only one quarter of the problem needs to be solved.

As the two meshes (steel mesh and flow mesh) are solved together and need to interact, the melt/mandrel interface needs to be marked by special type of boundary condition The Interface indicates a connection between two materials.

The mass flow rate input boundary condition was chosen at the entrance of the polymer melt. At the exit we have used an Output boundary condition. All of mentioned boundary conditions are shown in figure 36.

As material the HDPE Liten ML 71 was selected. The initial temperature for the isothermal walls and for the polymer melt was set to 160 °C. Mass flow rate of the polymer melt was set to 10 kg/h.

In figure 37 the decomposition of the calculated the flow domain with the mandrel is shown. Whole decomposition begins as a complete domain (flow domain + mandrel) and then it is decomposed on smaller part. In the end only ¼ of the mandrel and ¼ of the flow

domain are present. Calculation in 3DFem module were made only on ¼ of the whole flow channel.

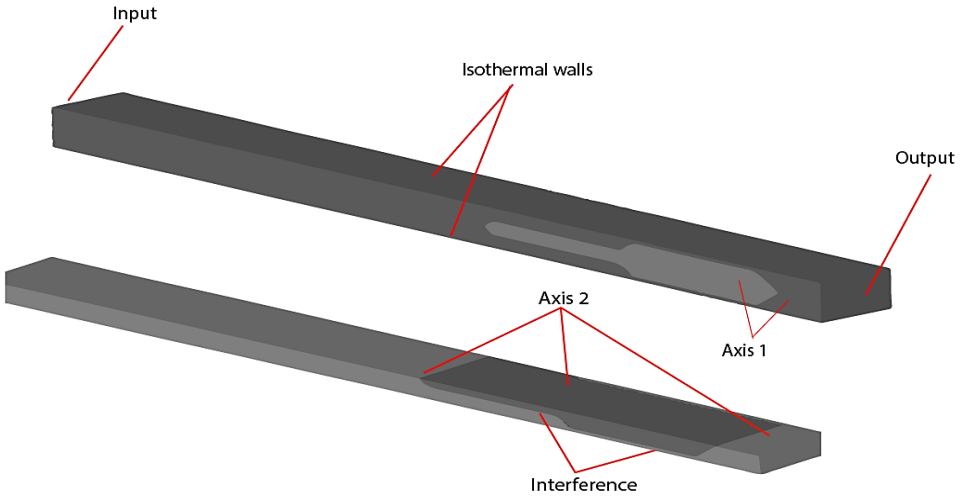

Figure 36: Boundary conditions of the flow domain with the mandrel

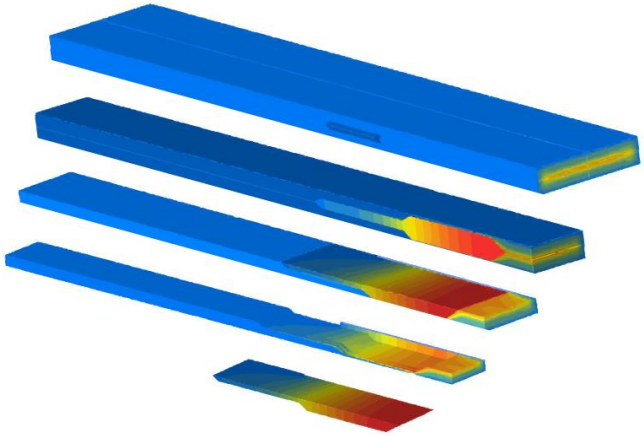

Figure 37: Decomposition of the 3D model (flow domain + mandrel) of the extrusion die

Temperature profile across the flow channel is shown in figure 38. Each from these curves have different position along the flow channel.

Temperature at the wall is 160 °C for all curves. Here it is assumed that the barrel has constant temperature and all conducted heat from the polymer melt is removed out. Temperature profiles close to the mandrel wall depends on the position in the flow channel. Figure 38 shows, that mandrel is heated up by dissipation from position 1 up to position 4. At position 4 mandrel is overheated up to 175 °C. Accepted heat is then part of the heat flow inside the mandrel. We can see in figure 37 that the mandrel is overheated mostly at the end and on the beginning it is cooled by the polymer melt.

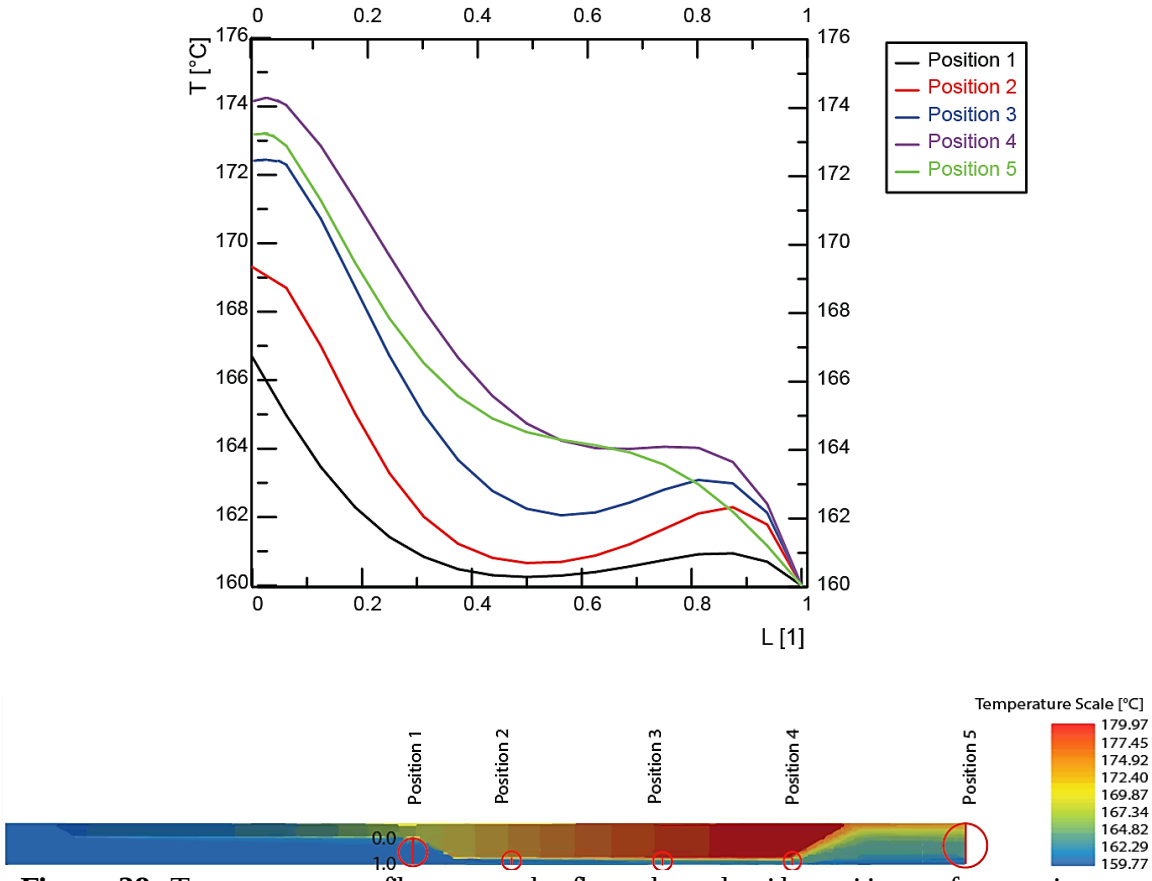

Figure 38: Temperature profile across the flow channel with positions of measuring

The major viscous heating occurs at the narrow gap channel. Mainly at the end the polymer gets really warm due to viscous heating. The heat is partly absorbed by outside body steel, non-negligible amount of energy comes also to the mandrel and heats it up. So it is not isothermal anymore. Temperature profile along the length of the mandrel (at the melt/mandrel interface) is shown in figure 39a). As it was mentioned, the mandrel has heat flow "loop".

The mandrel, however is more or less insulated inside the melt stream, it is connected to outer body only on its rear end. So the energy absorbed from the melt must be conducted back. Well as the heat in the mandrel comes back and heats the rear part of the mandrel too, it becomes warmer then the incoming polymer and also warmer than the outer walls. Then the mandrel is cooled by the polymer melt flowing slowly. At this part the channel is usually open and material flows slowly. There is minimal influence of dissipation. It means that polymer is cold and able to take out the heat from the mandrel.

From figure 39b) is obvious that temperature across the mandrel is constant so it is possible to neglect this factor in 2D simulation.

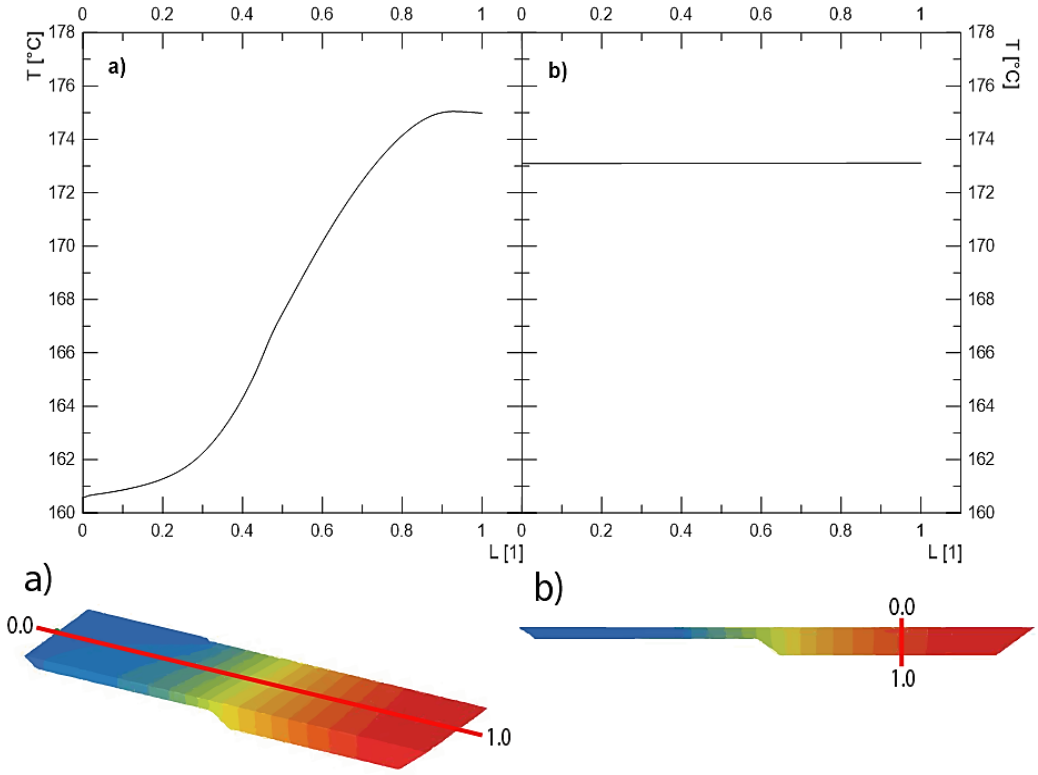

Figure 39: Temperature profile of the mandrel: a) along; b) across

Figure 40 shows temperature and pressure profile with help of the pathline, a path of a particle which seed was placed to the middle of the flow domain. Pressure curve is practically linear until channel depth decreased, then the pressure is consumed It means also that mechanical energy is transformed into the thermal energy, generation of the heat at the expense of pressure. Maximum value of pressure is 28 MPa and it decreases down to zero. Temperature in the middle of the flow domain increases its value up to 163 °C (and this is still not the hottest melt part).

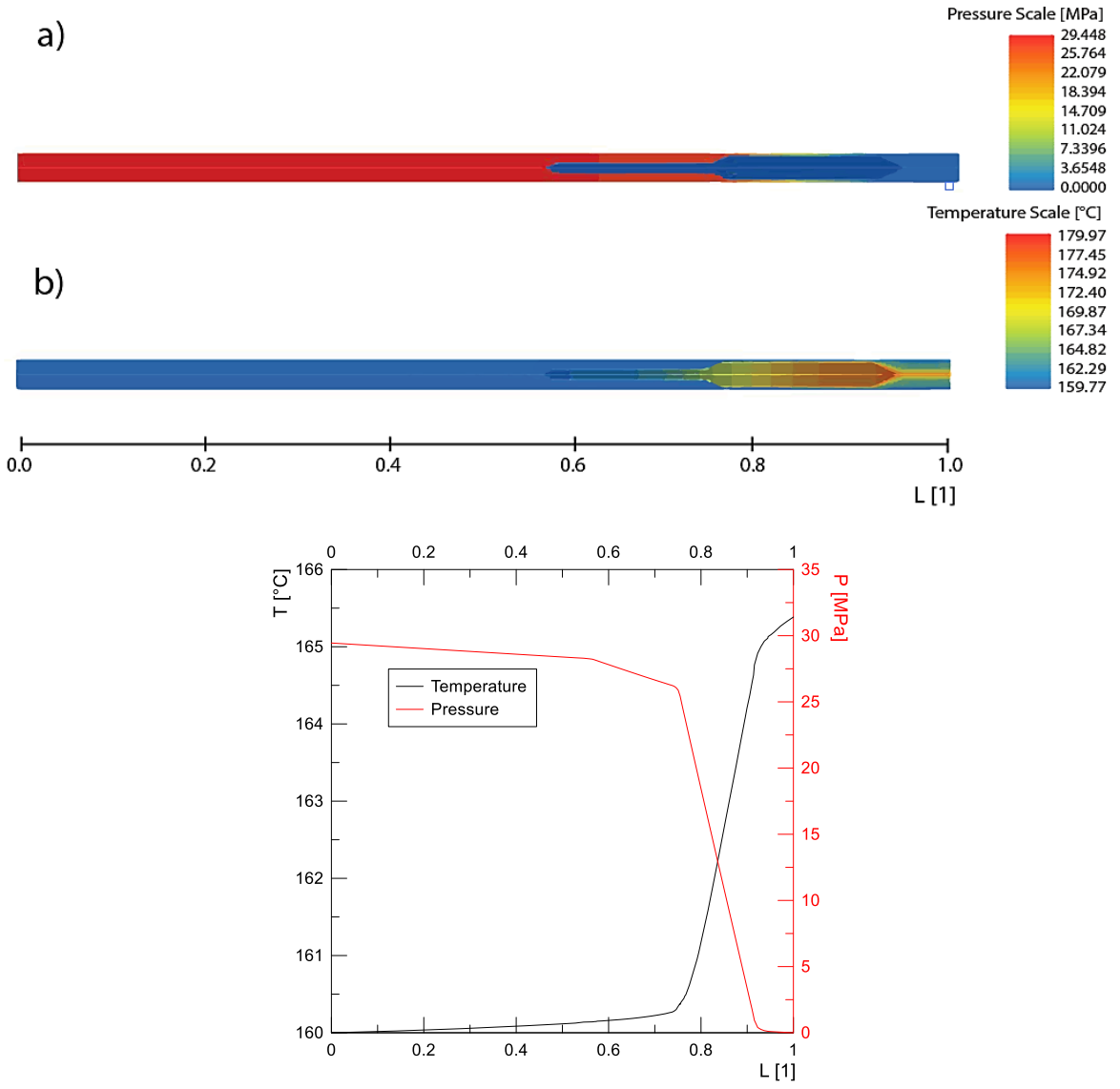

Figure 40: Graphs along the pathline located in the middle of the flow domain: a) pressure; b) temperature

7.3 2D Flow Domain

As we could see the 3DFem solution with mandrel steels walls is possible, however too complex for real life extrusion die simulation. The understanding obtained from the coupled steel and melt heat flow simulation using 3DFem, mainly the described heat "loop", helps us to find out reasonable simplification leading to very practical solution procedure. This approach could effectively lead to replacing the mandrel steel mesh by simple 1D heat transfer iterative solution. That simplifies the overall process of meshing, boundary assignment, and speeds up the solution. Such a calculation still keeps the mandrel / melt interaction and heat exchange.

We want to develop here a new simulation approach, in the 3DFem model it will become simply a new boundary condition for wall.

This boundary condition would be applicable to 3DFem simulation or even 2DFem simulation. For simplicity, we well use a 2DFem module of the software VEL^{TM} and derive the solution procedure here.

Nowadays the 2DFem module does not have the ability to include a steel mesh as a part for the solution, neither it has complex boundary conditions for steel tools (mandrels) inside the extrusion channels. Currently only isothermal and adiabatic boundary conditions are supported.

Geometry for 2DFem module is shown in figure 41. Red rectangle shows important area where most of our analysis were made. Description shows set of boundary conditions. Parameters of simulations were set as: Initial temperature 160 °C, mass flow rate 10 kg/h, temperature of walls 160 °C/insulted walls/new boundary condition.

7.3.1 The Isothermal Case of the 2D simulation

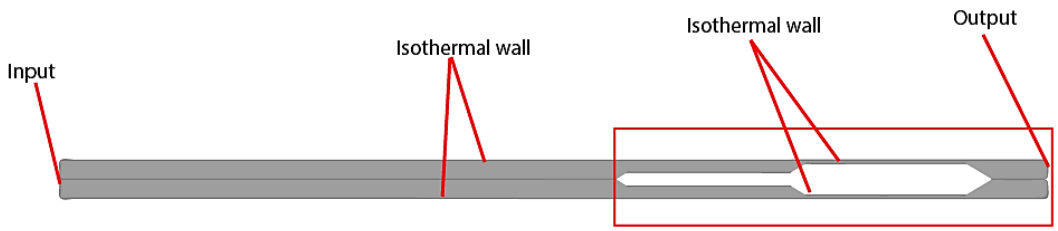

Figure 41: 2D geometry of the extrusion die with boundary conditions (isothermal case)

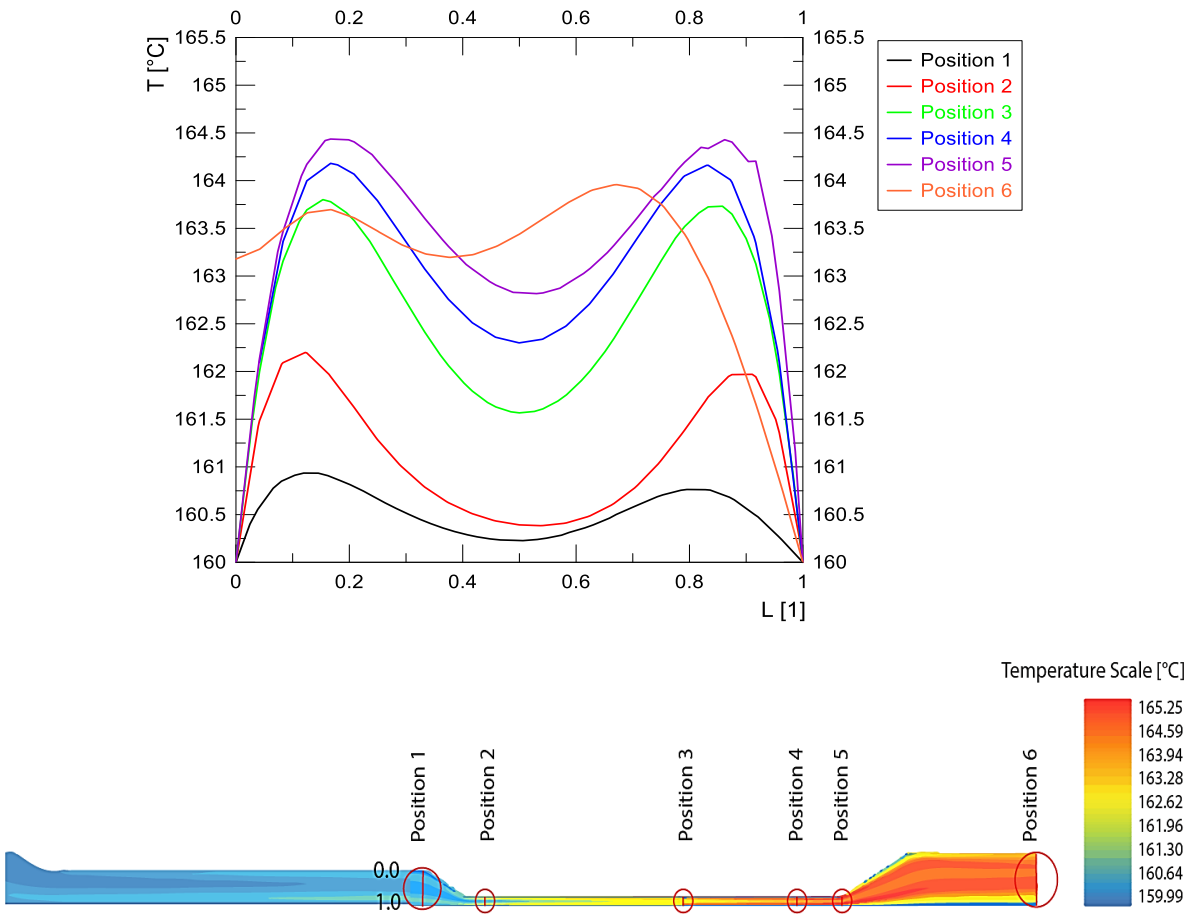

Figure 42: Temperature profile across the flow channel with positions of measuring (where mandrel is placed)

Cross section temperature profile of the flow channel for isothermal boundary condition is shown in figure 42. From position 1 where the flow channel decreases its depth, small influence of dissipation is present. Material starts to overheat. After position 1 dissipation increases its value until position 5, where the highest temperature is generated (164.5 °C). Here you may ask yourself, why the cross section temperature profile is not only linear curve without any peeks, when walls are removing the heat? Well, it is because of different thermal conductivity of materials. On one hand, thermal conductivity of steel is high, on the other hand, temperature of the polymer melt is very low. It took a time to remove out the heat from the polymer melt and because the velocity of polymer melt flow is also too high, then dissipation is present and material is overheated.

The only different in temperature profile is the one at position 6. Due to the sudden increase of the channel depth and bigger amount of material (connection of two symmetric parts) melt velocity slows down and the temperature decreases. Characteristic isothermal

behavior (except of position 6) is shown in figure 42. Curves have beginning and end at temperature 160 °C. All available heat is removed out from the walls to the free space.

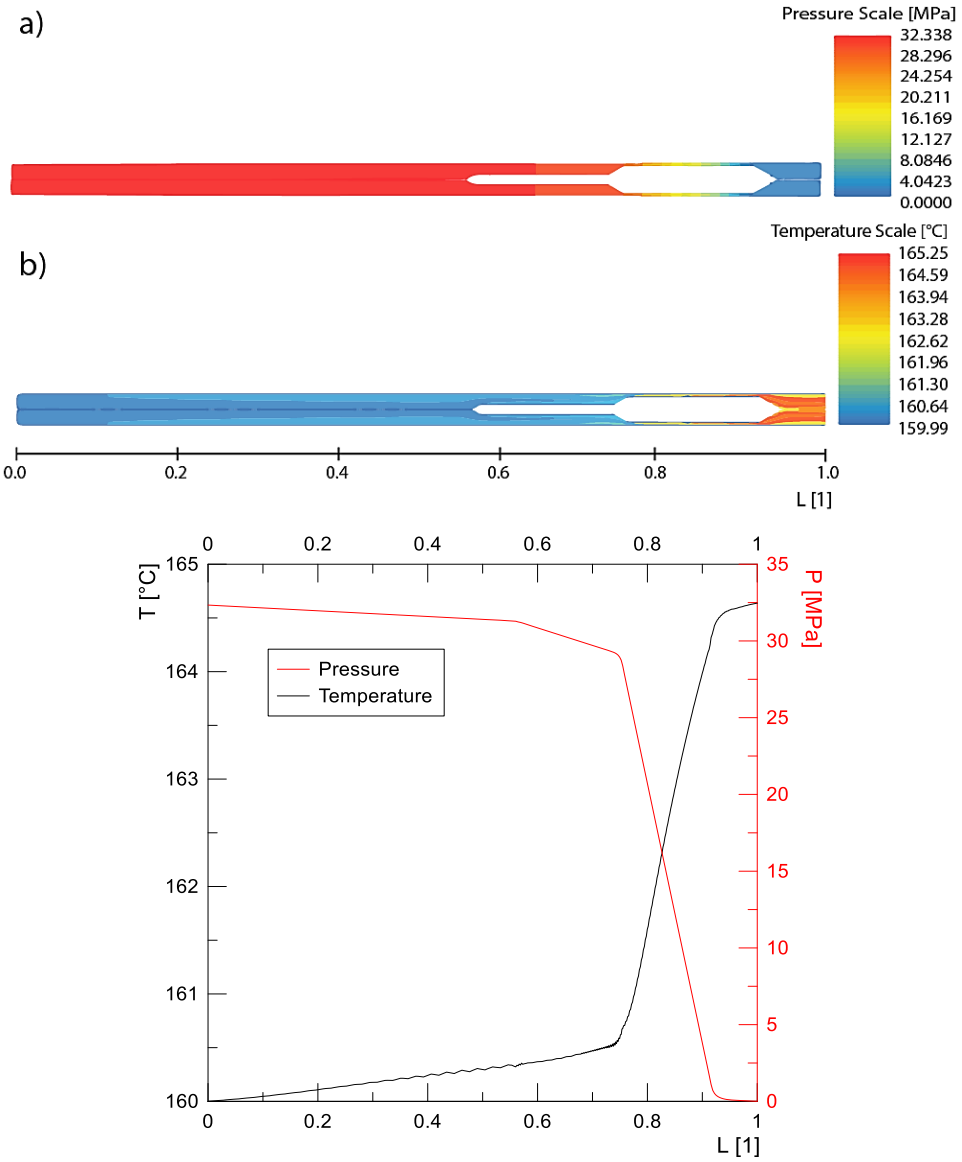

Figure 43: Pathline profiles in the middle of the flow domain (isothermal condition): a) pressure; b) temperature

Temperature and pressure profiles shown in figure 43 were described with help of pathline. This pathline seed was placed in the middle of the flow channel and the particle went through the whole length of the flow channel. In the three quarters of our geometry the pressure is consumed only a little bit. The decrease of the channel depth caused that large pressure is consumed in that section. Curves in figure 43 are interdependent. When pressure is consumed, the mechanical energy is consumed too and the temperature increases its value due to dissipation. In isothermal case can reach temperature as high as 164.5 °C.

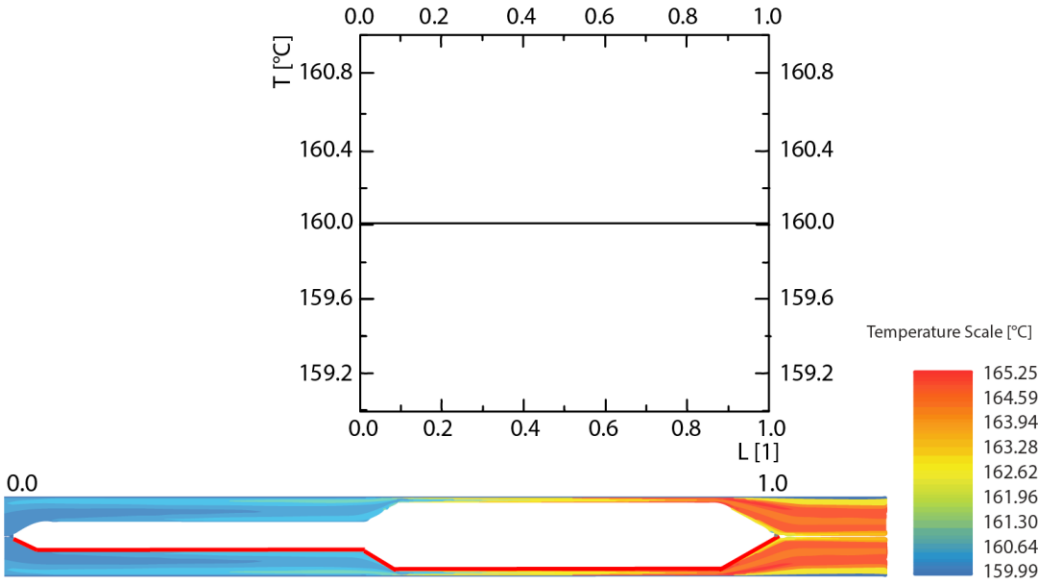

Figure 44: Temperature on the surface of the flow channel, where mandrel is placed (isothermal condition)

Temperature profile on the surface of the mandrel is shown in figure 44. All heat was removed out by steel to the free space. This boundary condition is not suitable for practical simulations. In reality it is not possible to remove out all heat from the mandrel walls. Temperature here is constant along the entire length.

Other interesting variables could be the shear stress along the wall, shear rate of the polymer melt and velocity. The highest shear stress along the wall in case of isothermal boundary is 271.67 kPa. In case of HDPE it could cause wall slip. Maximum value of shear rate at the walls 2270 s^{-1}. The highest velocity reached 192.23 mm/s.

7.3.2 The Adiabatic Case of the 2D simulation

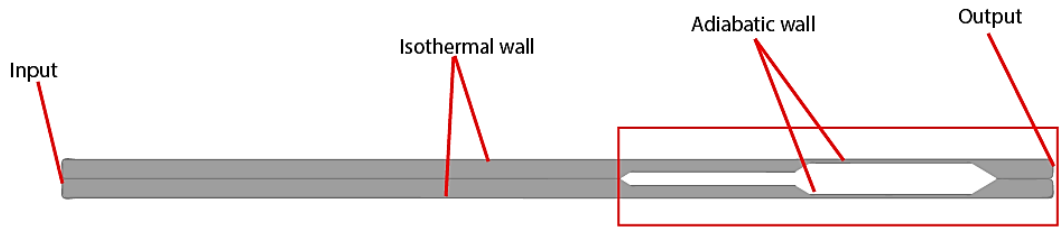

Figure 45: 2D geometry of the extrusion die with boundary conditions (adiabatic case)

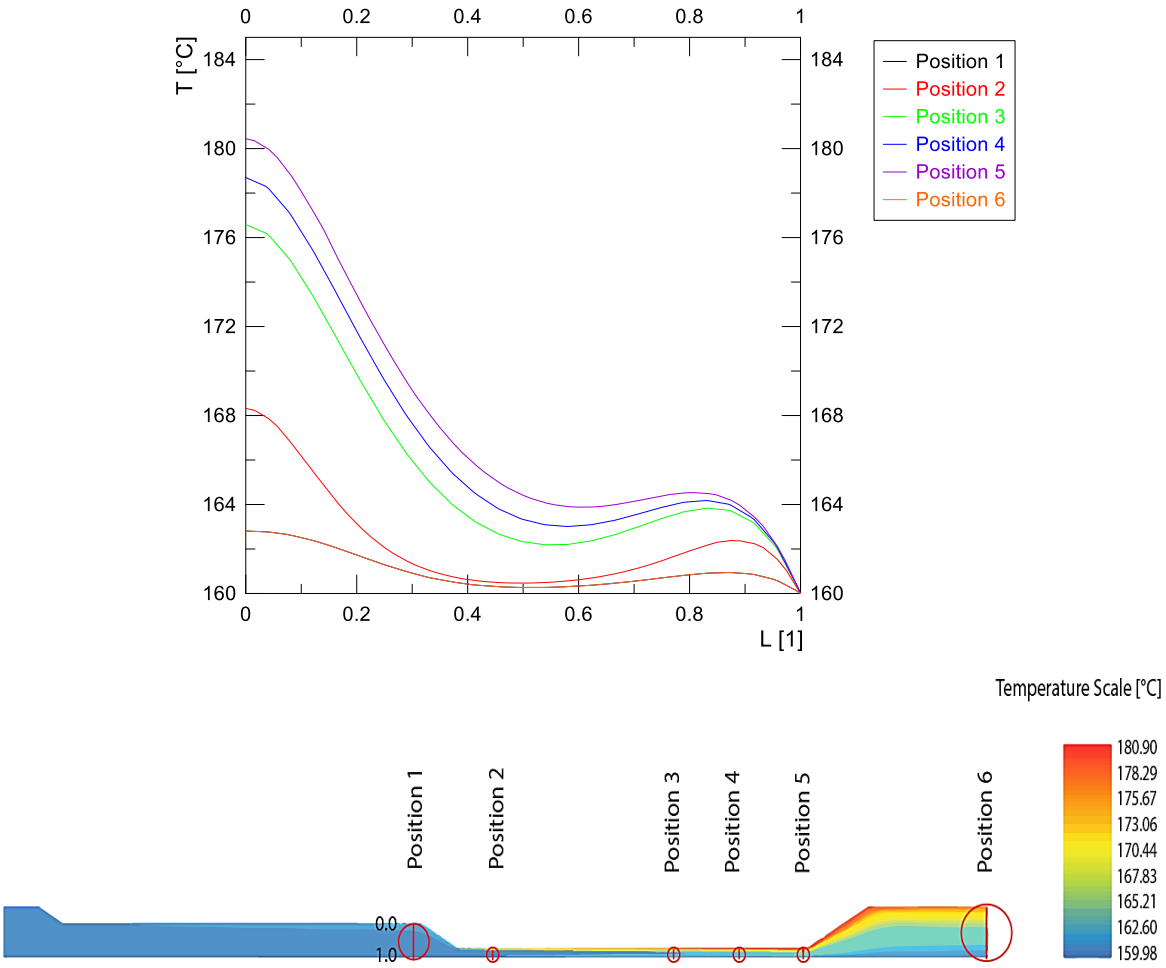

Figure 46: Temperature profile across the flow channel with positions of measuring (where mandrel is placed)

Temperature profile across the flow channel is displayed in figure 46. Positions of measuring with temperature scale are shown in figure under the graph. Here the trend of curves is different when comparing with isothermal boundary condition. Adiabatic boundary condition was set only at wall where mandrel is placed. Heat is not removed out from the surface of the mandrel and temperature gradient along the length is present. At position 1 influence of the heat generated by dissipation is not so strong. But with the next positions the influence becomes higher and higher and the temperature close to the mandrel increases its value. On the other hand, surface of the outside wall (body) was set as isothermal. It is the reason why on one side of the wall is constantly 160 °C and on the other side s temperature always higher than 160 °C, up to 180 °C, respectively. At the exit of the extrusion die (position 6) it is possible to see that temperature is decreased up to temperature at position 1. It is again because of lower velocity and bigger amount of material due to connection of two symmetric parts.

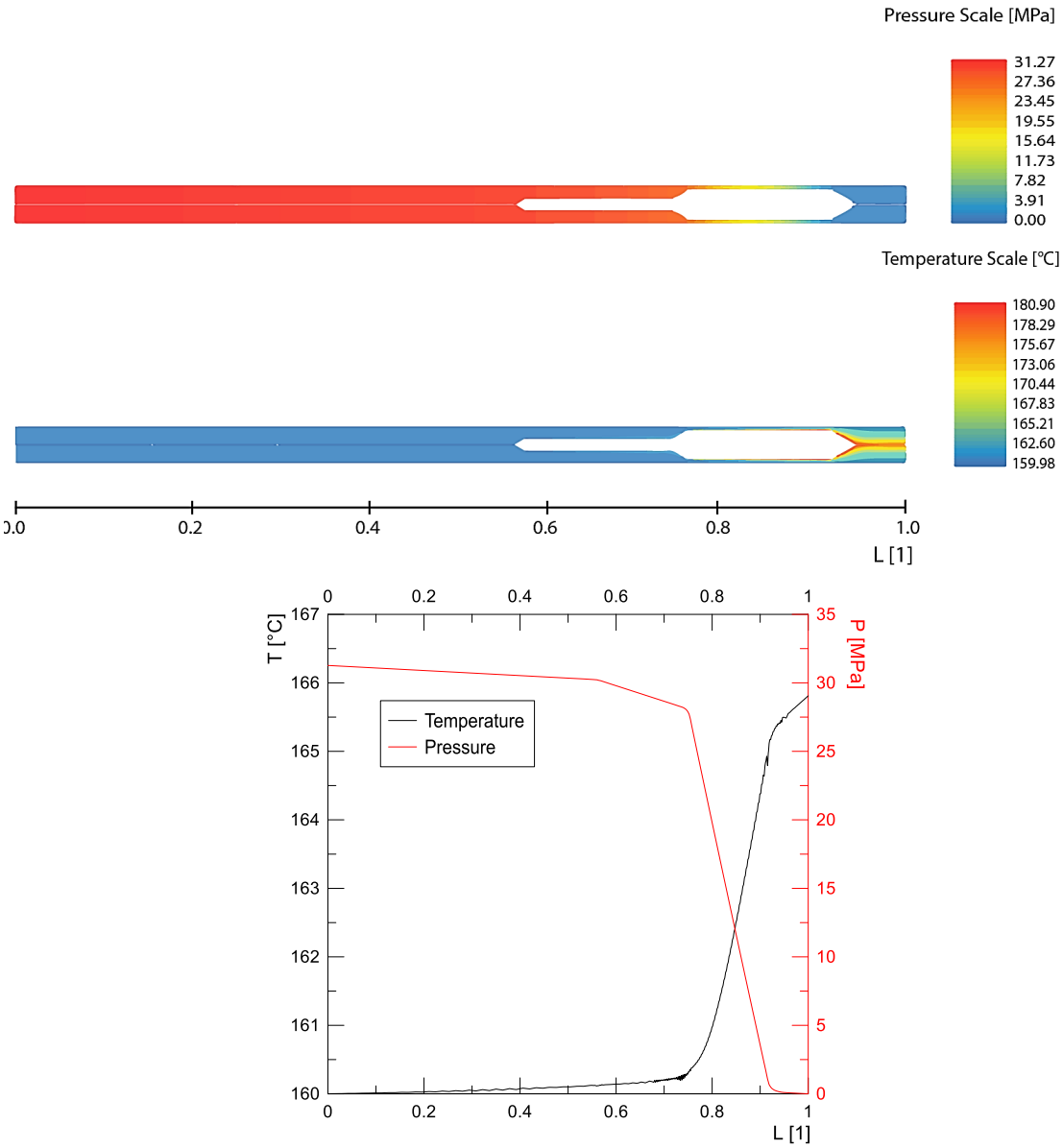

Figure 47: Pathline profiles in the middle of the flow domain (adiabatic condition): a) pressure; b) temperature

Temperature and pressure drop along the length of the flow channel is displayed in figure 47. These curves were obtained by using of pathline. Pathline was placed in the middle of the flow channel. Curves in figure 47 have similar trend as isothermal case of boundary condition at the wall of the mandrel. The only difference is the values reached. In case of adiabatic condition lower pressure was observed but higher temperature (due to higher temperature at the wall of the mandrel). Melt interface reaches the maximum temperature as the heat generated can be conducted (and then conveyed) away only by polymer.

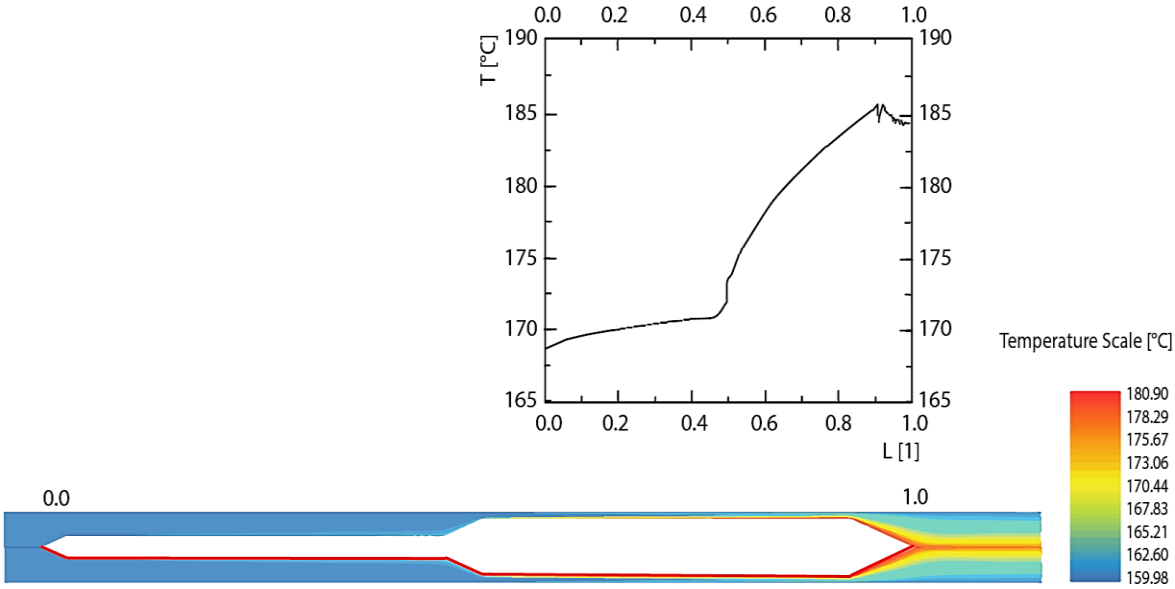

Figure 48: Temperature on the surface, where mandrel is placed (adiabatic condition)

Temperature curve on the surface of the mandrel is shown in figure 48. This curve has more realistic trend as the curve of isothermal condition case. It is because of adiabatic wall, which keeps the heat inside and the temperature is increased. Here is no assumption of heat flow inside the mandrel. It is assumed that the mandrel at each position is only heated up to get to the melt temperature (maximum found was 186 °C).

We can see that neither the isothermal, nor the adiabatic boundary conditions match the reality well. This is the reason why it is necessary to create a new boundary condition for steel tools (mandrel) inside the flow channel.

The highest shear stress along the wall in case of adiabatic boundary was found to be 267.22 kPa. Maximum value of shear rate at the walls reached 2190 s^{-1}. The highest velocity reached 190.98 mm/s.

7.3.3 The Developed New Boundary Condition for the 2D simulation

The developed new boundary condition is based on assumption that mandrel is described by 1D domain. This 1D domain is divided into 26 points. The energy equation was then solved by Finite difference numerical method. The solution was performed in software Maple. Example of model calculation is shown below.

The energy balance between the steel and polymer melt can be written as

$$k_{steel} \times \frac{\partial^2 T}{\partial x^2} = k_{melt} \times \frac{\partial^2 T}{\partial y^2} \tag{96}$$

and thermal conductivity of the polymer melt in direction y as:

$$\dot{S}_i = k_{melt} \int_{A_i} \frac{\partial T}{\partial y} \times d\, A_i \tag{97}$$

The second derivative can be (using Taylor series) expressed as:

$$\frac{\partial^2 T}{\partial x^2}^i = \frac{T_{i+1} - 2 \times T_i + T_{i-1}}{(\Delta x)^2} + O\left((\Delta x)^2\right) \tag{98}$$

If we make substitution:

$$\psi = \frac{k_{steel}}{(\Delta x)^2} \tag{99}$$

We can write:

$$\psi \times T_{i+1} - 2 \times \psi \times T_i + \psi \times T_{i-1} = \dot{S}_i \tag{100}$$

From equation 99 is expressed general matrix of heat flow inside the mandrel as:

$$\psi \times \begin{bmatrix} -2 & 1 & 0 & 0 & 0 \\ 1 & -2 & 1 & 0 & 0 \\ & \ldots & \ldots & \ldots & \\ 0 & 0 & 1 & -2 & 1 \\ 0 & 0 & 0 & 1 & -2 \end{bmatrix} \times \begin{bmatrix} T_0 \\ T_1 \\ \ldots \\ T_{n-1} \\ T_n \end{bmatrix} = \begin{bmatrix} \dot{S}_0 \\ \dot{S}_1 \\ \ldots \\ \dot{S}_{n-1} \\ \dot{S}_n \end{bmatrix} \tag{101}$$

The sum of the heat fluxes on isolated mandrel at steady state should be zero:

$$S = \sum_i S_i = 0 \tag{102}$$

Boundary condition for end nodes can be expressed as:

$$T_0 = const. \quad \text{and} \quad \left(\frac{\partial T}{\partial x}\right)_n = 0 \quad \text{respectively.} \tag{103}$$

What simplifies to

$$T_0 = T_{initial} \qquad \text{and} \qquad T_{ni} = T_{ni+1} \qquad \text{respectively.} \tag{104}$$

The tridiagonal matrix can be formed and the system of equation is:

$$\psi \times \begin{bmatrix} -1 & 1 & 0 & 0 & 0 \\ 1 & -2 & 1 & 0 & 0 \\ & \dots & \dots & \dots & \\ 0 & 0 & 1 & -2 & 1 \\ 0 & 0 & 0 & 1 & -1 \end{bmatrix} \times \begin{bmatrix} T_0 \\ T_1 \\ \dots \\ T_{n-1} \\ T_n \end{bmatrix} = \begin{bmatrix} 0 \\ \dot{S}_1 \\ \dots \\ \dot{S}_{n-1} \\ 0 \end{bmatrix} \tag{105}$$

Flow domain where simulation was made and boundary conditions which were chosen are shown in figure 49. As a boundary condition for outside walls an isothermal boundary condition was picked. Interference between the polymer melt and the mandrel is made by the developed boundary condition described above.

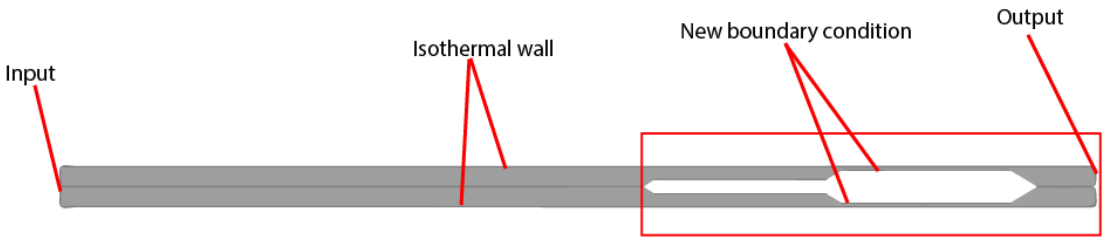

Figure 49: 2D geometry of the extrusion die with the developed new boundary condition

Temperature profile across the flow domain is shown in figure 50. Trend of the curves in figure 50 is very close as in the case of the 3D simulation. At the wall L=1 (Body) temperature is assumed to be constant. At the mandrel wall L=0 it is shown that the temperature along the mandrel increases. But from the derivation of the normal line in direction X we can find out if mandrel is cooled or heated. From figure 50 we can say, mandrel is cooled down until position 3, then is heated up. Heat migrates in or out to the mandrel, respectively

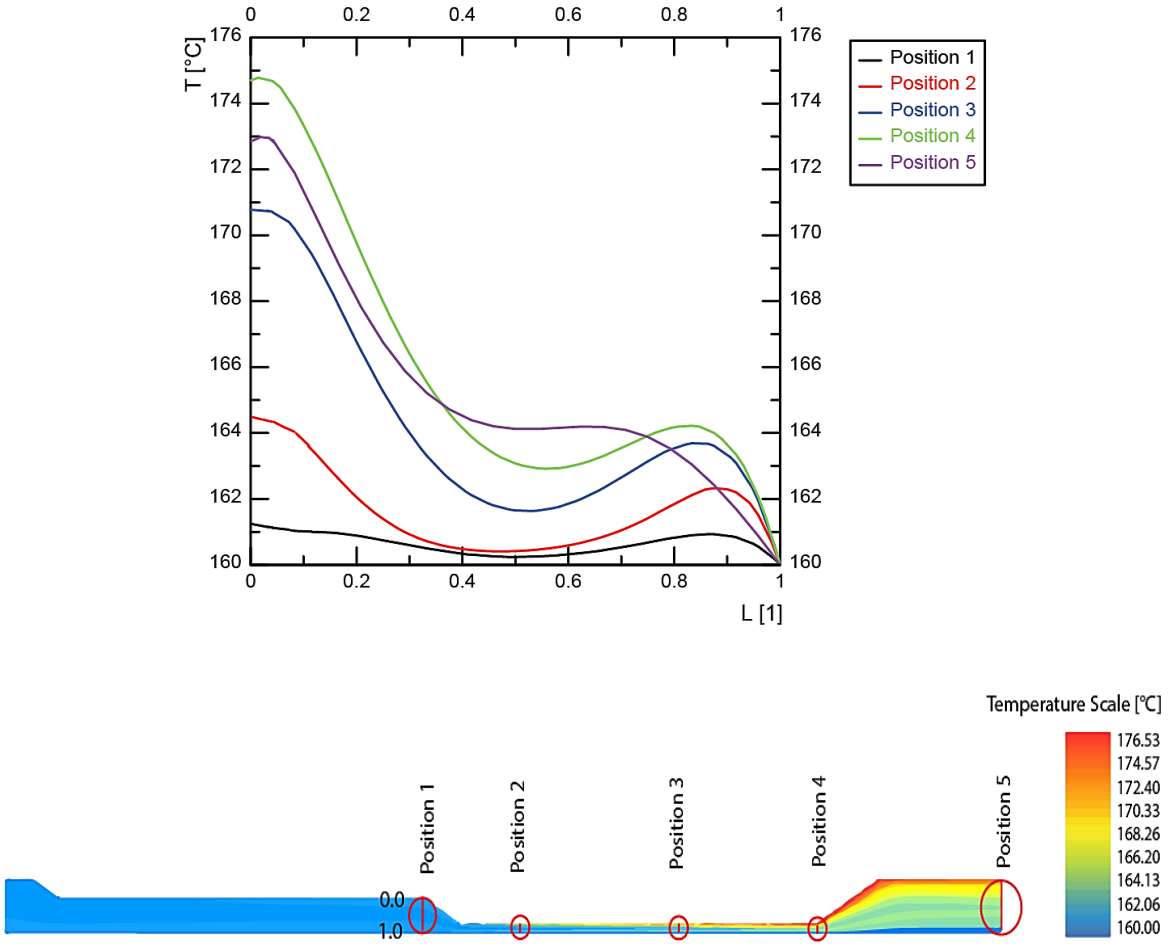

Figure 50: Temperature profile across the flow domain with positions of measuring (where mandrel is placed)

Figure 51 shows pressure and temperature profile along the length of the mandrel due to the pathline placed in the middle of the flow domain. Here it is similar trend as in previous cases, only difference is in values of pressures and temperatures. Temperature, dissipation is generated when pressure is consumed.

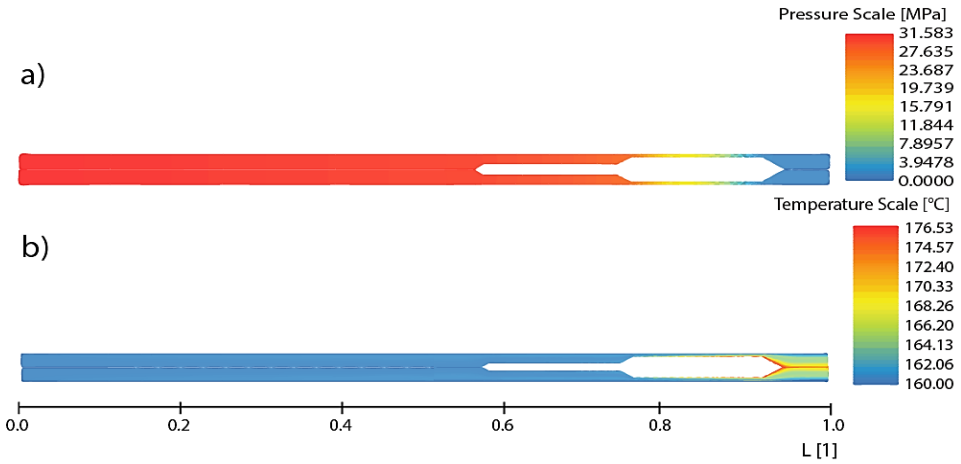

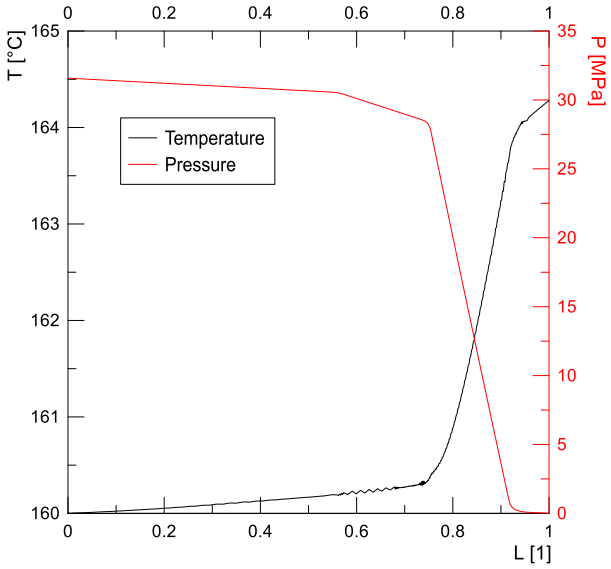

Figure 501: Pathline profiles in the middle of the flow channel (new boundary condition): a) pressure; b) temperature

Heat flow, temperature profile along the surface of the mandrel is shown in figure 52. As we simplified in 3D module, temperature profile inside the mandrel across the height is constant because of high thermal conductivity of steel. Trend of the curve in figure 52 is similar to the temperature profile in 3D module. In the end of the mandrel temperature reached up to 176.2 °C.

In comparison with results from 3DFem module the temperature is a little bit higher (difference 0.7 °C). It is because in 3D module the wall which fixes the mandrel to the body of the extrusion die is present. In case of 2D there is no possibility to have this wall in simulation. The wall mentioned cause some extra removal of the heat, resulting in smaller temperature profile.

In comparison with adiabatic condition, the mandrel is not overheated that much and it is partly cooled down by the cold polymer melt coming from the back of the die.

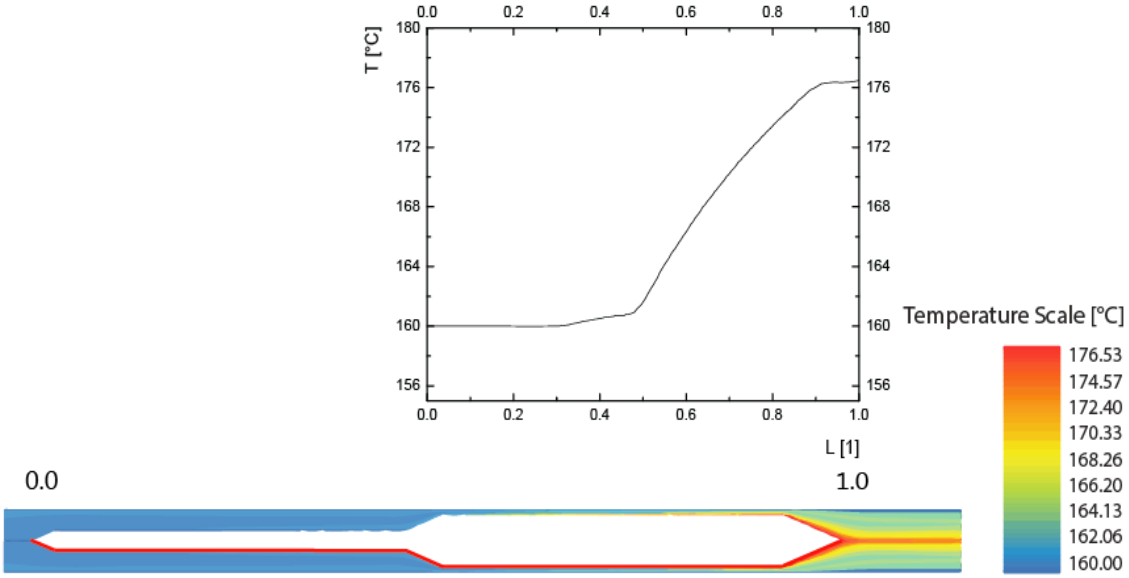

Figure 512: Temperature on the surface of the flow channel, where mandrel is placed (new boundary condition)

8

Real Extrusion Process

8.1 Extruder

As an extruder for extrusion process in submitted thesis was used BOCOMATIC EB 30 made by company Boco Pardubice Machines s. r. o. Technical parameters of used extruder are shown in table 3.

Table 3: Technical parameters of used extruder

Parameter	Unit	Value
Total electric load	kW	4
Screw speed	RPM	min. 5 – max. 80
Wattage of the machine	kW	7
Screw diameter	mm	40
Screw length	L/D	14
Screw type	1	single-thread pitch
Screw material	1	Nitride or armour
Barrel material	1	Nitride or bimetallic
Barrel cooling	1	Water cooling
Extruder length	mm	1030
Extruder width	mm	450

8.2 Extrusion Die

Extrusion die was constructed by company Compuplast s. r. o. Dimensions of the extrusion die are mentioned above.

Figure 523: Constructed extrusion die without heaters

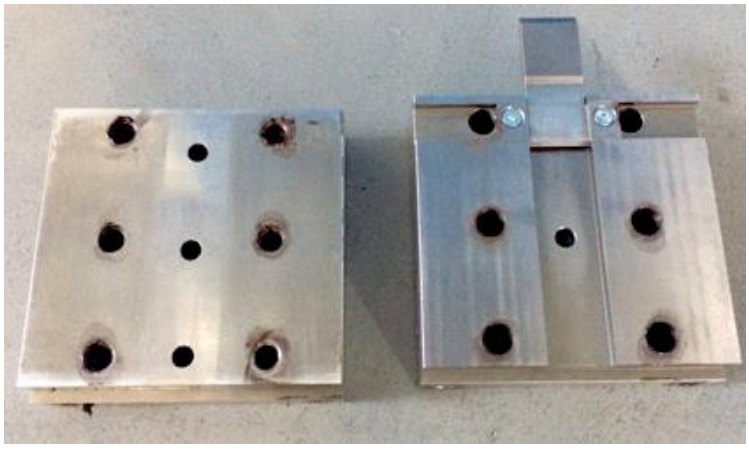

Figure 534: Constructed extrusion die channel with the mandrel

8.3 Measuring Tools

In this thesis three measuring tools were used. Infrared probe devices were used for measuring of melt temperature inside the extrusion die. Thermocouple wire was used for measuring of temperature inside the mandrel and pressure melt transducers were used for monitoring of the pressure.

For measuring of polymer melt temperature were used infrared probe devices instead of thermocouple sensors. It was because of fast response time and non-influence of heated up extruder barrels on our measuring (optical mechanism of infrared sensors) in case of infrared probe devices.

8.3.1 Infrared Probe Devices

In this thesis were used three high speed fiber optic infrared probes devices. Basically it is line of transmitters which measures a temperature range of 150 °C to 425 °C. The fiber optic cable behaves as a waveguide to bring the radiation (energy with specific wave length) to the infrared detector assembly in the electronics package. This electronic package works on mechanism of converting the infrared radiation delivered by optic cable into a reading system. The signal (emitted energy from surface of measured object) is transmitted optically and electrical or magnetic effects are neglected. This device consists from transmitter, type OS 4000, and polymer bolt probe assemblies, type 2108-650-RA-6, obtained from company Omega® (USA). The transmitter offers adjustable emissivity from 0.05 to 0.99, adjustable sensitivity of measuring and adjustable response time from 1 ms to 3200 ms. Emissivity value depends on the material and the surface conditions. Emissivity is the first approximatively measured by compering of measured temperature by infrared sensor with another test method (thermocouple). Technical draw of this sensor is shown in figure 55. As a recorder of the temperature profile was used software by company Omega. (Cheatle, 2006, Huddleston, 2007)

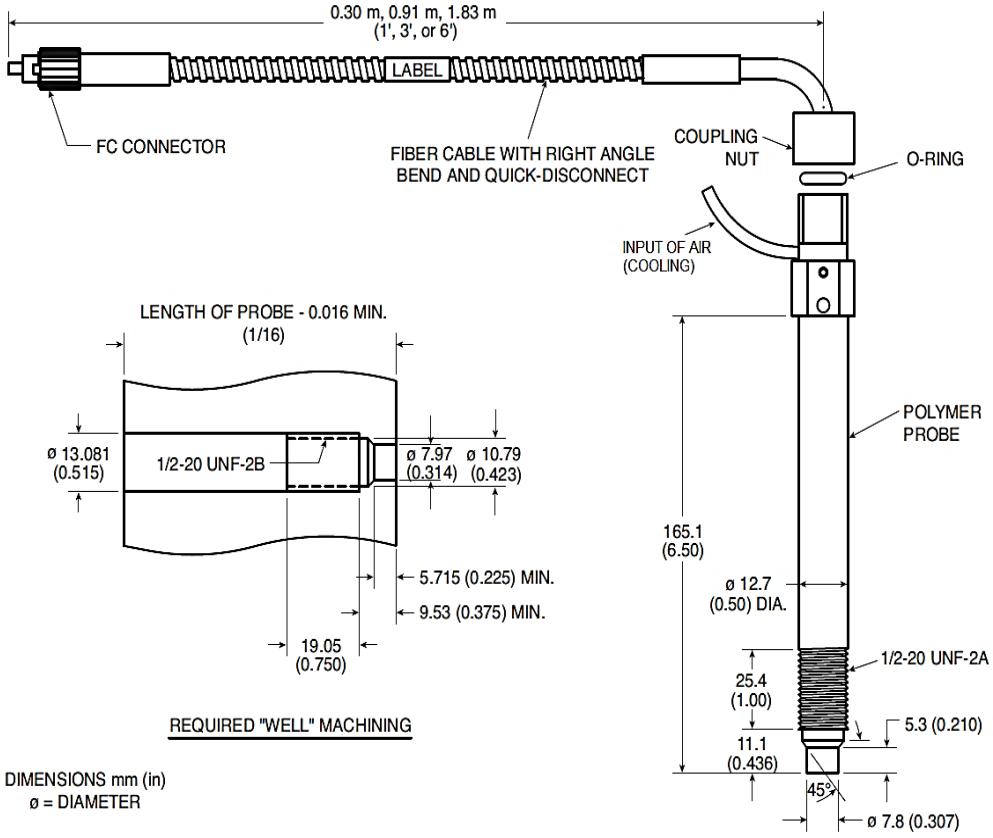

Figure 545: Technical draw of infrared probe device

8.3.2 Thermocouple Wire

In case of thermocouple wires is temperature measured electronically. Typical thermocouple set consists from pair of dissimilar metals, wires (positive and negative conductor), electrically joined together at the sensing point. The opposite ends of the wires are connected to the voltage device. When one end has different temperature than the end on the other side, thermal electromotive force is present in form of millivolts.

In other words, two wires, made from different materials, are joined at the point. This junction is placed at the point where is necessary to know actual temperature. If it is difference between temperatures of the junction location and the measuring location, then a small voltage is generated. The magnitude of the voltage is equal to the temperature gradient. Most of the thermocouple wires are insulted with help of heat resistant material jacketing. There are several types of thermocouple wires. They are classified according to the heat resistance and materials which they are come from. We recognize type J (Iron-Constantan), K (Chromel-Alumel), T (Copper-Constantan) and E (Chromel-Constantan). (Carniglia and Barna, 1992, Cheatle, 2006)

8.3.3 Pressure Transducers

Pressure devices measure pressure applied to an exposed surface of the pressure transducer. Polymer melt is measured by the melt pressure transducers. Melt pressure transducers are very often used in extrusion and blow molding processes. Mechanism of melt pressure transducers can be based on a hardened diaphragm, strain gages or piezoelectric effect. Hardened diaphragm is exposed to the melt. The deflection of the diaphragm causes the pressure in the fluid capillary to increase. Linear increase of pressure in the fluid capillary is achieved when amount of diaphragm deflection is small. The fluid capillary is of a length sufficient to isolate the sensors and electronics from the high heat. The capillary is often enclosed in an armored cable. (Kazmer, 2009)

For experimental measurement of submitted thesis were used pressure transducers (diaphragm mechanism) MDT 460FH with pressure range 0-700 bar, 0-500 bar, 0-350 bar and also transducers with built-in thermocouples TPT 4634H pressure range 0-100 bar and 0-700 bar. All of them were made by company Dynisco. As a recorder of pressure was used computer software Visco.

8.4 Extrusion Process Parameters

As sensible conditions for real extrusion process were chosen parameters shown in table 4. Screw speed was set as 40 RPM because when higher RPM were set, material achieved critical value of the shear stress and wall slip was occurred. It was recognized by the decreasing torque moment. Maximal mass flor rate of chosen extruder with the constructed extrusion die was determined as 2.3 kg/h.

Table 4: Conditions during real extrusion process

Parameter	Unit	Value
Room temperature	°C	20
Temperature of 1st zone	°C	145
Temperature of 2nd zone	°C	150
Temperature of 3rd zone	°C	153
Temperature of 4th zone	°C	157
Die temperature	°C	160
Screw speed	RPM	40
Mass flow	kg/h	2.3

8.5 Temperature and Pressure Measuring

During real extrusion process temperature and pressure were measured. Temperature was measured at two places. The first place was in position L= 0.4 and the second position was L= 0.9. These position are shown in figure 57. Position L= 0.4 was measured by thermocouple wire. This wire was put into the hole inside the mandrel (middle of the mandrel). Position L= 0.9 was measured by infrared probe device. Infrared probe device measured temperature at the surface of the mandrel. On the beginning of the process were both sensors calibrated with reference temperatures. In case of thermocouple wire it was reference liquid (hot water). Infrared probe device was calibrated with help of the temperature of the mandrel surface before polymer melt was present. Also emissivity of infrared probe device was set for material steel. Average temperature measured by thermocouple wire was 162.1 °C and average temperature measure by infrared device on the surface of the mandrel was 165.5 °C.

Pressure was measured in positons of mandrel: L= 0.1, L= 0.4 and L=0.9. Values of pressure were shown in software Visco. For position L= 0.1 was pressure measured as 18.3 MPa, for position L= 0.4 as 16.8 MPa and for position 0.9 was measured as 1.7 MPa.

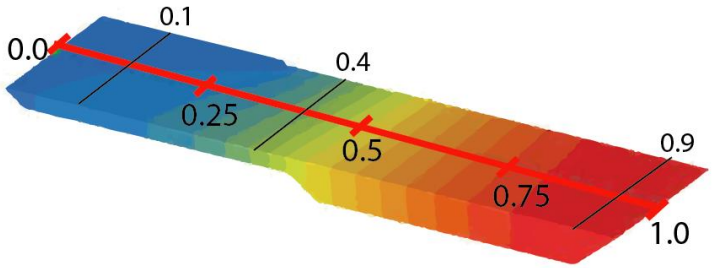

Figure 56: Mandrel with positions of measuring

The results of temperature measuring are shown in figures 57 and 58. Figure 57 shows data´s obtained by thermocouple wire and figure 58 shows curve obtained by infrared probe device. These curves confirmed our expectations. Temperature on the beginning is lower, than temperature achieved at the end of the mandrel. Dissipation is generated by decreasing of the channel depth. Comparison of measured temperatures with simulation will be discussed in next chapter. Figure 57, thermocouple wire, describes temperature profile inside the mandrel from the beginning of the extrusion process. It means from the time, when polymer melt starts to flow. Figure 58, infrared device, describes only steady temperature profile on the surface of the mandrel during extrusion. It means, polymer melt is already in steady flow.

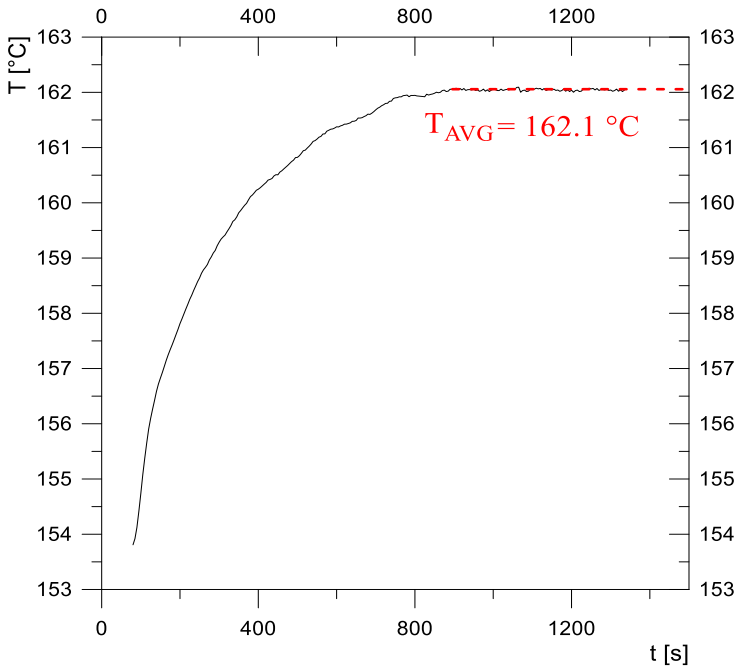

Figure 57: Temperature measuring at position 0.4 along the mandrel

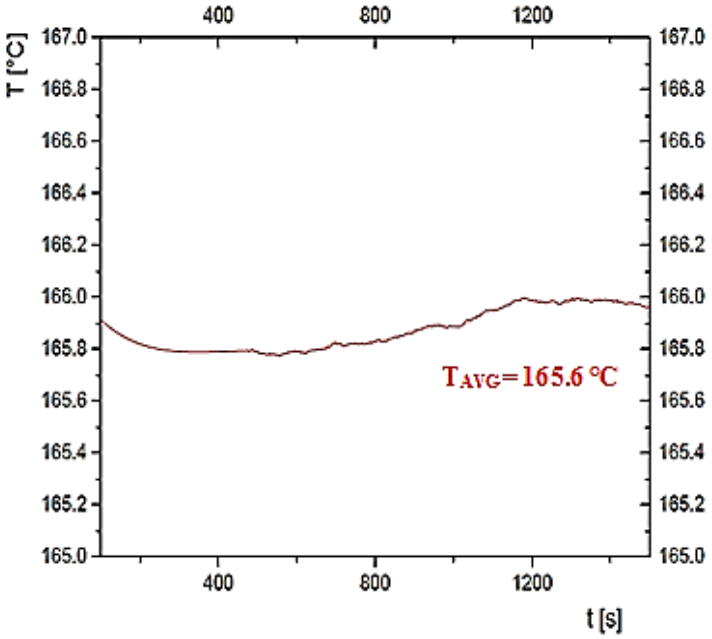

Figure 558: Temperature measuring at position 0.9 along the mandrel

9

Results Comparison

Results from the real extrusion process and results calculated by simulation in 2D and 3D module will be discussed in this chapter.

During real extrusion experiment the material at high production speeds exhibited wall slip. For that reason, we were limited by the maximum of the mass flow rate. Simulation was recalculated for lower mass flow rate, which was 2.3 kg/h. Initial conditions were set as before, outside isothermal walls on temperature 160 °C and temperature of the polymer melt was set on 160 °C as well.

From real measurement we obtained two values of temperature and three values of pressure along the length of the mandrel. All of these results are shown in table 5.

Table 5: Results from real measuring

Variable [1]	Position [1]	Value [1]
Pressure [MPa]	0.1	18.3
	0.4	16.8
	0.9	1.7
Temperature [°C]	0.4	162.1
	0.9	165.5

Figure 59 shows temperature profile along the mandrel. Curves have similar trend, the only differences are at the beginning and also that the curve obtained by 2D module shows more linear trend of increasing temperature. When we compare these curves with curves obtained in previous case (mass flow rate 10kg/h) we can see more gradual increase of temperature. It is probably because polymer melt has lower velocity, it means lower value of pressure is generated leading to lower influence of energy dissipation. Also the difference between temperature of the mandrel and that of the polymer melt is not big.

Values of the temperature are in both cases similar, at least qualitatively. Average temperature for position L= 0.4 reaches 161.5 °C and for position L= 0.9 reaches 165.1 °C. In comparison with the real results we can see just minor differences. On the beginning of the mandrel L=0.4 it is 0.6 °C and in case of position L= 0.9 the difference is 0.5 °C. These differences are probably because of incorrect boundary condition assumed at the wall which connects mandrel with the body of the extrusion die. Extrusion body probably cools down the mandrel a bit and then the difference occurs along the whole length of the mandrel.

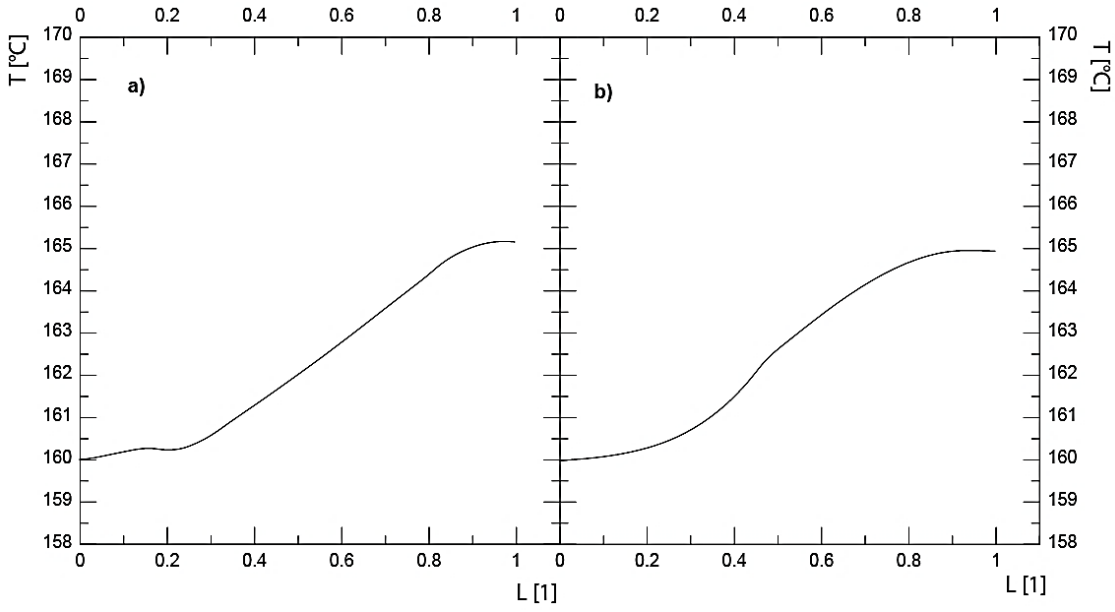

Figure 569 Comparison of temperature profile along the length of the mandrel (simulation): a) 2D module; b) 3D module

Temperature profile across the height of the flow domain is displayed in figure 60. Trend of the curves obtained by 2D and 3D simulation are quite similar. We can see that with lower mass flow rate the temperature profile is practically linear. As it was mentioned it is mainly because of smaller velocity of the polymer melt, lower influence of the thermal conductivity,

respectively. On the beginning of the area, where the mandrel is placed, the temperature profiles are similar with the case when mass flow rate was equal to 10 kg/h. Positions 4 and 5, the end of the mandrel, have more linear trend. Heating of the mandrel by the polymer melt is almost linear.

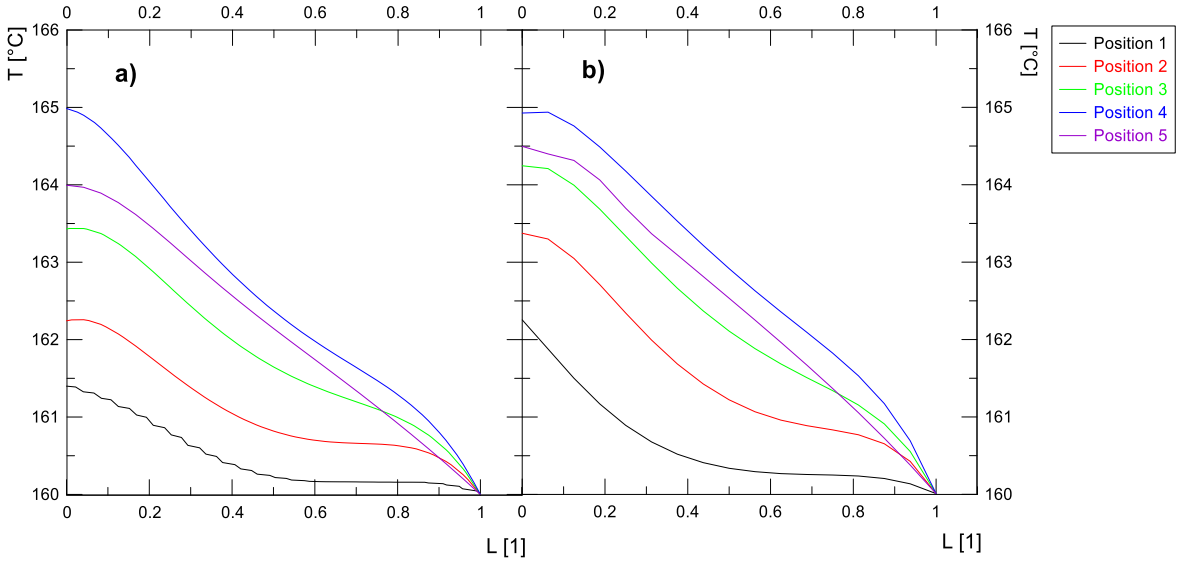

Figure 60: Comparison of temperature profile across the height of the flow domain (simulation): a) 2D module; b) 3D module

Pressure and temperature profiles in the middle of the flow domain were described as a functions along the pathline. In comparison with real measurement the pressure is smaller. The difference corresponds to that of the temperature. Mechanical energy is transformed into generated heat.

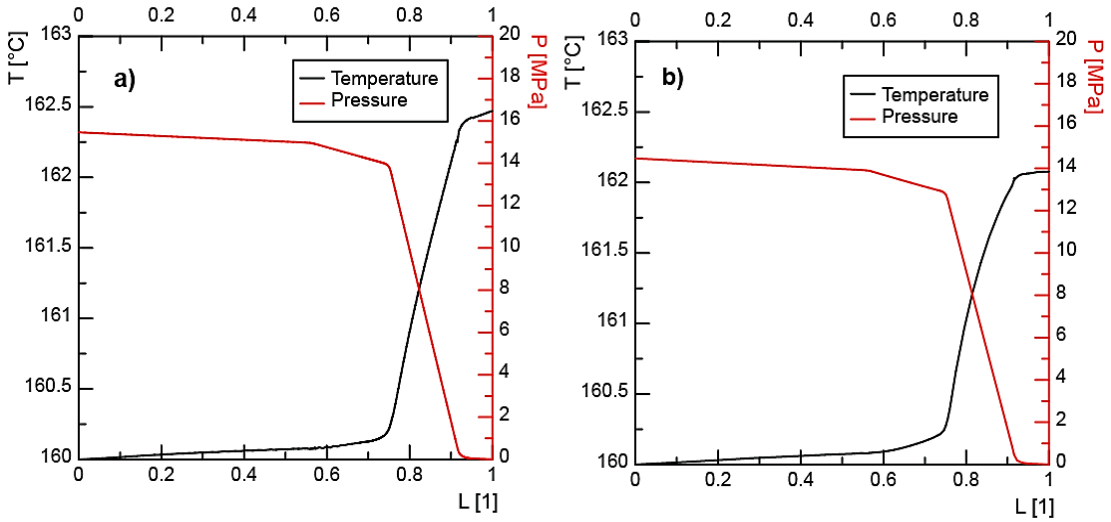

Figure 6157: Comparison of temperature and pressure profiles in the middle of the flow domain (simulation): a) 2D module; b) 3D module

Conclusion

"A day without laughter is a day wasted"

Charlie Chaplin

Simulations of the extrusion process can help as a prediction of the real extrusion conditions. The submitted thesis is focused on understanding of the thermal behavior inside the extrusion die as well as developing of the new boundary condition for 2D (later also for 3D) module of the computer program Virtual Extrusion Laboratory™ 6. 9. from company Compuplast®. The developed new boundary condition solves problems of simulation programs nowadays.

Significant thermal effects occurred in the extrusion die for example in regions where the channel depth is small. In these regions the pressure is consumed and mechanical energy is transformed into heat energy. Such a situation can be caused by presence of the mandrel. Understanding of the mandrel thermal behavior was crucial for this thesis. Most of the simulation programs calculate mandrels as an isothermal or an adiabatic state. The submitted thesis demonstrates that mandrel shows totally different thermal behavior.

Our results show that mandrel is possible to be divided into two parts. One of these parts is cooled down by the polymer melt and the other one is heated up. Cooling of the mandrel is happening at its beginning, while heating of the mandrel is prevailing at the end. In the submitted thesis the mandrel was replaced by the 1D model. The energy equation has been simplified to incorporate the heat fluxes between the mandrel and polymer and also the heat conduction along the mandrel. The model was solved iteratively using Finite difference numerical method.

Simulation in 2DFem module was made after successful design of the new boundary condition. Comparison of our new boundary condition results with those of the 3DFem module shows good match. Subsequently the developed boundary condition approach was compared with real extrusion measurement. This measurement was made by an infrared probe device and thermocouple wire. Results from real extrusion process showed a little bit higher values of temperature and pressure (in case of temperature circa 0.5°C, in case of pressure

circa 2 MPa). It is probably caused by the wall which connects the mandrel with body of the extrusion die.

In summary thermal behavior of the mandrel was described by the new boundary conditions. It will help to provide fast and more accurate predictions of the extrusion dies, where mandrel is included, in computer simulation program VEL^{TM} 6.9.

References

BIRD, R., ARMSTRONG, R. C., HASSAGER, O. **1987**. *Dynamics of Polymer Liquids*, New York, John Willey and Sons.

BIRD, R., STEWART, E., LIGHTFOOT, E. N. **2007**. *Transport Phenomena*, New York, John Wiley and Sons.

BRALLA, J. G. **2007**. *Handbook of Manufacturing Processes - How Products, Components and Materials are Made*. Industrial Press.

CAMPBELL, G. A., SPALDING, M. A. **2013**. *Analyzing and Troubleshooting Single-Screw Extruders*. Hanser Publishers.

CANTOR, K. **2006**. *Blown Film Extrusion - An Introduction*. Hanser Publishers.

CARLEY, J. F., MALLOUK, R. S., MCKELVEY, J. M. **1953**. *Simplified Flow Theory for Screw Extruders*. Industrial & Engineering Chemistry, 45**,** 974-978.

CARLEY, J. F., MCKELVEY, J. M. **1953**. *Extruder Scale-Up Theory and Experiments*. Industrial & Engineering Chemistry, v. 45**,** pp. 989-992.

CARLEY, J. F., STRUB, R. A. **1953a**. *Application of Theory to Design of Screw Extruders*. Industrial & Engineering Chemistry, v. 45**,** pp. 978-982.

CARLEY, J. F., STRUB, R. A. **1953b**. *Basic Concepts of Extrusion*. Industrial & Engineering Chemistry, v. 45**,** pp. 970-973.

CARNIGLIA, S. C., BARNA, G. L. **1992**. *Handbook of Industrial Refractories Technology - Principles, Types, Properties and Applications*. William Andrew Publishing/Noyes.

CHEATLE, K. R. **2006**. *Fundamentals of Test Measurement Instrumentation*. ISA.

CHHABRA, R. P., RICHARDSON, J. F. **2008**. *Non-Newtonian Flow and Applied Rheology - Engineering Applications* (2nd Edition). Elsevier.

CHUNG, C. I. **2011**. *Extrusion of polymers: Theory and Practice*. Cincinnati, Hanser

CIVAN, F. **2016**. *Reservoir Formation Damage - Fundamentals, Modeling, Assessment, and Mitigation* (3rd Edition). Elsevier.

COMPUPLAST. **2003**. *Polymer Rheology and Extrusion*.

DRURY, B. **2009**. *Control Techniques Drives and Controls Handbook* (2nd Edition). Institution of Engineering and Technology.

ERHARD, G. **2006**. *Designing with Plastics*. Hanser Publishers.

FREIRE, F. B., MUJUMDAR, A., FREIRE, F., FREIRE, J. **2014**. *Trends in Modeling and Sensing Approaches for Drying Control*. Drying technology, v. 32**,** pp. 1524-1532.

GHOSHDASTIDAR, P. S. **2012**. *Heat Transfer (2nd Edition).* Oxford University Press.

GILES, H. F., WAGNER, J. R., MOUNT, E. M. **2005**. *Extrusion - The Definitive Processing Guide and Handbook*. William Andrew Publishing/Plastics Design Library.

GORDON, R. J. **1987**. *Calculation and Measurement Techniques for Momentum, Energy and Mass Transfer*. New York, American Institute of Chemical Engineers.

GORE, W. L. **1953**. *Introduction - Theory of Extrusion.* Industrial & Engineering Chemistry, v. 45**,** pp. 969-970.

GRELLMANN, W., SEIDLER, S. **2013**. *Polymer Testing* (2nd Edition). Hanser Publishers.

HALLEY, P. J., GEORGE, G. A. **2009**. *Chemorheology of Polymers - From Fundamental Principles to Reactive Processing.* Cambridge University Press.

HAN, C. D. **2007**. *Rheology and Processing of Polymeric Materials, Polymer Processing.* Oxford University Press.

HUDDLESTON, C. **2007**. *Intelligent Sensor Design - Using the Microchip*. Elsevier.

IBRAHIM, B., KADUM, K. **2010**. *Influence of Polymer Blending on Mechanical and Thermal Properties*. Modern Applied Science, v. 4

JEPSON, C. H. **1953**. *Future Extrusion Studies.* Industrial & Engineering Chemistry, v. 45, pp. 992-993.

KAZMER, D. O. **2009**. *Plastics Manufacturing Systems Engineering - A Systems Approach.* Hanser Publishers.

KOLAT, P. **2001**. *Prenos Tepla a Hmoty,* Ostrava, Technical University of Ostrava.

KOSTIC, M., REIFSCHNEIDER G. L. **2006**. *Design of Extrusion Dies.* Encyclopedia of Chemical Processing.

KUTZ, M. **2011**. *Applied Plastics Engineering Handbook - Processing and Materials.* Elsevier.

LYONS, W. C., PLISGA, G. J., LORENZ, M. D. **2016**. *Standard Handbook of Petroleum and Natural Gas Engineering (3rd Edition).* Elsevier.

MALKIN, A. Y. **1984**. *Rheology Fundamentals.* ChemTec Publishing.

MALKIN, A. Y., ISAYEV, A. I. **2012**. *Rheology - Concepts, Methods, and Applications* (2nd Edition). ChemTec Publishing.

MALLOUK, R. S., MCKELVEY, J. M. **1953**. *Power Requirements of Melt Extruders.* Industrial & Engineering Chemistry, v. 45**,** pp. 987-989.

MANAS, M., VLCEK, J. **2001**. *Aplikovana reologie.* Zlin: Tomas Bata University.

MASOCO, C. W. **1993**. *Rheology: Principles, Measurements, and Applications,* New York, John Willey and Sons.

MCCRUM, N. G., BUCKLEY, C. P., BUCKNALL, C. B. **1997**. *Principles of Polymer Engineering* (2nd Edition). Oxford University Press.

MCKELVEY, J. M. **1953**. *Experimental Studies of Melt Extrusion.* Industrial & Engineering Chemistry, v. 45**,** pp. 982-986.

MICHAELI, W. **2004**. *Extrusion Dies for Plastics and Rubber - Design and Engineering Computations* (3rd Edition). Hanser Publishers.

MORRISON, F. A. **2001**. *Understanding Rheology.* Oxford University Press.

MUSIL, J. **2008**. *Development of Improved Entrance Pressure Drop Technique for Extensional Viscosity Determination.* Master Thesis, Tomas Bata University.

NICOUD, R. M. **2015**. *Chromatographic Processes - Modeling, Simulation, and Design,* Cambridge University, Cambridge University Press.

OSSWALD, T., HERNÁNDEZ-ORTIZ, J. P. **2006**. *Polymer Processing - Modeling and Simulation.* Hanser Publishers.

OSSWALD, T., RUDOLPH, N. **2015**. *Polymer Rheology - Fundamentals and Applications*. Hanser Publishers.

OSSWALD, T. A., MENGES, G. **2012**. *Material Science of Polymers for Engineers* (3rd Edition). Hanser Publishers.

ÖZIŞIK, M. N. **2002**. *Boundary Value Problems of Heat Conduction.* Dover Publications.

PAL, S., BHUNIA, S. C. **2015**. *Engineering Mathematics.* Oxford University Press.

PATTERSON, E. **1968**. *C.A.D. the First Voice of a New Technology.* Computer-Aided Design, v. 1**,** pp. 3-4.

PAVLOU, D. G. **2015**. *Essentials of the Finite Element Method - For Mechanical and Structural Engineers.* Elsevier.

PEPPER, D. W., CARRINGTON, D. **2009**. *Modeling Indoor Air Pollution.* World Scientific.

PETHRICK, R. A., AMORNSAKCHAI, T., NORTH, A. M. **2011**. *Introduction to Molecular Motion in Polymers.* Whittles Publishing.

PLACEK, L. **2002**. *The Bahavior of Plastic Profiles After Exiting Extrusion Die.* Doctoral Thesis, Tomas Bata University.

POEHLS, D. J., SMITH, G. J. **2009**. *Encyclopedic Dictionary of Hydrogeology.* Elsevier.

RATHAKRISHNAN, E. **2005**. *Fundamentals of Engineering Thermodynamics,* Prentice-Hall of India, Asoke K. Ghosh.

RAUWENDAAL, CH. **1991**. *Mixing in Polymer Processing,* New York, Plastics engineering (Marcel Dekker).

RAUWENDAAL, CH. **2014**. *Polymer Extrusion* (5th Edition). Hanser Publishers.

ROOS, Y. H., DRUSCH, S. **2016**. *Phase Transitions in Foods (2nd Edition).* Elsevier.

SCHUBERT, G. **2015**. *Treatise on Geophysics.* Elsevier.

SINGLER, I. L., POLLOCK, H. M. **1992**. *Fundamentals of Friction: Macroscopic and Microscopic Processes*, Netherlands, Springer.

STEVENS, M. J., COVAS, J. **1995**. *Extruder Principles and Operation,* Netherlands, Springer.

TADMOR, Z., GOGOS, C. G. **2006**. *Principles of Polymer Processing*, New Jersey, John Willey and Sons.

TANNOUS, K. **2015**. *Innovative Solutions in Fluid-Particle Systems and Renewable Energy Management*. IGI Global.

TORRES, J. M., WANG, C., VOGT, B. D. **2011**. *Influence of Chain Stiffness on Thermal and Mechanical Properties of Polymer Thin Films.* Macromolecules, v. 44**,** pp. 9040-9045.

TUCKER, L. C. **1989**. *Computer Modeling for Polymer Processing,* Munich Vienna New York, Hanser Publishers.

WHITE, J. L., POTENTE, H. **2003**. *Screw Extrusion,* Munich, Hanser Publishers.

WILKINSON, A., RYAN, A. **1998**. *Polymer Processing and Structure Development,* Netherlands, Springer.

ZATLOUKAL, M. **2015**. *Applied Rheology Textbook*. Tomas Bata University.

List of Abbreviations

2D	two dimensional
3D	three dimensional
™	trade Mark
®	trade Mark registered with the US Patent & Trade Mark Office
TBU	Tomas Bata University
CAD	computer aided design
P	total pressure
exp	exponential function
const.	constant
$f_{b,\,s}$	the friction coefficients of the solid bed, of the screw
Z_b	the down channel distance at barrel surface
mm	unit millimeter
$\dot{Q}$	polymer flow rate
S	channel area
v	speed
kPa, MPa	unit kilo, mega pascal
ΔT	temperature difference
ΔP	pressure loss
ρ	density
C_p	heat capacity with constant pressure
De	Deborah number
λ	relaxation time
Θ	observation time
$\dot{\gamma}$	shear rate

τ	stress tensor
$\dot{\tau}$	shear stress
G	Young module
μ	material coefficient
x, y, z	direction X, Y, Z
$v_{x, y, z}$	speed in directions x, y, z
D_{ij}	total rate of the deformation tensor
t	time
L_{ij}	velocity gradient tensor
d_{ij}	symmetric part
ω_{ij}	asymmetric part
F_x	force in direction X
N_1, N_2	normal stresses
η	shear viscosity
$\psi_{1/2}$	coefficient of the first/second normal stress difference
A	thermal sensitive constant
T	temperature
η_{ref}	initial shear viscosity
β	thermal sensitive constant
R	universal gas constant (8.314 J/mol.°C)
Ea	activation energy
s	unit second
K, K_1, K_2	material constants
α	material constant
M_v	average molecular weight

M_w	weight average molecular weight
M_N	number average molecular weight
n	index of non-Newtonian behavior
m	index of consistency
II_D	second invariant of velocity-deformation tensor
$\dot{\varepsilon}$	elongation rate
η_E	elongation viscosity
ΔE	change of internal energy
W	work done by the system
Q	heat absorbed by the system
ΔU	internal change of energy
ΔE_k	kinetic energy change
ΔE_p	potential energy change
H	enthalpy
V	volume
C_V	heat capacity with constant volume
$\dot{E}_{acc}$	energy of accumulation
$\dot{E}_{conv}$	convection energy
$\dot{E}_{cond}$	conduction energy
$\dot{E}_{diss}$	dissipation energy
$\dot{S}$	energy source
k, λ	thermal conductivity
∇	Nabla mathematical vector operator
:	mathematical operator (double dot product of two tensors is a scalar)

·	mathematical operator (single dot product of two tensors is a vector)
H_r	amount of heat per unit volume
c	degree of cure
P	rate of reversible work affiliated with volume changes (Eq. 56)
q	heat flux
ε	emissivity (Eq. 63)
σ	Boltzmann constant ($1.381\times10^{-23} J/K$)
α	heat transfer coefficient (Eq. 65)
f_{ij}	function with nodes in location i, j
MFR	mass flor rate
HDPE	high density polyethylene
mLLDPE	metallocene linear low density polyethylene
LLDPE	linear low density polyethylene
UV	ultraviolet light
Kg	unit kilogram
m^3	unit volume cubic meter
g	unit gram
W	unit watt
°C	unit degree of Celsius
J	unit joule
ISO	International Organization for Standardization
ASTM	American Society for Testing and Materials
kN	unit kilo newton
%	unit percent
L/D	ratio of length/diameter
π	constant Pi (3.14159)

d_{cn}	diameter of capillary
r_{cn}	radius of capillary
L, l	length
log	logarithmic function
cm	unit centimeter
cm^2	square centimeter
No.	number of
N	unit newton
min	unit minute
DSC	differential scanning calorimetry
kW	unit kilo watt
min.	minimum
max.	maximum
USA	United States of America
ms	unit millisecond
RPM	unit ramps per minute
h	unit hour
ψ	substitution (Eq.)

List of Figures

Figure 1: Schematic of a basic extrusion process (Giles et al., 2005) 15
Figure 2: Classification of feeders for polymer materials 17
Figure 3: Basic screw zones of extruders (Rauwendaal, 2014) 17
Figure 4: Tadmor melting model 19
Figure 5: Drag downstream and pressure upstream side by side (Cantor, 2006) 20
Figure 6: Screw characteristic curves (Newtonian fluid) (Osswald and Menges, 2012) 20
Figure 7: Die swell on exiting the extrusion die (Pethrick et al., 2011) 21
Figure 8: Distribution of extrusion dies 23
Figure 9: Cross section and pressure distribution of the coat-hanger die (Osswald and Menges, 2012) 24
Figure 10: Types of sheeting die: a) The T-shape die; b) The Fishtail die; c) The coat-hanger die (Rauwendaal, 2014) 24
Figure 11: Examples of a) in-line die; b) cross-head die (Rauwendaal, 2014) 25
Figure 12: Examples how to avoid weld lines (Michaeli, 2004) 26
Figure 13: Difficulty of profile die designs (Kostic and G., 2006) 27
Figure 14: Divided flow system into Cartesian coordinates 31
Figure 15: Shear flow deformation 34
Figure 16: Influence of temperature and shear rate on viscosity 37
Figure 17: Uniaxial elongation flow 40
Figure 18: Schema of numerical methods 50
Figure 19: Construction of a grid for finite difference approximations 51
Figure 20: Curve for calculation of ΔP 61
Figure 21: Flow curve of HDPE Liten ML 71 62
Figure 22: Temperature dependency of time for measuring of thermal conductivity 63
Figure 23: Heat capacity dependency of temperature curve 64
Figure 24: Extrusion die: 1 Input; 2 Flow channel; 3 output with the pressure controller 65
Figure 25: Cross section of the extrusion die 65
Figure 26: Cross section of the channel flow where dissipation is occurred 66

Figure 27: Cross section of the channel flow where mandrel is placed 66
Figure 28: Mandrel of the extrusion die 66
Figure 29: The flow situation with isothermal boundary condition of the surface (Temperature field displayed): a) view on top, b) longitudinal section, c) 3D view of a body 68
Figure 30: Temperature profiles across the flow channel at the end of the die with different thermal conductivity (isothermal boundary condition) 69
Figure 31: Temperatures in the steel body and flow channel for isothermal boundary condition: a) values at the polymer melt/steel interface - along, b) values across the flow channel 70
Figure 32: The flow situation with adiabatic boundary condition of the surface (Temperature field displayed): a) view on top, b) longitudinal section, c) 3D view of a body 71
Figure 33: Temperature profiles across the flow channel at the end of the die with different thermal conductivity (adiabatic boundary condition) 71
Figure 34: Temperatures in the steel body and flow channel for adiabatic boundary condition: a) values at the polymer melt/steel interface - along, b) values across the flow channel 72
Figure 35: Longitudinal section temperature profile of the mandrel.....73
Figure 36: Boundary conditions of the flow domain with the mandrel.....75
Figure 37: Decomposition of the 3D model (flow domain + mandrel) of the extrusion die 75
Figure 38: Temperature profile across the flow channel with positions of measuring 76
Figure 39: Temperature profile of the mandrel: a) along; b) across 77
Figure 40: Graphs along the pathline located in the middle of the flow domain: a) pressure; b) temperature 78
Figure 41: 2D geometry of the extrusion die with boundary conditions (isothermal case).....79
Figure 42: Temperature profile across the flow channel with positions of measuring (where mandrel is placed) 80
Figure 43: Pathline profiles in the middle of the flow domain (isothermal condition): a) pressure; b) temperature 81

Figure 44: Temperature on the surface of the flow channel, where mandrel is placed (isothermal condition) 82

Figure 45: 2D geometry of the extrusion die with boundary conditions (adiabatic case) 82

Figure 46: Temperature profile across the flow channel with positions of measuring (where mandrel is placed) 83

Figure 47: Pathline profiles in the middle of the flow domain (adiabatic condition): a) pressure; b) temperature 84

Figure 48: Temperature on the surface, where mandrel is placed (adiabatic condition) 85

Figure 49: 2D geometry of the extrusion die with the developed new boundary condition 87

Figure 50: Temperature profile across the flow domain with positions of measuring (where mandrel is placed) 88

Figure 51: Pathline profiles in the middle of the flow channel (new boundary condition): a) pressure; b) temperature 89

Figure 52: Temperature on the surface of the flow channel, where mandrel is placed (new boundary condition).....90

Figure 53: Constructed extrusion die without heaters 92

Figure 54: Constructed extrusion die channel with the mandrel 92

Figure 55: Technical draw of infrared probe device.....93

Figure 56: Mandrel with positions of measuring.....96

Figure 57: Temperature measuring at position 0.4 along the mandrel 96

Figure 58: Temperature measuring at position 0.9 along the mandrel 97

Figure 59: Comparison of temperature profile along the length of the mandrel (simulation): a) 2D module; b) 3D module 99

Figure 60: Comparison of temperature profile across the height of the flow domain (simulation): a) 2D module; b) 3D module 100

Figure 61: Comparison of temperature and pressure profiles in the middle of the flow domain (simulation): a) 2D module; b) 3D module 100

List of Tables

Table 1: Typical material properties of Liten ML 71 59
Table 2: Values for weight and density of measured samples:.....63
Table 3: Technical parameters of used extruder 91
Table 4: Conditions during real extrusion process.....95
Table 5: Results from real measuring 98

APPENDIX I: MICHAELIS DIAGRAM

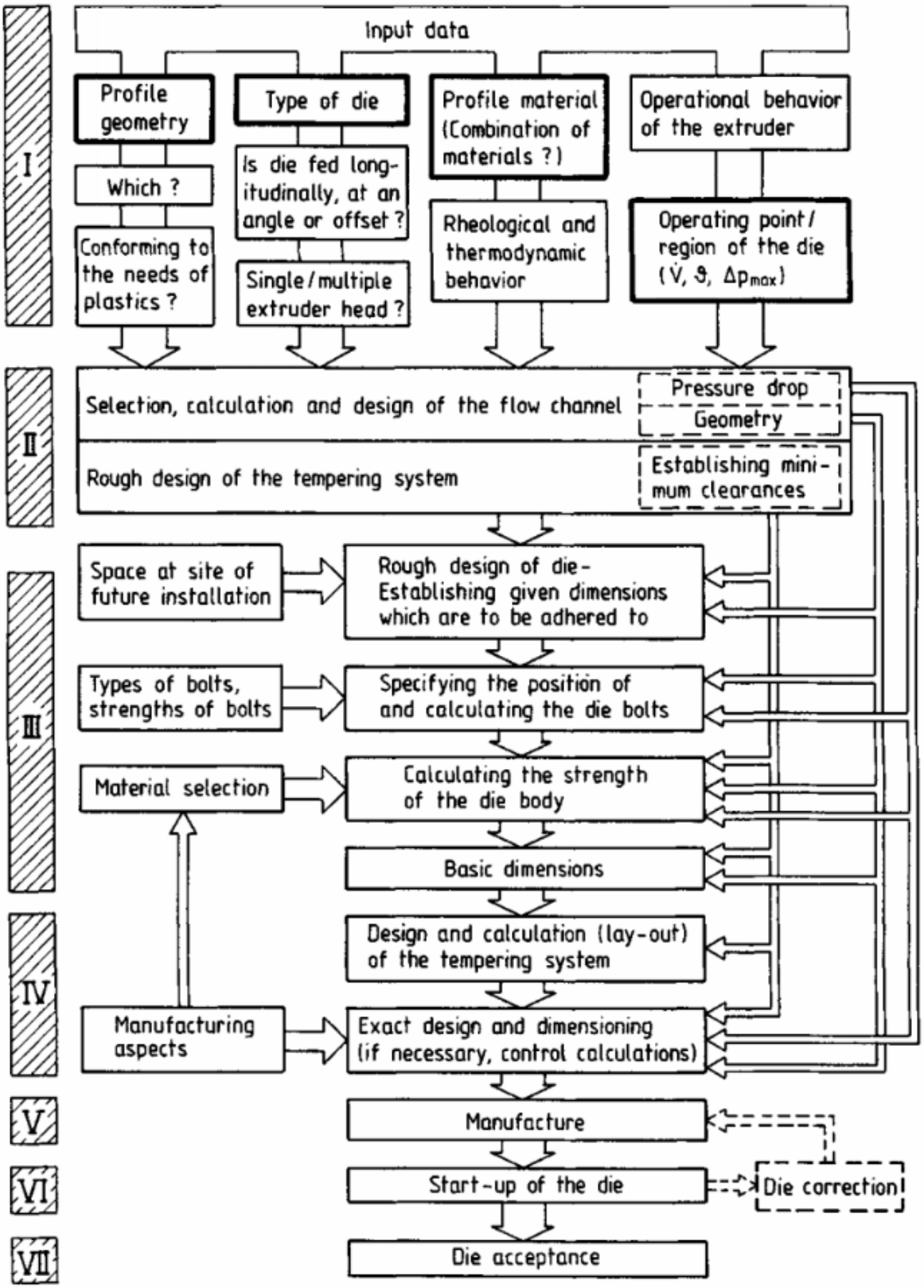

APPENDIX II: FINITE DIFFERENCE EXPRESSIONS FOR COMMON DERIVATES

$$\left.\frac{\partial f}{\partial x}\right|_{i,j} = \frac{f_{i+1,j} - f_{i,j}}{\Delta x} + O[(\Delta x)]$$

$$\left.\frac{\partial f}{\partial x}\right|_{i,j} = \frac{f_{i,j} - f_{i-1,j}}{\Delta x} + O[(\Delta x)]$$

$$\left.\frac{\partial f}{\partial x}\right|_{i,j} = \frac{f_{i+1,j} - f_{i-1,j}}{2\,\Delta x} + O[(\Delta x)^2]$$

$$\left.\frac{\partial f}{\partial x}\right|_{i,j} = \frac{-3f_{i,j} + 4f_{i+1,j} - f_{i+2,j}}{2\Delta x} + O[(\Delta x)^2]$$

$$\left.\frac{\partial f}{\partial x}\right|_{i,j} = \frac{3f_{i,j} - 4f_{i-1,j} + f_{i-2,j}}{2\Delta x} + O[(\Delta x)^2]$$

$$\left.\frac{\partial^2 f}{\partial x^2}\right|_{i,j} = \frac{f_{i+1,j} - 2f_{i,j} + f_{i-1,j}}{(\Delta x)^2} + O[(\Delta x)^2]$$

$$\left.\frac{\partial^2 f}{\partial x^2}\right|_{i,j} = \frac{f_{i,j} - 2f_{i+1,j} + f_{i+2,j}}{(\Delta x)^2} + O[\Delta x]$$

$$\left.\frac{\partial^2 f}{\partial x^2}\right|_{i,j} = \frac{2f_{i,j} - 5f_{i+1,j} + 4f_{i+2,j} - f_{i+3,j}}{(\Delta x)^2} + O[(\Delta x)^2]$$

$$\left.\frac{\partial^2 f}{\partial x^2}\right|_{i,j} = \frac{f_{i,j} - 2f_{i-1,j} + f_{i-2,j}}{(\Delta x)^2} + O[\Delta x]$$

$$\left.\frac{\partial^2 f}{\partial x^2}\right|_{i,j} = \frac{-f_{i-3,j} + 4f_{i-2,j} - 5f_{i-1,j} + 2f_{i,j}}{(\Delta x)^2} + O[(\Delta x)^2]$$

$$\left.\frac{\partial^2 f}{\partial x \partial y}\right|_{i,j} = \frac{1}{\Delta x}\left[\frac{f_{i+1,j} - f_{i+1,j-1} - f_{i,j} + f_{i,j-1}}{\Delta y}\right] + O[\Delta x\,\Delta y]$$

$$\left.\frac{\partial^2 f}{\partial x \partial y}\right|_{i,j} = \frac{1}{\Delta x}\left[\frac{f_{i+1,j+1} - f_{i+1,j-1} - f_{i,j+1} + f_{i,j-1}}{2\Delta y}\right] + O[\Delta x, (\Delta y)^2]$$

$$\left.\frac{\partial^2 f}{\partial x \partial y}\right|_{i,j} = \frac{1}{2\Delta x}\left[\frac{f_{i+1,j+1} - f_{i+1,j} - f_{i-1,j+1} + f_{i-1,j}}{\Delta y}\right] + O[(\Delta x)^2, \Delta y]$$

$$\left.\frac{\partial^2 f}{\partial x \partial y}\right|_{i,j} = \frac{1}{2\Delta x}\left[\frac{f_{i+1,j+1} - f_{i+1,j-1} - f_{i-1,j+1} + f_{i-1,j-1}}{2\Delta y}\right] + O[(\Delta x)^2, (\Delta y)^2]$$

$$\left.\frac{\partial^3 f}{\partial x^3}\right|_{i,j} = \frac{f_{i+2,j} - 2f_{i+1,j} + 2f_{i-1,j} - f_{i-2,j}}{2\Delta x^3} + O[(\Delta x)^2]$$

$$\left.\frac{\partial^4 f}{\partial x^4}\right|_{i,j} = \frac{f_{i+2,j} - 4f_{i+1,j} + 6f_{i,j} - 4f_{i-1,j} + f_{i-2,j}}{(\Delta x)^2} + O[(\Delta x)^2]$$

APPENDIX III: TECHNICAL DRAW OF THE EXTRUSION DIE